MULTIFOCAL LIDAR SYSTEMS

A THESIS SUBMITTED TO
THE GRADUATE SCHOOL OF NATURAL AND APPLIED SCIENCES
OF
MIDDLE EAST TECHNICAL UNIVERSITY

BY

KORAY ÜRKMEN

IN PARTIAL FULFILLMENT OF THE REQUIREMENTS
FOR
THE DEGREE OF DOCTOR OF PHILOSOPHY
IN
MICRO AND NANOTECHNOLOGY

AUGUST 2022

Approval of the thesis:

MULTIFOCAL LIDAR SYSTEMS

submitted by **KORAY ÜRKMEN** in partial fulfillment of the requirements for the
degree of **Doctor of Philosophy** in **Micro and Nanotechnology, Middle East
Technical University** by,

Prof. Dr. Halil Kalıpçılar
Dean, Graduate School of **Natural and Applied Sciences** _____

Prof. Dr. Deniz Üner
Head of the Department, **Micro and Nanotechnology** _____

Assoc. Prof. Dr. Emre Yüce
Supervisor, **Micro and Nanotechnology, METU** _____

Examining Committee Members:

Assoc. Prof. Dr. Halil Berberoğlu
Physics, Ankara Hacı Bayram Veli University _____

Assoc. Prof. Dr. Emre Yüce
Micro and Nanotechnology, METU _____

Assoc. Prof. Dr. Kıvanç Azgın
Mehnacial Engineering, METU _____

Assist. Prof. Dr. Abdullah Demir
UNAM, Bilkent University _____

Assist. Prof. Dr. Ihor Pavlov
Physics, METU _____

Date: 29.08.2022

I hereby declare that all information in this document has been obtained and presented in accordance with academic rules and ethical conduct. I also declare that, as required by these rules and conduct, I have fully cited and referenced all material and results that are not original to this work.

Name Last name : Koray Ürkmen

Signature :

ABSTRACT

MULTIFOCAL LIDAR SYSTEMS

Ürkmen, Koray
Doctor of Philosophy, Micro and Nanotechnology
Supervisor : Assoc. Prof. Dr. Emre Yüce

August 2022, 150 pages

LIDAR systems are commonly used in automation applications, autonomous vehicles, military systems, and other new application areas that are increasingly expanding with the recent developments in LIDAR technology. LIDAR systems are used for getting 3 Dimensional information about the target which is very important for most of the advanced systems and algorithms that are used for the recognition and identification of objects. The most well-known distance measurement techniques for LIDAR systems are the direct "time of flight" (ToF), AMCW (Amlitude Modulated Continuous Wave), and FMCW (Frequency Modulated Continuous Wave) range measurement techniques. In the direct ToF technique, depth resolution is limited by the rise time of the transmitted pulse and measurement speed of the LIDAR system. AMCW and Linear Chriped AMCW techniques are limited in maximum measurement range by ambiguity. FMCW technique needs high-speed electronics with a single pixel resolution and its maximum measurement range is limited by the coherence length of the light source. This study, it is aimed to achieve up to mm scale depth resolution capability at a medium target range by combining multifocal imaging concepts with LIDAR measurement techniques. With this study, Multifocal LIDAR Imaging techniques with higher resolution, have been first introduced, designed, and analyzed. The results show that, with the introduced

Multifocal LIDAR Imaging technique, a good improvement has been achieved in depth resolution for the direct ToF technique and measurement range for the AMCW technique without decreasing the depth resolution of AMCW. Introduced new techniques by this thesis can have a large application area such as robotic applications.

Keywords: LIDAR, Depth of Field, Multifocal Imaging, Dispersion, AM Modulation

ÖZ

MULTİFOKAL LİDAR SİSTEMLERİ

Ürkmen, Koray
Doktora, Mikro ve Nanoteknoloji
Tez Yöneticisi: Doç. Dr. Emre Yüce

Ağustos 2022, 150 sayfa

LIDAR sistemleri otomasyon, otonom araçlar, askeri sistemler gibi farklı alanlarda kullanılmakta ve LIDAR teknolojisindeki gelişmeler ile birlikte farklı kullanım alanları artarak genişlemektedir. LIDAR sistemleri, obje tanımlanması ve sınıflandırılması için kullanılan birçok sistem ve algoritma için çok önemli olan 3B hedef bilgisinin elde edilmesi için kullanılmaktadır. LIDAR mesafe ölçüm tekniklerinden en bilinenleri direkt uçuş zamanı ölçüm tekniği ile Genlik Modüleli LIDAR ve Frekans Modülasyonlu LIDAR teknikleridir. Direkt uçuş zamanı ölçüm tekniğinde elde edilebilen derinlik çözünürlüğü lazerin darbe genişliği ve sistemin ölçüm hızı ile sınırlıdır. Genlik Modüleli LIDAR ve Linear Frekans Kaymalı Genlik Modüleli LIDAR sistemlerinin ölçüm mesafesi belirsizlik mesafesi tarafından sınırlanmaktadır. Frekans Modüleli LIDAR sistemleri tek piksel çözürlükle yüksek hızlı elektronik sistemlere ihtiyaç duymakta ve ölçüm mesafesi ışık kaynağının uyumluluk mesafesi ile sınırlanmaktadır. Bu çalışmada, orta hedef mesafelerinde mm seviyesinde derinlik çözünürlüğe ulaşılabilmesi için Multifokal görüntüleme tekniği ile farklı LIDAR tekniklerinin birleştirilmesi amaçlanmıştır. Bu çalışma ile standart daha yüksek derinlik çözünürlüğe sahip Multifokal LIDAR Görüntüleme tekniği ilk defa tanımlanmış, tasarlanmış ve analiz edilmiştir. Elde edilen sonuçlar

önerilen Multifokal LIDAR tekniği ile direkt uçuş zamanı ölçüm tekniğinde derinlik çözünürlüğünde ve Genlik Modüleli indirekt ölçüm tekniğinde, Genlik Modüleli tekniğin çözünürlüğünü azaltmadan ölçüm mesafesinde önemli iyileşmeşler sağlandığını göstermektedir. Bu tezle tanımlanan yeni tekniğin, robotik uygulamarı gibi geniş bir uygulama olabilecektir.

Anahtar Kelimeler: LIDAR, Görüş Alanı Derinliği, Multifokal Görüntüleme, Dispersiyon, Genlik Modülasyonu

This Study dedicated to my son Umut Deniz ÜRKMEN

ACKNOWLEDGMENTS

TABLE OF CONTENTS

LIST OF TABLES

LIST OF FIGURES

FIGURES

xviii

LIST OF ABBREVIATIONS

ABBREVIATIONS

DFF   : Depth From Focus

FOR   : Field of Regard

FOV   : Field of View

FPA   : Focal Plane Array

IFOV   : Instantaneous Field of View

MEMS   : Micro Electro Mechanical Structure

S/N   : Signal to Noise Ratio

ToF   : Time of Flight

LIST OF SYMBOLS

SYMBOLS

σr   : Depth Resolution

Δφ   : Phase Shift

λ   : Wavelength

CHAPTER 1

INTRODUCTION

RADAR term is first used in 1940 by the United States Navy [1] as the acronym for "Radio Detection and Ranging". The RADAR systems basically send electromagnetic radiation in RF (Radio Frequency) band to the target area and collect the reflected radiation for detection of the possible targets. The spatial and depth resolution of the RADAR systems is limited by the wavelength of the transmitted signal. So the RADAR systems can be used for the detection of large systems with low spatial and depth resolution. The Laser Radar or LIDAR technique can be defined as a kind of RADAR technique that uses Laser light instead of RF signals. Because the wavelength of Laser light is much smaller than the RF signals, it is possible to achieve much higher resolutions in both spatial space and range.

The LIDAR techniques are studied since the 1960s for different applications such as probing the lower atmosphere and studying meteorological phenomena [15], detecting the aerosols from long distances, and getting 3 Dimensional information on the area of interest. 3 Dimensional information is very valuable for different kinds of applications such as target detection, recognition, and identification applications in large application areas such as defense, security, automotive and robotic applications. The depth information gathered by LIDAR systems, not only can be used to distinguish the real targets from the false ones but also gives some other valuable information about targets such as target range and target speed. So, the LIDAR techniques are also very useful for mapping the surfaces in 3 dimensions for geographic and archeological applications.

The basic working principle of 3D LIDAR systems is based on illuminating the target with a known signal shape and measuring the flight time of the signal between LIDAR and target with the help of receiving time of the returned signal. The speed of light is almost constant in air, and the time difference between the transmitted and returned pulse can be used for measuring the distance between the target and LIDAR. The depth resolution is determined by the Time of Flight (ToF) measurement precision which is limited by the rise time of the signal pulse and the bandwidth of the detector systems. To achieve centimeter depth resolution by the traditional LIDAR systems, pulse rise times in picoseconds as discussed under section 1.1.1, as well as larger detector bandwidths in GHz, are required. Moreover, at an increased distance the signal-to-noise ratio (SNR) decreases. These factors further limit the depth resolution. There are also studies for increasing the depth resolution of the LIDAR systems without decreasing signal pulse rise time or increasing detector bandwidths where they still need signal rise time times in nanoseconds and bandwidths in of the order of GHz to achieve mm-scale resolutions [5]. Alternatively, indirect ToF measurement techniques such as modulation of the transmitted signal can be used for higher depth resolution, as detailed in section 1.1.4. The maximum measurement range is limited by the ambiguity or coherence length in these indirect ToF measurement applications [8, 20].

On the other hand, depth data can also be derived by some other passive techniques such as Multifocal Imaging or Depth from Defocus which uses the de-focusing level of the target in the image plane regarding its distance to the optical system [3]. It is known that the image of closer targets is reconstructed at a longer distance in the image plane whereas the image of the far targets is reconstructed at a closer distance in the image plane. Based on this fact, the distance between the image plane and the lens can give relative information about the target distance. Or in another way, the different target distances will cause de-focusing or blurring of the image, and the level of de-focusing on the image can give some information about the target distance. There exist several algorithms for estimating the depth data on the target

plane from the amount of the blurring effect on the image plane [2,11]. The blurring effect also depends on the circle of confusion size, which can be resolved by the detector on the image plane, and respectively depth of field of the optical system. However, these algorithms mainly require a 2D camera that does not provide an avalanche process at a low cost which is essential for the extensive deployment of LIDARs in various fields.

Alternatively, the multi-focal imaging technique can also be used for gathering depth data due to focusing point change in the image plane. Multifocal imaging techniques basically use the Depth of Field to distinguish different depths on the target surface as detailed in section 1.2 The narrower depth of field gives higher depth resolution for the Multifocal Imaging techniques. So, a multifocal imaging system's depth resolution is also inversely limited by the width field of depth of the system so this technique can be used for commonly in microscopy systems [24] where magnification is very high and Field of Depth is very narrow.

1.1   LIDAR Systems

A basic LIDAR system commonly uses a light source for generating the controlled light generation, an optical system for pointing the transmitted light to the interest area and collecting the reflected light from the targets, and data processing electronic to process the collected data for generating a 3-dimensional picture of the area of interest. The spatial resolution of the image can be transmitted by array-type detectors or optical scanner systems where the depth information is gathered by the time of flight measurement of the received signal.

In today, different types of LIDAR systems have been developed such as Flash LIDARs, Solid State LIDARs, Optical Phase Array LIDARs, and MEMS-based LIDARs. In all of these techniques, the target is illuminated by the predefined codded illumination by the LIDAR system. The range between the LIDAR and target is

calculated by the electronic devices with help of the time difference between the transmitted and received codes. The received signal amplitude shall be higher than the Signal to Noise Ratio (S/N) for detection where S/N is determined by the design to avoid false alarms that can be caused by the detector or background noises. So the intensity of the transmitted light and selection of sensor material and electronic circuits plays an important role for the higher detection range of the system. Other important parameters that determine the higher range in terms of the received signal can be given as the target reflectivity, atmospheric transmission (if the target is far away), Reflection characteristic of the target, optical transmission coefficient of the LIDAR optic and clear aperture size of the collection optic. So the basic LIDAR equation can be written as;

$$I_{Received} = I_{Transmitted} R_T D_T T_{AT} T_{AR} T_O A \tag{1-1}$$

where $I_{Received}$ is the received power of the signal, $I_{Received}$ the power of the transmitted signal, R_T the target reflection coefficient, D_T the diffusion caused by the reflection from the target, and T_{AT} the atmospheric transmission that is faced during the illumination of the target, T_{AR} the atmospheric transmission that faced on the back way of the light, T_O the optical transmission of the receiver optic and A is the clear aperture of the receiver optic. Atmospheric transmission can be calculated as;

$$T_{AT} = T_{AR} = e^{-\frac{\sigma D}{1000}} \tag{1-2}$$

Where, R is the distance between the LIDAR and target, σ is the atmospheric absorption coefficient.

For the Lambertian reflection, the diffused intensity of the light can be found as;

$$D_T = \frac{cos\alpha}{\pi D^2} \tag{1-3}$$

4

Where α is the reflection angle on the target surface and if both Light Source and Receiver Optic is on the same optical path α will be 0, then

$$D_T = \frac{1}{\pi D^2} \tag{1-4}$$

By using equations (1-2) and (1-4); equation (1-1) can be re-written as;

$$I_{Received} = \mathrm{I}_{Transmitted} R_T \frac{1}{\pi D^2} \mathrm{e}^{-\frac{2\sigma R}{1000}} T_O A \tag{1-5}$$

LIDAR systems can generate 3D target information basically measuring the distance for different spatial points on the target. Different kinds of electronic or optical scanner systems, sensor matrixes (Focal Plane Arrays, FPA), and or MEMS mirror systems [10] can be used for gathering spatial coordinates on the target. Because the distance measurement shall be done for each pixel in spatial space, the direct ToF limits the overall imaging frame rate of the system. Modulation techniques have greater advantages for increasing the overall frame rate of the system where there is no need to wait for receiving back a single pulse and measurement can be done with any part of the modulation.

1.1.1 Direct Time of Flight (ToF) Measurement

The basic working mechanism of a direct ToF LIDAR system is given in Figure 1-1. The basic principle of time of flight measurement is sending a controlled light pulse to the target and measuring the time difference between the pulse generation and received pulse detection which is reflected back from the target surface. So by the time of flight (Δt) measurement, the range between the LIDAR system and the target can be found by the equation (1-6).

$$D = \frac{c\Delta t}{2} \qquad (1\text{-}6)$$

Where, D is the distance between the LIDAR and Target, c the speed of light and Δt the time of flight.
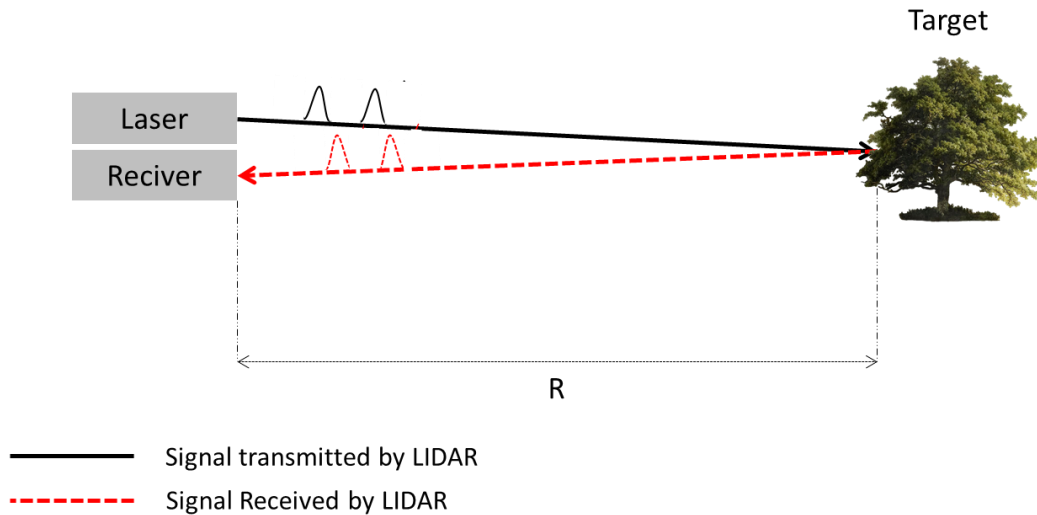
Figure 1-1: Direct Time of Flight Measurement

It is also known that the resolution (σr) of a ToF system is dependent on rise time of the light pulse and can be defined as in equation (1-7) [12];

$$\sigma_r \propto \frac{c}{2} \cdot t_{rise} \cdot \frac{1}{\sqrt{S/N}} \qquad (1\text{-}7)$$

Where σr is the resolution in range, t_{rise} is the rise time of the light pulse, c the speed of light and S/N the signal to noise ratio of the detector system.

In real life applications Signal to Noise Ratio shall always be greater than 1, to distinguish the signal from the noise. As a best-case scenario, if we assume that S/N is 1; then the equation becomes;

$$\sigma_r = \frac{c}{2} \cdot t_{rise} \tag{1-8}$$

$$\sigma_r = \frac{2.998 \; 10^8 \; ^m/_s}{2} \cdot t_{rise} \tag{1-9}$$

$$\frac{2\sigma_r}{2.998 \; 10^8 \; ^m/_s} = t_{rise} \tag{1-10}$$

To achieving 1 cm resolution, required time resolution can be found as;

$$t_{rise} \approx 6.67 \; 10^{-11} \; s \tag{1-11}$$

So, the rising time of the pulse shall be equal to or smaller than 66.7 picoseconds for 1 cm depth resolution, which is hard to easily achieve by widely available low cost commercial products.

1.1.2 Coherent Systems (Homodyne)

Coherent systems are using a coherent source and calculate the ToF by the phase difference of the transmitted and received signal. The coherent detection techniques are also known as homodyne detection techniques [4]. By the coherent detection techniques, it is possible to get a very high resolution in depth which is smaller than the wavelength of the source signal. This source signal wavelength can be the

wavelength of the used light or the wavelength of the modulation that is used to modulate the light source. The wavelength of the light can be used for micro and/or nanoscale measurements from the long ranges as done in intelligence systems for detecting the voice records from the surface of window or Chemical and Biological Reconnaissance systems that detects the suspended aerosols in the air (or cloud) at the infected area [21,22]. The different kinds of interferometer systems can be used for precise measurement of the phase shift at the wavelength of light in such applications. On the other hand, the main limitation of this technique is the coherence length of the light source. After the coherence length of the source, the signal lose its coherency which causes measurement errors in range.

1.1.3   Non Coherent Systems (Heterodyne)

Direct ToF measurement can be given as an example of the non-coherent measurement method. It directly measures the ToF between transmitted and received signals by measuring the time difference between the transmission of the pulse and reception of the back signal. There is no need to have a coherent source for measuring the time difference between two signals. So non-coherent systems are free from the coherence length limitation such as in coherent measurement techniques, but the range measurement resolution of the non-coherent systems is limited by the modulation wavelength or pulse shape (rise time) of the signal.

1.1.4   Indirect Time of Flight Measurement Techniques

Indirect measurement methods are some kind of mixed measurement technique that uses different types of modulation techniques to get a higher resolution in non-coherent or coherent measurement techniques. The most well-known modulation techniques are Amplitude Modulation (AM) and Frequency Modulation (FM) techniques. These modulation techniques are also very well-known and well-studied techniques in Radar technology so this gives the advantage of using well-known

Radar measurement techniques, algorithms, and circuit architecture for LIDAR applications.

Indirect ToF techniques can gather higher resolution than the direct ToF technique where they use the wavelength of the modulation. AMCW and Chirped AMCW techniques do not require a coherent light source because they use the coherency of the modulation whereas FMCW techniques require a coherent light source because it is modulating the frequency of the used light. Indirect ToF measurement techniques are also limited by the ambiguity for non-coherent techniques and the coherence length for coherent techniques. For Amplitude Modulation and Chirped Amplitude Modulation techniques, the limitation wavelength is the modulation wavelength which is much higher than the wavelength of the light.

Both AM and FM modulation techniques require slower electronics than the direct ToF measurement [7]. This makes modulation techniques more feasible for different kinds of applications.

1.1.4.1   Amplitude Modulation (AM)

One of the well-known non-coherent measurement techniques in LIDAR systems is the Amplitude Modulation technique. In this technique, the light source is simply modulated in amplitude to get a signal waveform with the desired wavelength. The phase shift between the transmitted signal and received signal is measured to calculate ToF and then calculate the range information between the LIDAR system and the target. Basic transmitted and received signal forms are given in Figure 1-2. The phase shift ($\Delta \boldsymbol{\Phi}$) and range correlation is given with the equation (1‑12) [4].
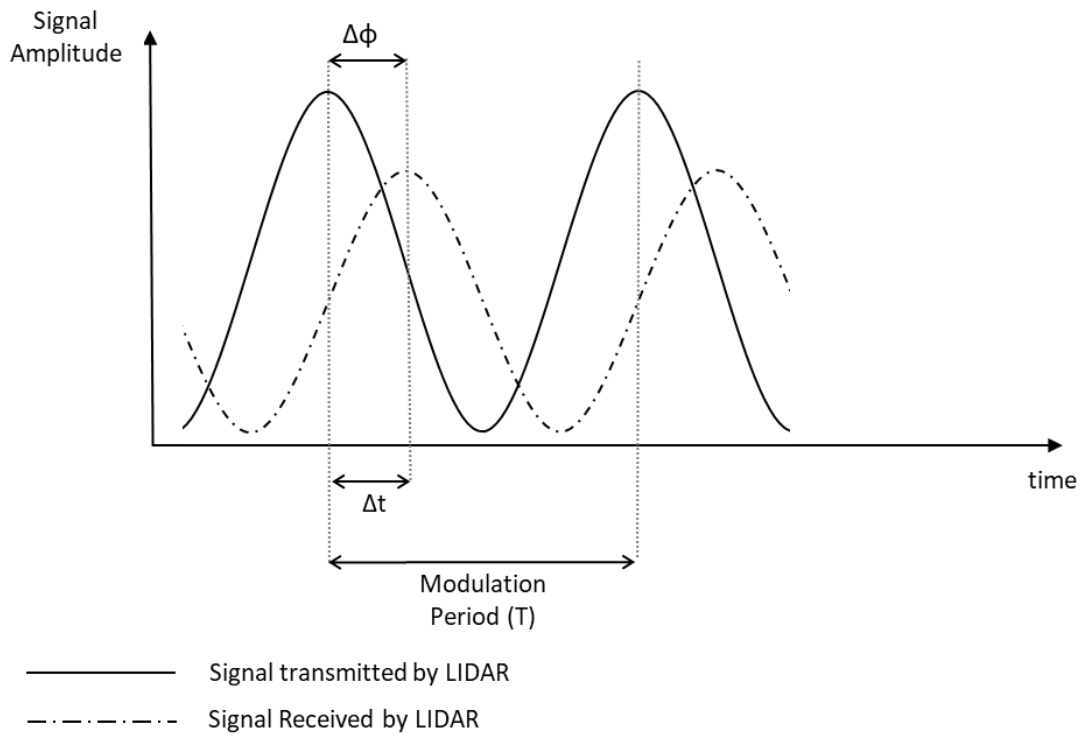
Figure 1-2: Amplitude Modulation

$$\Delta\Phi = \frac{2wD}{c} \qquad (1\text{-}12)$$

$$D = \frac{c\Delta\Phi}{2w} \qquad (1\text{-}13)$$

Where,

$$w = 2\pi f_M \qquad (1\text{-}14)$$

Then,

$$D = \frac{c}{2} \frac{\Delta\Phi}{2\pi f_M} \qquad (1\text{-}15)$$

Where D is the distance between the LIDAR system and the target, c is the speed of light, $\Delta\Phi$ is the phase shift and f_M is the modulation frequency. The relation between the modulation frequency and depth resolution can be defined as [19]

$$\sigma r = \frac{1}{\sqrt{2} \cdot SNR} \cdot \frac{1}{2\pi} \frac{c}{2 \cdot f_M} \qquad (1\text{-}16)$$

Since the AMCW techniques are looking for the phase shift ($\Delta\Phi$) in the wavelength of the emitted light or modulation wavelength, and the phase shift is the same for $\Delta\Phi$, $2\pi+\Delta\Phi$ and $4\pi+\Delta\Phi$, and (any multiplies of 2)$\pi+\Delta\Phi$, it is not possible to dissolve the range larger than the wavelength of the signal. This limitation is also known as ambiguity.

For $\Delta\Phi = N2\pi$, where N is an integer, the sinusoidal equation (1-17) gives the same Amplitude value for N numbers. So, for a phase shift $\Delta\Phi$ over than 2π, it is not possible to distinguish the actual range with the phase shift measurement method.

$$A(t) = A_0 \mathrm{Sin}(\mathrm{wt} + \Delta\Phi) \qquad (1\text{-}17)$$

Where, A_0 is the maximum amplitude, w is the angular frequency and t is the time. The AM modulation techniques may need high-speed electronics (in units of MHz) for modulation of light whereas low-speed electronics will be enough for measurement of ToF from the received signal after de-modulation [7]. So one of the

advantages of AM modulation is, having no necessity for complicated or high-speed read-out circuits.

1.1.4.2   Frequency Modulation (FM Modulation)

In Frequency Modulation (FM) technique, basically, the frequency of the transmitted light is modulated by a local oscillator in units of GHz. The frequency difference (so the phase shift of the modulation signal) between the transmitted signal and received signal is measured to calculate ToF and then calculate the range information between the LIDAR system and the target. Basic transmitted and received signal forms are given in Figure 1-3. The phase shift ($\Delta\Phi$) and range correlation is given with the equation (1-22) [15].
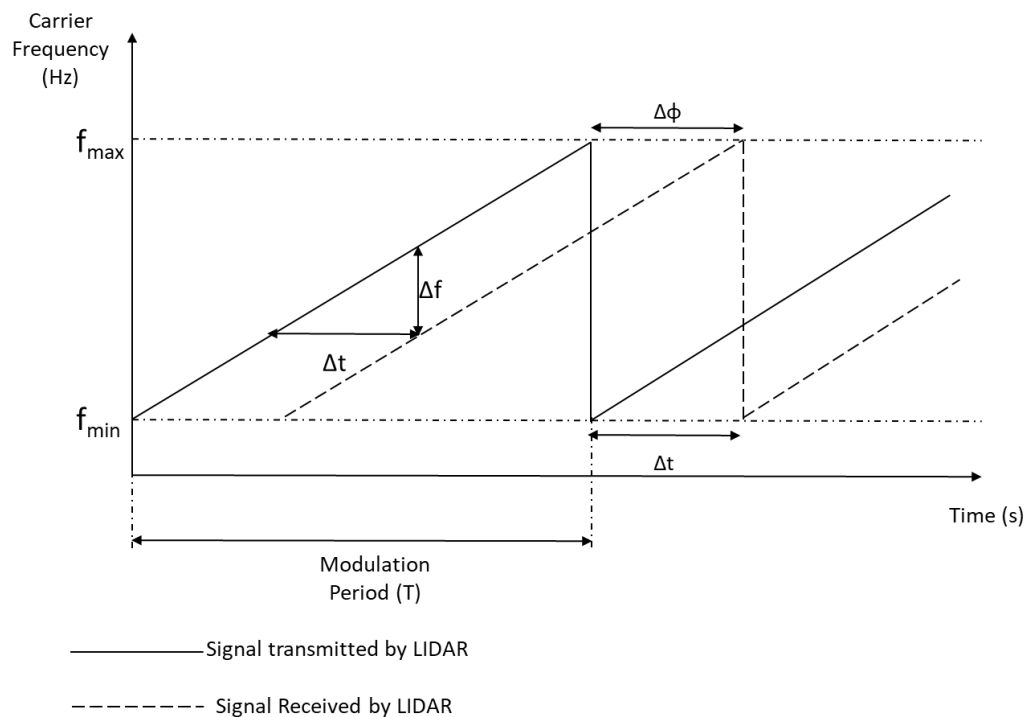
Figure 1-3: Frequency Modulation

$$\Delta f = \text{slope}.\Delta t \tag{1-18}$$

Where,

$$\text{slope} = \frac{f_{max} - f_{min}}{T} \tag{1-19}$$

Then,

$$\Delta f = \frac{f_{max} - f_{min}}{T} \Delta t \tag{1-20}$$

With using equation (1-6),

$$\Delta f = \frac{f_{max} - f_{min}}{T} \frac{2D}{c} \tag{1-21}$$

Finally, The target distance can be given as,

$$D = \Delta f \frac{cT}{2(f_{max} - f_{min})} \tag{1-22}$$

The FM method can also be determined as a different approach where it can be defined as a homodyne technique in the Fourier Domain. The depth resolution of the FMCW technique is limited by the frequency measurement resolution and also the

bandwidth of the frequency modulation. The relation between the modulation bandwidth and depth resolution can be defined as [21]

$$\sigma r \; = \frac{c}{2(f_{max} - f_{min})}$$

(1-23)

FM modulation technique gives more accurate data in the outdoor application where the amplitude of the signal can be affected by the other noise sources and can achieve higher measurement ranges regarding frequency bandwidth used [15].

The main limitation for this application is the coherence length [20] of the light source which depends on environmental effects and mainly coherence specs of the tunable source that is used. The coherence length can be calculated by the equation (1-24) as

$$L_{coh} = \frac{c\pi}{\Delta v_{FWHM}}$$

(1-24)

Where Lcoh is the coherence length, c is the speed of light, Δv_{FWHM} is the source linewidth full-with-half-minimum.

Alternatively, the amplitude of the signal can be modulated by a linear frequency change (named chirped AM) to overcome the ambiguity problem of the AMCW technique, but modulation frequency bandwidth in units of GHz is required for centimeter resolution which is hard to achieve.

1.2   Multi-Focal Imaging

Multifocal imaging gets depth data on a single frame by using different sensors or Focal Plane Arrays in the image plane that focuses on the different depth on the target surface. The basic diagram of multifocal imaging is given in Figure 1-4.

14
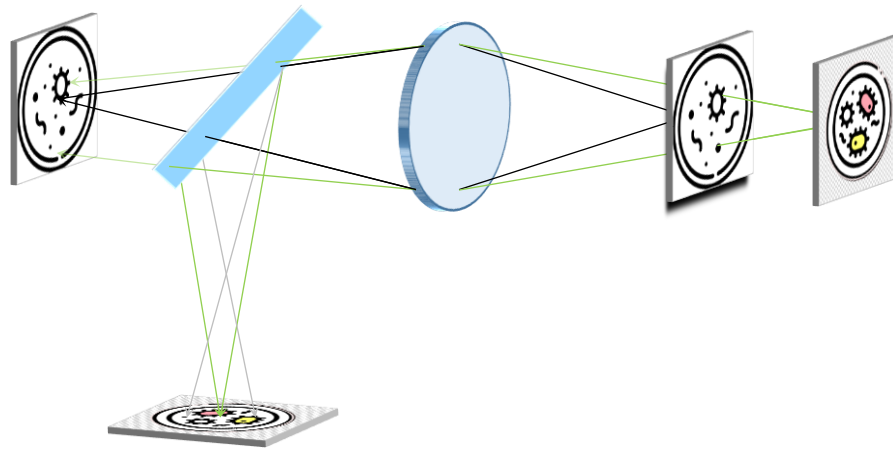
Figure 1-4:Multifocal Imaging

Multifocal imaging techniques basically use the Depth of Field to distinguish different depths of the target surface. Multifocal imaging is commonly used as a microscopy technique where it requires very high magnifications and so very narrow Field of Depth. In microscopy, the microscope system can only focus in a narrow range of a distance regarding the objective magnification. The distinguishable depth in this narrow range is determined by the Depth of Field which is inversely proportional to the magnification of the microscope and the clear aperture of the objective [6]. Small depth changes on the target plane make the object out of the Depth of Field which means blur images and low-intensity on the image plane. For seeing different depths on the target plane focusing point in the image plane is changed (which is called focusing of the objective). The multifocal plane microscopy uses this phoneme by using different FPAs (or detectors) on different focusing points in the image plane to distinguish the depth information on the target. In such a case each FPA will focus on a specific different depth on the target and get a clear image of that specific depth only because the light comes from other depths will be blurred regarding the Depth of Field of the system. So the maximum depth resolution is limited by the Depth of Field. The multifocal imaging technique is a well-studied

technique in microscopy where the magnification is so high and then the Depth of Field is small enough to get high-resolution depth data from the target surface.

1.2.1 Depth of Focus / Depth of Field

The depth of field is the maximum and minimum range limitation of an objective system that can be imaged without blurring effect. The basic diagram of a simple objective system is given in Figure 1-5 [6]. In Figure 1-5, f is the effective focal length of the lens system; D the target distance; C the circle of confusion diameter; N f# of the lens system, and d_1 the nearest object distance from the D, d_2 the farthest object distance from the D and so d is the depth of field.
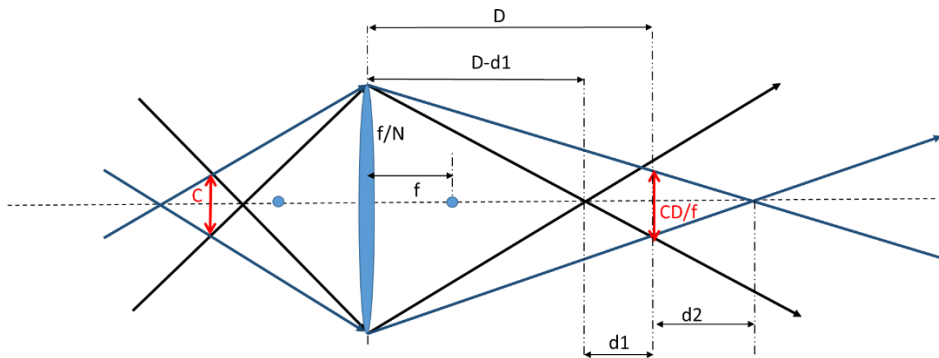
Figure 1-5: The schematic representation of the depth of field.

With using similar triangular relations;

$$\frac{d1}{D-d1} = \frac{CD/f}{f/N} \tag{1-25}$$

16

And,

$$\frac{d2}{D + d2} = \frac{CD/f}{f/N} \qquad (1\text{-}26)$$

We can derive d1 from equation (1-25) as,

$$d1 = \frac{CD^2/f - d1CD/f}{f/N} \qquad (1\text{-}27)$$

$$d1 + \frac{d1CD/f}{f/N} = \frac{CD^2/f}{f/N} \qquad (1\text{-}28)$$

$$d1\left(\frac{f/N + CD/f}{f/N}\right) = \frac{CD^2/f}{f/N} \qquad (1\text{-}29)$$

$$d1 = \frac{CD^2/f}{f/N + CD/f} \qquad (1\text{-}30)$$

Similarly d2 can be derived from equation (1-26) as;

$$d2 = \frac{CD^2/f}{f/N - CD/f}$$

(1-31)

So;

$$d = d1 + d2 = \frac{2NCD^2 f^2}{f^4 - N^2 C^2 D^2}$$

(1-32)

Where, d is the depth of field; N is the numerical aperture of the objective, C is the circle of confusion diameter, D is the target distance, f is the focal length of the objective.

For small ranges, $N^2 C^2 D^2$ is negligible so the equation (1-32) can simply re-written as;

$$d = d1 + d2 = \frac{2NCD^2}{f^2}$$

(1-33)

The closest distance that getting a sharp focus for the infinity objects is called hyperfocal distance D_H and can be calculated by the equation (1-34) [23].

$$D_H = f + \frac{f^2}{NC}$$

(1-34)

So, because we will not able to distinguish different target distances that over than the hyperfocal distance, we can define the hyperfocal distance as a limit for the maximum target distance that multifocal imaging can be used.

18

The depth of focus s can also be calculated by using equation (1-33) as;

$$s = \frac{2NCD^2}{f^2} \cdot \frac{f}{D} = \frac{2NCD}{f}$$

(1-35)

1.2.2 Depth Estimation by Depth of Focus (Depth From Focus, DFF)

The intensity on a FPA pixel is maximum for the focus condition and spot sizes begin to increase so the image gets blurred and the intensity on the pixel decreases for out-of-focus conditions. Basically, the Depth From Focus technique uses the change in the intensity of the pixels to estimate the focus and out-of-focus conditions on an image. Measuring the degree of this intensity change is used to estimate the degree of out-focusing and finally depth change on the target plane which causes out-focusing. For estimation of depth, different kinds of algorithms can be used [13] or predefined data sets for different degrees of un-focus conditions can be used [14]. Although it is a basic technique that uses only computing sources for estimation of depth from classical images, the depth resolution is proportional to the magnification of the optic and so inversely proportional to the depth of field as in Multi-Focal imaging and so limited by the depth of field of the optical system. Also, different reflection coefficients on the target or non-uniform illumination on the target, etc. can cause secondary measurement errors where the measurement is using the intensity changes on the pixels.

CHAPTER 2

LIMITATION OF DEPTH MEASUREMENT TECHNIQUES

2.1   Limitations of LIDAR Techniques

The general depth resolution limitations are discussed in chapter 1.1.1 for Direct ToF LIDAR systems and chapter 1.1.4 for indirect LIDAR techniques. Basically, the rise time of the pulse and speed of the electronic devices are the main direct limitations for the depth resolution of the direct ToF measurement LIDAR systems where the light source peak power and ambiguity are the main limitations of AM LIDAR systems. The speed of the electronic devices and the ambiguity is the main limitation for FM LIDAR systems. These limitations can be defined for a depth resolution of a single pixel measurement system, especially for the FM technique. In real life, for most of the applications, high spatial resolution is required so depth measurement shall be taken for different spatial coordinates to create 3D information. In field deployed LIDAR systems, several techniques can be used for getting depth data at different spatial coordinates. These systems can be flash LIDAR systems with FPA structure [16,17], or different kinds of scanning systems can be used such as optical wedges [18], polygonal mirrors, micro mirrors, etc. [10]. In platform deployed LIDAR systems, the movement of the platform can also be used as a scanning mechanism in one direction.

For getting 3D data, the depth (or range) data shall be measured for each spatial coordinate (pixels) separately. This can be done at the (nearly) same time for all pixels such as in flash LIDAR systems or can be done sequentially such as in scanning systems or can be done with mixed techniques that include both detector arrays and scanner systems. Because, high-speed electronics and readout are required for the ToF measurement, the spatial resolution of the FPA's is still limited with the

low resolution (such as 128 x 128 pixels or lower) in today [16,17]. Limitations in array sizes of LIDAR detectors can cause some extra limitations for LIDAR systems such as frame rate limitations. As defined by equation (1-6), the total time of flight (∆t) is depending on the target range. In direct ToF measurement ∆t can be defined as the necessary time for transmitting and receiving back the signal. For close target distances and low spatial resolutions, spending ∆t is not a limiter for frame rate but for longer distances and high spatial resolutions it can become a limiter for an effective LIDAR imaging system. In an ideal case to achieve a 30 Hz frame rate, the whole image shall be created in 0.033 seconds, so the system shall have 0.033 seconds for the depth measurement in all pixels. If we ignore the time losses in the reading circuits, electronics, and scanner systems, and we assume that the next measurement starts immediately for the next spatial coordinate without any time loss, the upper limits of the ToF for each pixel can be calculated as,

$$ToF_{limit} = \frac{0.033}{\# \ of \ pixels}$$

(2-1)

The results for different spatial resolutions are given in Table 2.1

Table 2.1 ToF limitations and Corresponding Range Limits for achieving 30 Hz Frame Rate in ideal conditions

# of the Pixels	ToF Limit (microseconds)	Corresponding Range Limit (m)
1	33,333.33	4,996,666.67
128 x 128	2.03	304.97
256 x 256	0.51	76.24
512 x 512	0.13	19.06
640 x 480	0.11	16.27

Even in the ideal case, without any time loss in electronics or scanner mechanisms, if the one-pixel detector is used for generating a 640 x 480 pixels resolution image at 30 Hz, by using equation (2-1) the maximum measurement time can be calculated as;

$$ToF_{limit} = \frac{0.033}{640.480} \approx 108.5 \ ns$$

(2-2)

So, by using equation (1-6), for getting 640 x 480 pixels resolution with 30 Hz frame rate, the maximum measurement range D_{max} can be calculated as,

$$D_{max} = \frac{108.5 \ ns \ . \ 2.998 \ 10^8 m/s}{2} \approx 16,27 \ m$$

(2-3)

To exceed this limitation, the detector arrays can be used or indirect time of flight techniques, which do not require waiting for all ToF, can be used. Since the signal is continuous in AMCW or FMCW modulation techniques, the measurement can be taken at any time from any part of the signal so the ToF can be calculated without waiting for ToF for each pixel. So to achieve 3D information that also satisfies the high resolution in spatial coordinates, the high speed and high-cost FPA's or indirect ToF techniques shall be used.

2.2 Limitations of Multifocal Imaging

As described in chapter 1.2, multifocal systems use the focal shift in the image plane and the depth resolution of the system is the proportional depth of field of the optical system. Then the multifocal systems can distinguish the small depth differences only for narrow depth of fields, so for high magnification optics. As given in equation

(2-4) high magnification optics means high optical focal length where high focal length means a very narrow Instantaneous Field of View (IFOV) as described by equation (2-5).

$$M = \frac{f}{D} \tag{2-4}$$

$$IFOV = \tan^{-1} \frac{Pixel\ Pitch}{2 * f} \tag{2-5}$$

The total spatial area that can be imaged is then limited by the horizontal and vertical Field of Views which can be calculated equations (2-6) and (2-7).

$$FOV_{Horizontal} = \#Pixels_{Horizontal}.IFOV \tag{2-6}$$

$$FOV_{Vertical} = \#Pixels_{Vertical}.IFOV \tag{2-7}$$

In other words, to get a high depth resolution, the system is losing from the total imaging area and may need some scanning system to get a higher Field of Regard with scanning for imaging required target area in most of the applications. Similar to the previous chapter, using a scanner system also inversely affects the frame rate of the system. On the other hand, for a good depth resolution, an optical system shall be needed with high focal distances and some stabilization systems may be needed for the operation of such systems. So, because of these reasons, the high depth resolution of the multi-focal imaging techniques is limited with the microscopy applications.

2.3   Increasing Depth Resolution Of Lidar Technique By Multifocal Imaging

The depth resolution, spatial resolution, and frame rate limitations of LIDAR systems and Multifocal imaging systems have been discussed above. In this work, our main aim is to increase the depth resolution of direct ToF LIDAR technique and improve the measurement range of indirect ToF measurement techniques by combining LIDAR techniques with multifocal imaging techniques and developing a new Multi-Focal LIDAR imaging system by getting the advantages of each systems (Figure 2-1).
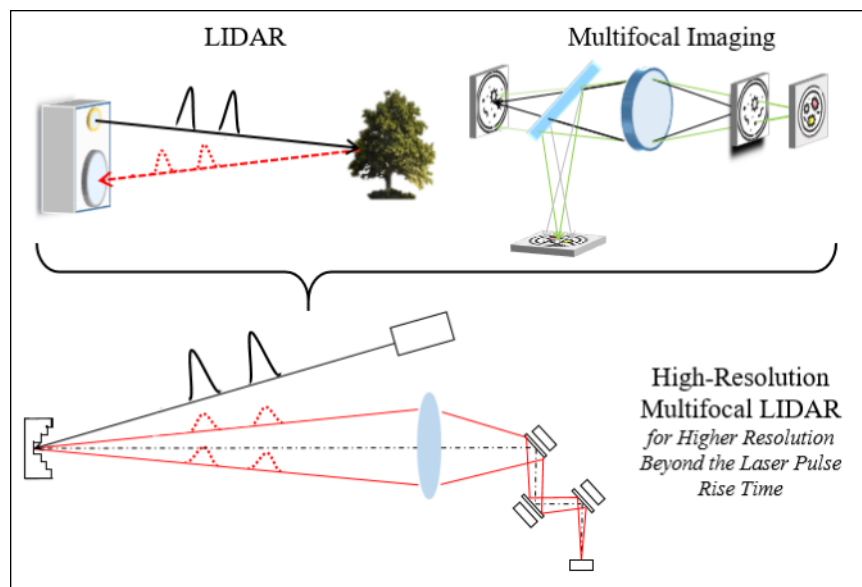
Figure 2-1: High Resolution Multifocal LIDAR System.

In this work, a new Multifocal LIDAR Imaging system technique has been introduced, designed, and analyzed. The thesis work starts with a proof of concept and also goes on with advanced solutions which have been introduced, designed, and analyzed in the following chapters.

The main idea of the multifocal LIDAR technique is to use direct ToF techniques for a rough measurement of the target distance and use the multifocal imaging technique

for higher depth resolutions. Basically the depth measurement of the different depth layers on the target plane with higher depth resolution simultaneously with the different sensors that are placed on different positions on the image plane by using the multifocal imaging technique.

By this newly introduced technique, only the reference (rough) distance of the target is measured with the direct ToF technique and then the multifocal imaging technique is used for depth in higher resolution. This newly introduced technique also does not require waiting flight time for measuring the depth layers by multifocal imaging. The optical system and analysis for proof of concept design are given in chapter 3. Some chromatic enhancements on the Multifocal LIDAR Imaging system to achieve easier productibility are also worked and newly introduced techniques are given in chapters 4 and 5.

With the positive results of the proof of concept of the Multifocal LIDAR Imaging system, an Advanced Multifocal LIDAR system has been designed and introduced in chapter 6 with mm depth resolution, in moderate target ranges with easier productibility.

Finally, the AMCW Multifocal LIDAR system design has been introduced in chapter 7 with high depth resolutions in mm and with great measurement ranges higher than the Multifocal LIDAR system and the ambiguity limitations of the AMCW LIDAR technique. In the AMCW Multifocal LIDAR system, the multifocal imaging technique is differently used for creating measurement gates to enlarge the maximum measurement range of the system over to ambiguity ranges.

In this thesis work, two new types of LIDAR systems have been introduced as the combination of standard LIDAR techniques and multifocal imaging techniques. The combination with multifocal imaging technique provides the advantage of higher depth resolution to direct ToF measurement technique in new proposed Multifocal LIDAR Imaging technique and provides an advantage to AMCW Multifocal LIDAR

Imaging technique to enhancing measurement range over then the ambiguity limitations without losing high depth resolution. All proposed systems have mm depth resolution so provide high depth resolution beyond the pulse rise time limitation of the direct ToF measurement techniques.

CHAPTER 3

OPTICAL DESIGN FOR COMBINING LIDAR AND MULTIFOCAL IMAGING TECHNIQUES FOR HIGHER DEPTH RESOLUTION

In this chapter, the Multifocal LIDAR Imaging System (MLIS) is introduced and the optical design is detailed. Aldo the analysis results are given for proof of concept to show that the main idea of the system is working. The schematic diagram of the introduced Multifocal LIDAR Imaging system is given in Figure 3-1.
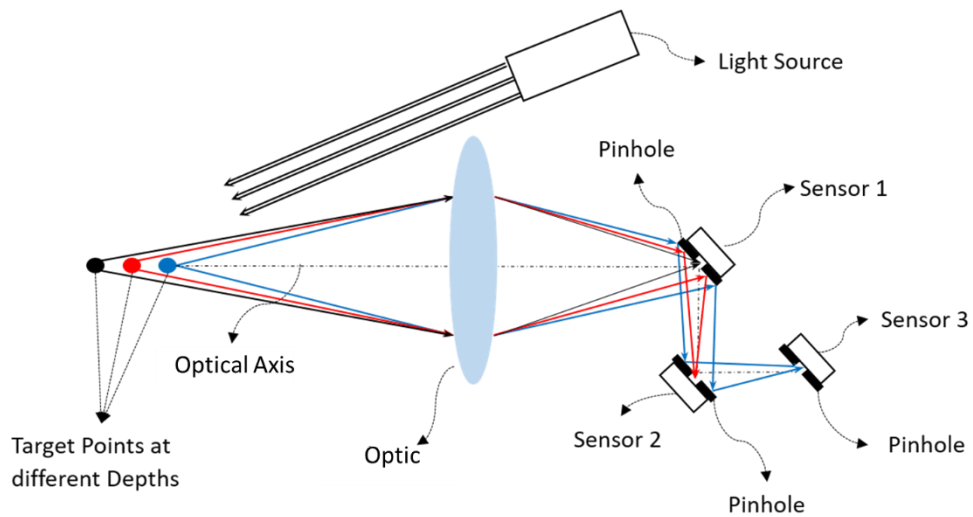
Figure 3-1: The schematic representation of the combination of the LIDAR and Multifocal imaging techniques

In this method, the pulse is transmitted to the target with the help of the controlled light source and the time difference between transmission time and reception time of any sensor is measured for calculation of the target distance D with the equation (1-6). After the reference target distance D is calculated by the direct ToF technique,

the images taken by the sensor-1, sensor-2, and sensor-3 are used for the measurement of different depth layers on the Target plane by the multifocal technique. As described in Figure 3-1, For a target layer-1 at 500 mm (0 mm height in the object plane), it is observed that the collected light focused perfectly on the first sensor, S1. The signal on S1 after the pinhole provides a focal image. The remaining signal is reflected and directed to the second detector. For the target layer-2 at 498 mm (2 mm height in the object plane), the collected rays are reflected by the pinhole reflector that is in front of the first sensor. Similar to the first detector a focal signal on the second sensor plane will be observed. The remaining signal is again reflected by the reflective pinhole in front of the second detector and directed to the third detector. Lastly, for the target layer-3 at 496 mm (4 mm height in the object plane), the reflected rays from the first and second sensor are focused on the third sensor plane. This result will gather low intensity on the S1 and S2 where high intensity on S3. The places of the sensors are fixed in the image plane, so the distances between the layers are known. Because the narrow depth of field is required to achieve distinguishable depth layers, a closer target plane range (50 cm) is studied with a high focal distance objective for proof of concept study. To achieve such an optical system, a basic optical relay system is designed for proof of concept and related analysis.

3.1   Design Criteria

For proof of concept study, it is aimed at very well distinguished depth layers on the target plane with 2 mm depth differences, where such a depth resolution requires picosecond pulse rise time in direct ToF measurement technique. It is also aimed to have a moderate clear aperture to avoid very big ones which are very expensive and difficult to produce.

Table 3.1 The Design Inputs for Multifocal LIDAR Imaging Optical System

Parameter	Design Data
Target Distance	0.5 m
Clear Aperture	60 mm
Depth of Field	2 mm
Working wavelength	850 nm

3.2 Optical Design

Because well-distinguished depth layers on the target plane with 2 mm depth resolution require high magnification and so closer target range with high focal distance, a basic relay optic is designed for proof of concept study. The optical layout of the designed system is given in Figure 3-2. 3 sensors are located in the image plane with the help of reflective mirrors for different depth imaging as given in Figure 3-3 which is a zoomed part of the image plane.
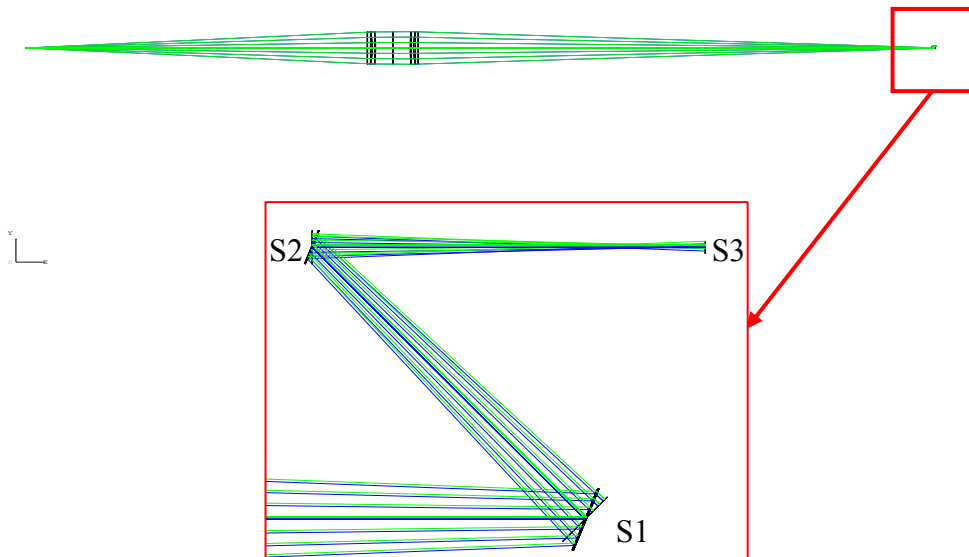
Figure 3-2: The optical design layout of new introduced Multifocal LIDAR Imaging system.

The relay system is designed and optimized for 500 mm target distance and better image quality in the image plane on sensor-1, and sensor-1 is placed on the optimized point in the image plane. The first reflective mirror is placed and then the relay system is optimized for 498 mm target distance and better image quality in the image plane on sensor-2, and sensor-2 is placed on the optimized point in the image plane. Finally, the second reflective mirror is placed and the relay system is optimized for 496 mm target distance and better image quality in the image plane on sensor-3, and sensor-3 is placed on the optimized point in the image plane. The distances between the optimized points for sensor-1, sensor-2, and sensor-3 planes have been measured as 4.5 mm.
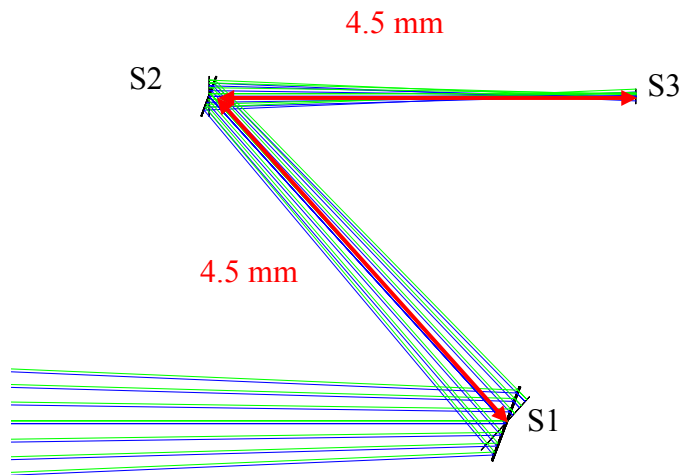
Figure 3-3: The sensor locations layout of new proposed LIDAR and Multifocal imaging system.

The spot diagrams, MTF graphs, and encircled energy diagrams have been checked for each sensor plane and 496 mm, 498 mm, and 500 mm target distances, to present the image quality of the system and further analysis. The design results of the system for 496 mm target distance and well in-focus condition on sensor-3 (which is the longest effective focal length condition of the system) are given in Table 3.2. The pinhole radius of the system is determined as 10 µm by the encircled energy graphs

on sensors which will be detailed in chapter 3.3. The output parameters of the optical design are given in Table 3.1. The IFOV is calculated by using equation (2-5) as,

$$\frac{IFOV}{2} = \tan^{-1}\frac{10\ \mu m}{317mm} = 0.0018º \tag{3-1}$$

Table 3.2 The Design Outputs of Multifocal LIDAR Imaging Optical System

Parameter	Design Data
Effective Focal Length (f)	317 mm
Pinhole Radius	10.0 μm
Calculated Depth of Field	~0.5 mm
Calculated Hyperfocal Distance	951 m
IFOV	0.0036º ~ 0.03 mm

3.3   Results

Results of the optical design have been examined in three different target ranges with 2 mm layer depth differences between each other.

For the first target layer at a distance of 500 mm, the target image is constructed on Sensor-1 as seen in Figure 3-4. In this condition, the rays are in a good in-focus condition on sensor-1, and the reflected parts of the rays from the pinhole mirror of sensor-1 continue their ways but they will be out-of-focus conditions on sensor-2 and sensor-3.

For the second target layer at a distance of 498 mm, the rays are in out-of-focus condition on sensor-1, and then they reflected from the pinhole mirror of the sensor-1 and the target image is constructed on Sensor-2 as seen in Figure 3-4. The other rays that reflected from the pinhole mirror of sensor-2 also continuous their ways but they will be out-of-focus condition on sensor-3.

For the last and third target layer (which is the closest one to the multifocal LIDAR system) at a distance of 496 mm, the rays are in out-of-focus condition on sensor-1 and sensor-2 planes, then they reflected from the pinhole mirrors of the sensor-1 and sensor-2 and the target image is constructed on Sensor-3 as seen in Figure 3-4.

The MTF graphs and spot diagrams on each sensor for each target layers are worked below for analyzing the results.

3rd Target Layer
(Height: 4mm)

S2

S3

S1
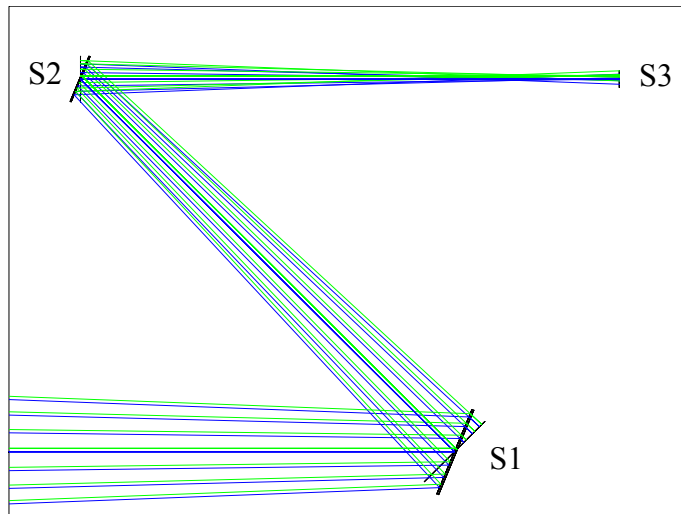
2nd Target Layer
(Height: 2mm)

S2

S3

S1
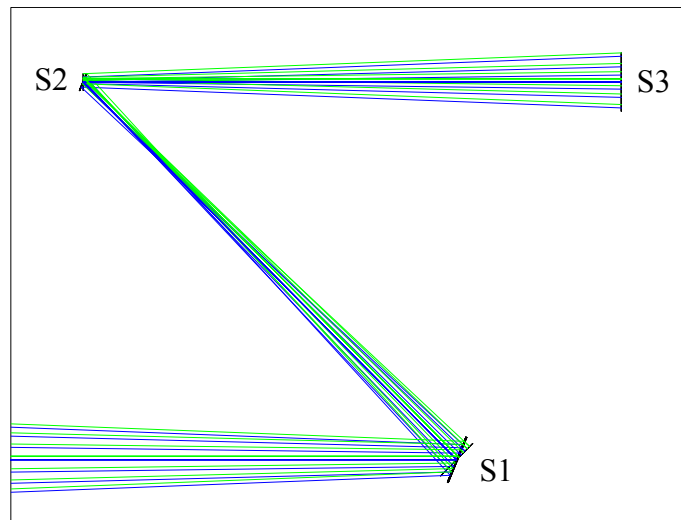
1st Target Layer
(Height: 0mm)

S2

S3

S1
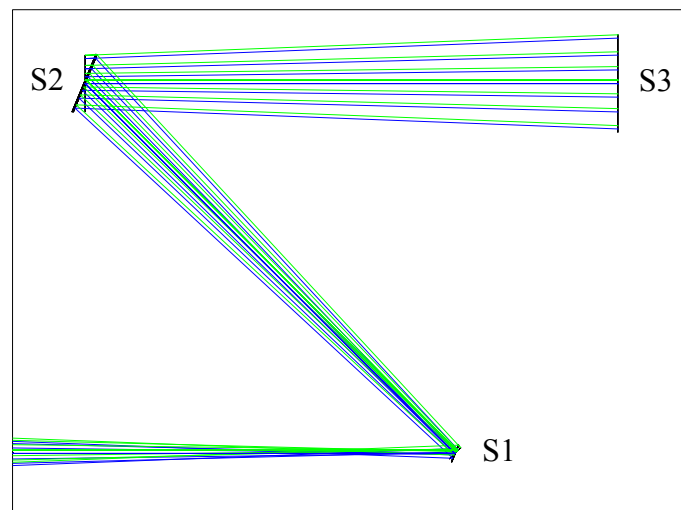
Figure 3-4: The optical paths and sensor layouts for 1st, 2nd and 3rd Target Layers

Spot diagram results of sensor-1, sensor-2 and sesnor-3 planes are given in Figure 3-5 for the first, second and third target layers. In the spot diagram, it is clearly seen that

- on the sensor plane-1
    – the spot size is smaller than the airy disk for Target Layer-1 which means that the optical design is diffraction limited. So a very good image quality is expected on sensor-1 plane for the first target layer.
    – the spot sizes are bigger for Target Layer-2 and Target Layer-3 and far away from the airy disk which means that blurred images will be constructed with low intensity for Target Layer-2 and Target Layer-3.

- the spot size on the sensor plane-2
    – the spot size is smaller than the airy disk for Target Layer-2 which means that the optical design is diffraction limited. So a very good image quality is expected on sensor-2 plane for the second target layer.
    – the spot sizes are bigger for Target Layer-1 and Target Layer-3 and far away from the airy disk which means that blurred images will be constructed with low intensity for Target Layer-1 and Target Layer-3.

- the spot size on the sensor plane-3
    – the spot size is smaller than the airy disk for Target Layer-3 which means that the optical design is diffraction limited. So a very good image quality is expected on sensor-3 plane for the third target layer.
    – the spot sizes are bigger for Target Layer-1 and Target Layer-2 and far away from the airy disk which means that blurred images will be constructed with low intensity for Target Layer-1 and Target Layer-2.

Figure 3-5: The Spot Diagram results of target layers 1,2 and 3 for the Sensor-1, Sensor-2 and Sensor-3 Planes

MTF results of sensor-1, sensor-2 and sesnor-3 planes are given in Figure 3-6 for the first, second and third target layers. For 10 μm pinhole radius, the required spatial frequency in cycles per mm can be calculated as,

$$\# \; of \; Cycles = \frac{1mm}{2 \, . \, pinhole \; diameter} = \frac{1mm}{2 \, . \, 2. \, 10 \mu m} = 25 \qquad (3\text{-}2)$$

In Figure 3-6 MTF results are clearly shows that;

- on the first Target Layer
  - The OTF value of sensor-1 plane is bigger than 0.6 for the first target layer where industrial rule of thumb is 0.5 for a good image quality. So a very good image quality is expected on sensor-1 plane for the first target layer.
  - the OTF values for sensor-2 and sensor-3 planes are almost 0 which means that totally blurred images will be constructed on sensor-2 and sensor-3 planes.

- on the second Target Layer
  - The OTF value of sensor-2 plane is bigger than 0.6 for the second target layer. So a very good image quality is expected on sensor-2 plane for the second target layer.
  - the OTF values for sensor-1 and sensor-3 planes are almost 0 which means that totally blurred images will be constructed on sensor-1 and sensor-3 planes.

- on the third Target Layer
  - The OTF value of sensor-3 plane is bigger than 0.6 for the third target layer. So a very good image quality is expected on sensor-3 plane for the first target layer.
  - the OTF values for sensor-1 and sensor-2 planes are almost 0 which means that totally blurred images will be constructed on sensor-1 and sensor-2 planes.
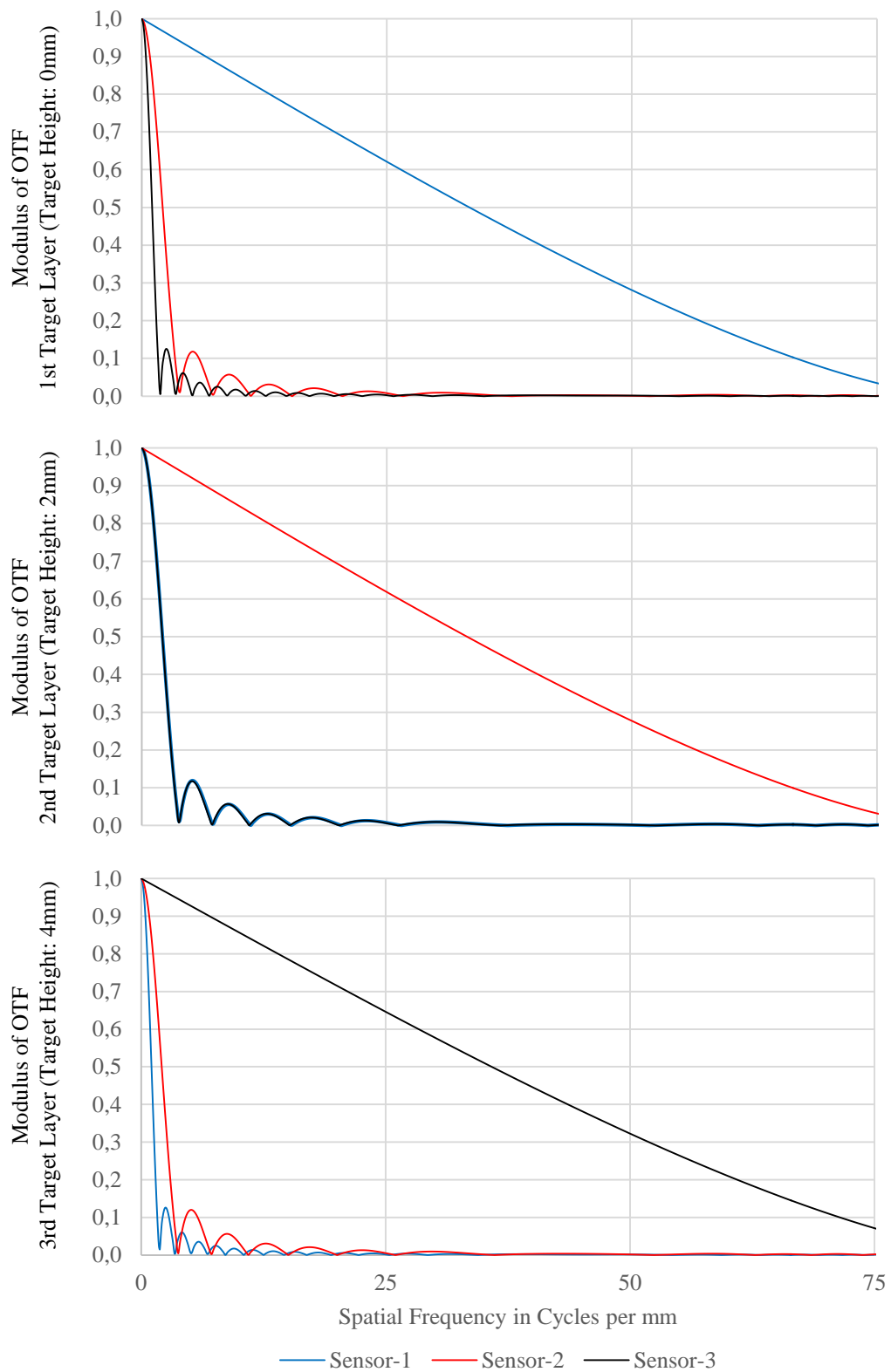
Figure 3-6: The MTF graph on Senor-3 for 496 mm target distance

Encircled Energy diagram results are given in Figure 3-7 for the third target layer at 496 mm distance. It is seen that over than %80 of the optical energy is collected with a 10 μm radius size, where it slowly increases after 10 μm radius size. So pinhole size has been selected as 10 μm for observing the highest intensity changes between the sensor planes for different target layers.
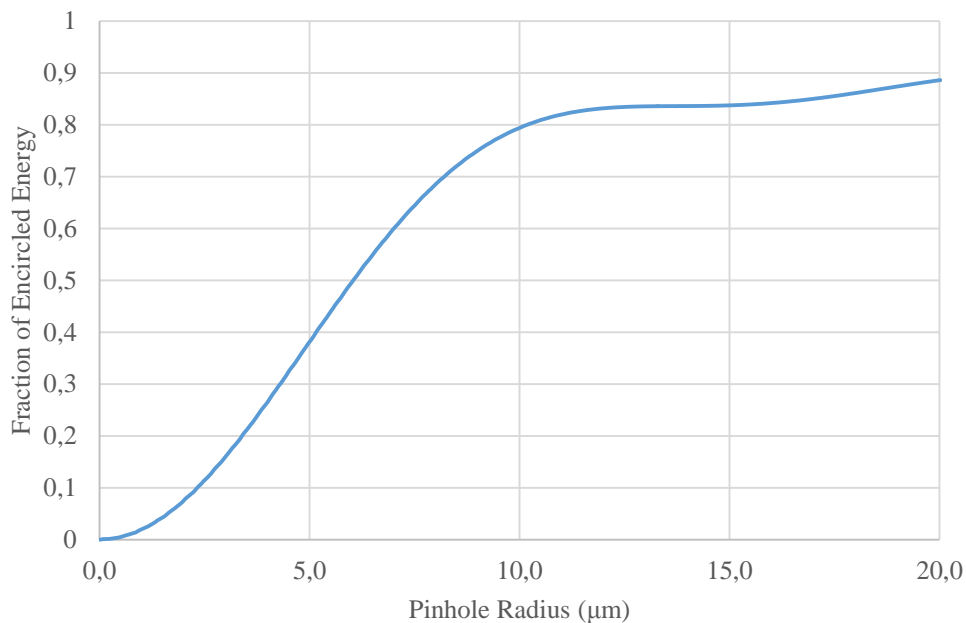
Figure 3-7: The Encircled Energy Diagram on Senor-3 for 496 mm target distance.

3.4   Chapter Discussion

The optical design and Multifocal LIDAR Imaging concept optical results are given and discussed in chapters 3.2and 3.3. In the results, it is seen that for the first target layer at 500 mm, OTF values and spot sizes are good enough for a clear image construction on the sensor-1 plane where OTF values and spot sizes are not good for sensor-2 and sensor-3 planes which means that blurred images are expected on sensor-2 and sensor-3 planes.

Similarly, results show that, for the second target layer at 498 mm OTF values and spot sizes are good enough for a clear image construction on sensor-2, and for the third target layer at 496 mm OTF values and spot sizes are good enough for a clear image construction on sensor-3, OTF values and spot sizes are not good sensor-1 and sensor-2 planes for second target layer OTF values and spot sizes are not good sensor-2 and sensor-3 planes for third target layer.

Also for better representation of the constructed images on different sensor layers for different target layers, geometric image analysis tools are used for further analysis, and the results are given in Figure 3-8 for the first target layer, in Figure 3-9 for the second target layer and Figure 3-10 for third target layer. As expected from the MTF and Spot diagram results of sensor-1, sensor-2, and sensor-3 planes, it is clearly seen that a good image is constructed in the sensor-1 plane for the first target plane where there are only optical noises on sensor-2 and sensor-3 planes as given in Figure 3-8. Similarly, a good image is constructed in the sensor-2 plane for the second target plane where there are only optical noises on sensor-2 and sensor-3 planes as given in Figure 3-9. And finally, a good image is constructed in the sensor-3 plane for the third target plane where there are only optical noises on sensor-2 and sensor-3 planes as given in Figure 3-10.
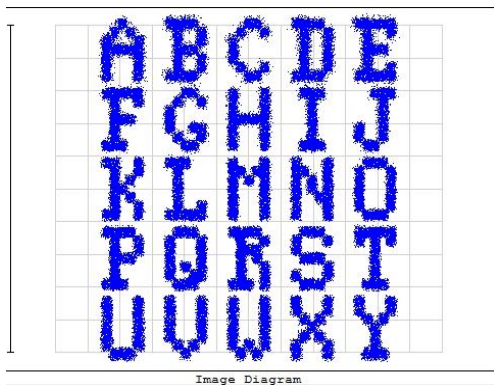
Image diagram at Sensor-1 Plane   Image diagram at Sensor-2 Plane
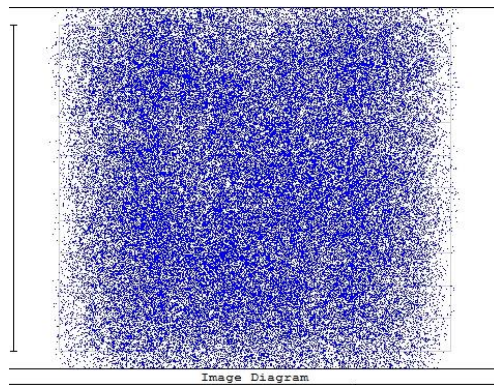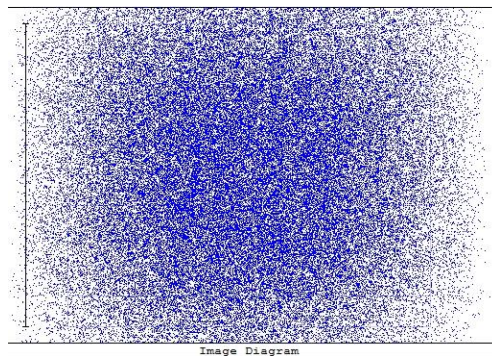
Image diagram at Sensor-3 Plane

Figure 3-8: The Image Diagrams on Sensors for 500 mm target distance
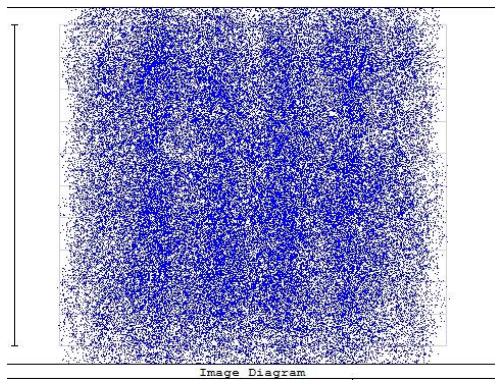
Image diagram at Sensor-1 Plane
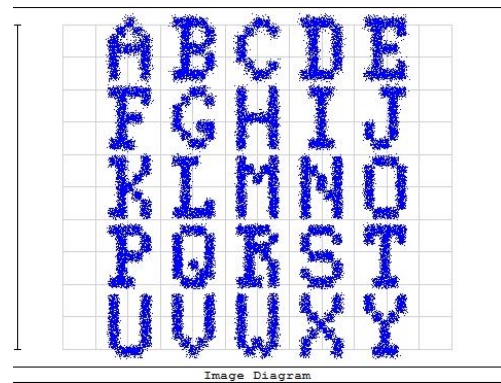
Image diagram at Sensor-2 Plane
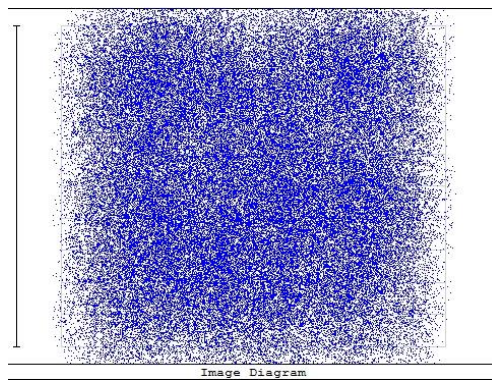
Image diagram at Sensor-3 Plane

Figure 3-9: The Image Diagrams on Sensors for 498 mm target distance.
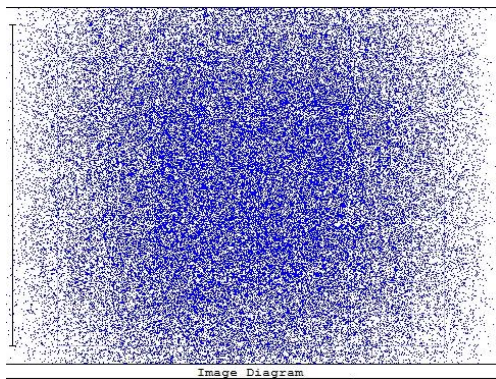
Image diagram at Sensor-1 Plane   Image diagram at Sensor-2 Plane
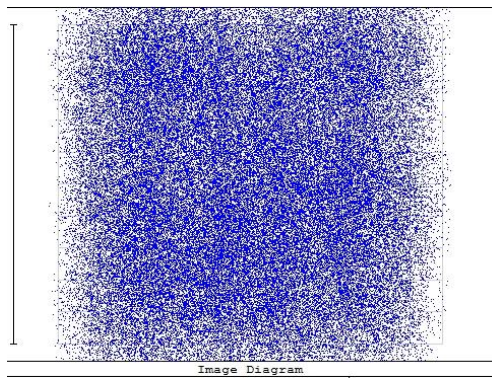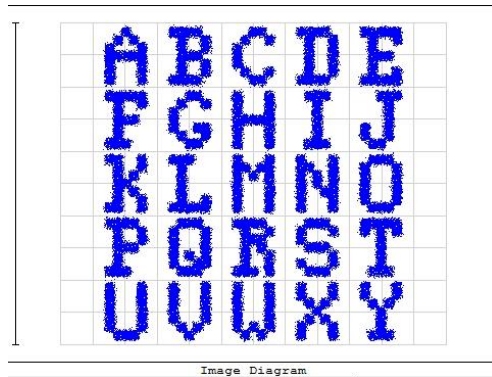
Image diagram at Sensor-3 Plane

Figure 3-10: The Image Diagrams on Sensors for 496 mm target distance.

The relation between the optical layout of the rays, spot sizes for the different target layers, and corresponding height on the target plane is summarized in Figure 3-11. Here, it can be seen that any objects on the target plane are getting focused on the sensor-1 plane, any objects that have 2mm height from the target plane are getting focused on the sensor-2 plane and any objects that have 4mm height from the target plane is getting focused on the sensor-3 plane.
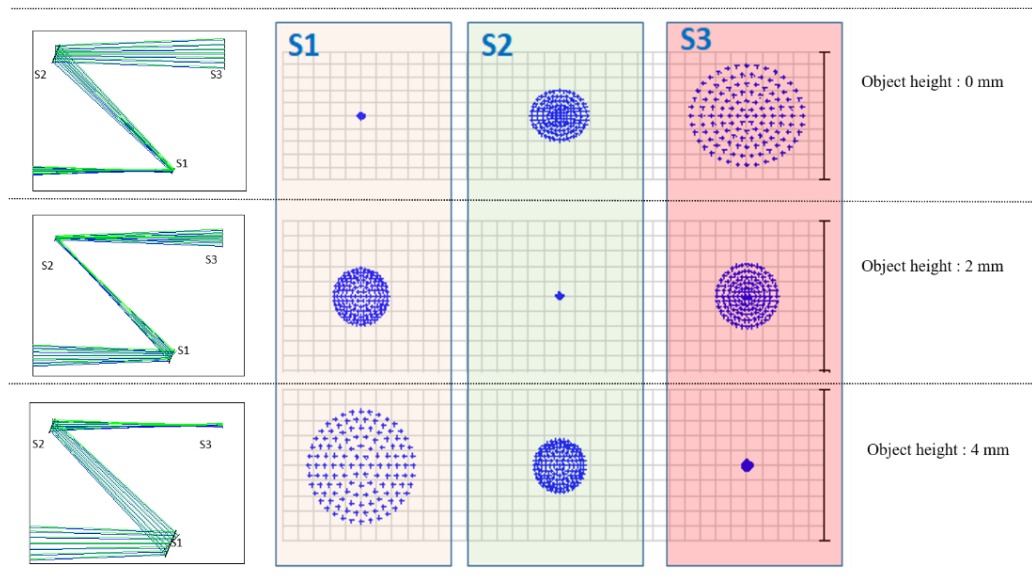
Figure 3-11: The optical paths and spot diagrams for 0, 2 and 4 mm target point heights in Target Plane

For further analysis, the normalized energy levels on each sensor plane are measured by the encircled energy analysis tool of the optical program, for observing the energy changes on the sensor planes regarding different object heights on the target plane. The results of the normalized energy diagram are given in Figure 3-12. It is seen that the concept works for the determined target layers and the energy is collected on the corresponding sensor planes for each 2mm separated target layer. Figure 3-12 shows that not only a clear (not blurred) image is constructed on the corresponding sensor plane, also there will be very low-intensity noise levels on the other sensor planes.
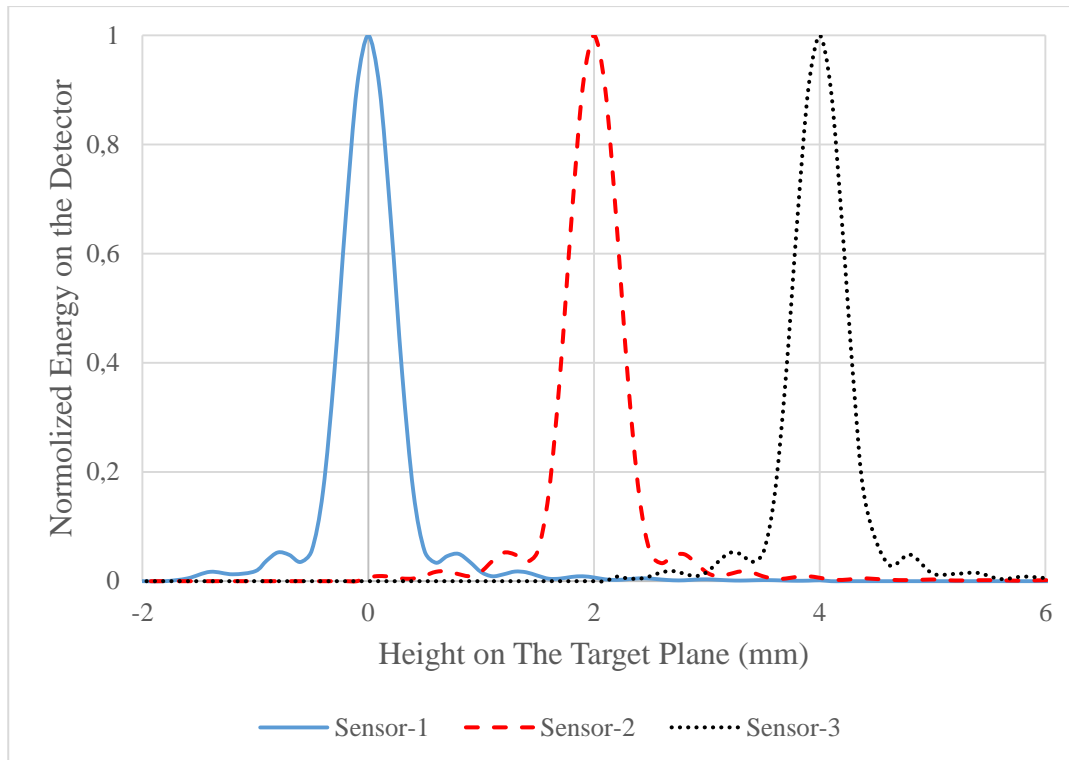
Figure 3-12: The Encircled Energy change on 10,0 µm Pinholes of Sensor-1 (s1), Sensor-2 (s2) and Sensor-3 (s3) via target point heights on the target plane

As the final step of the analysis, a 3D sample is created (Figure 3-13) and the corresponding images on sensor-1, sensor-2, and sensor-3 planes are analyzed for an ideal detector system. In this work, also the constructed optical noise levels on sensor-1 for the second and third target layers are added to the constructed image of the first target layer on sensor-1 to see the effect of the noise levels caused by the other target layers. Similarly, the same work was done for the constructed images on sensor-2 and sensor-3 planes. The constructed images for sensor-1, sensor-2, and sensor-3 planes are given in Figure 3-14, Figure 3-15, and Figure 3-16 respectively.
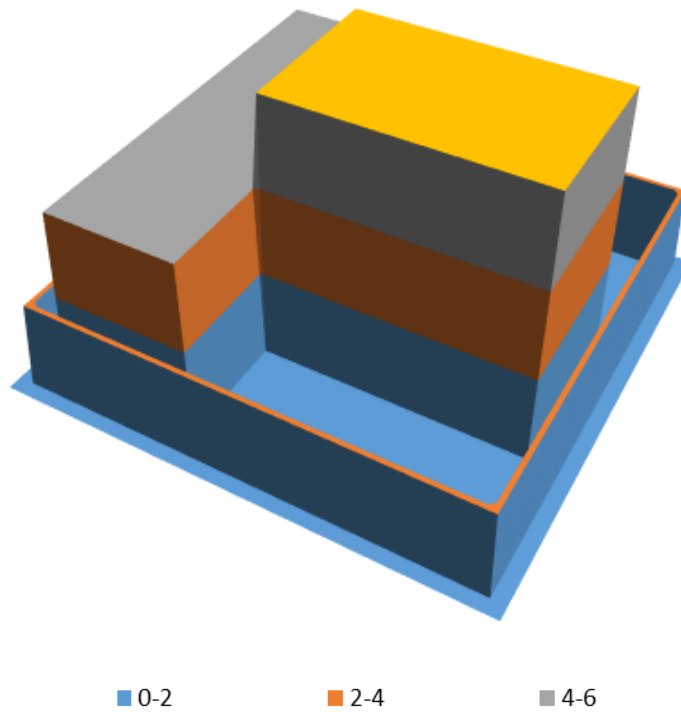
Figure 3-13: The 3D Target Sample for further analysis of Multifocal LIDAR
Imaging System (Each color represents the points in corresponding 2 mm
thickness)
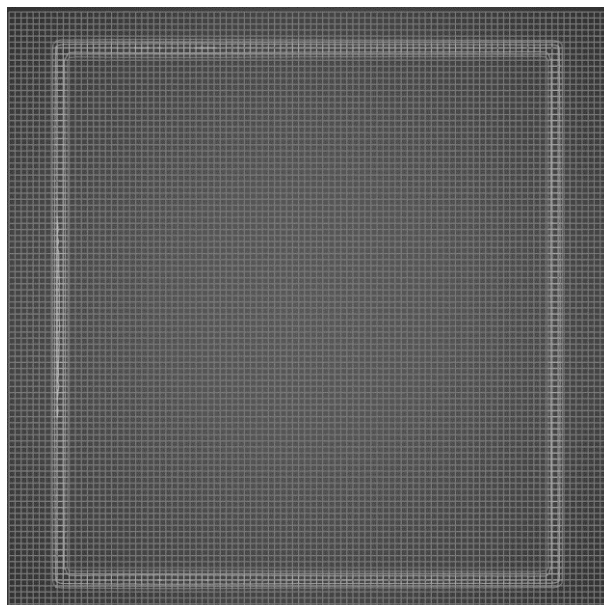
Figure 3-14: The constructed image of the test sample on sensor-1 plane
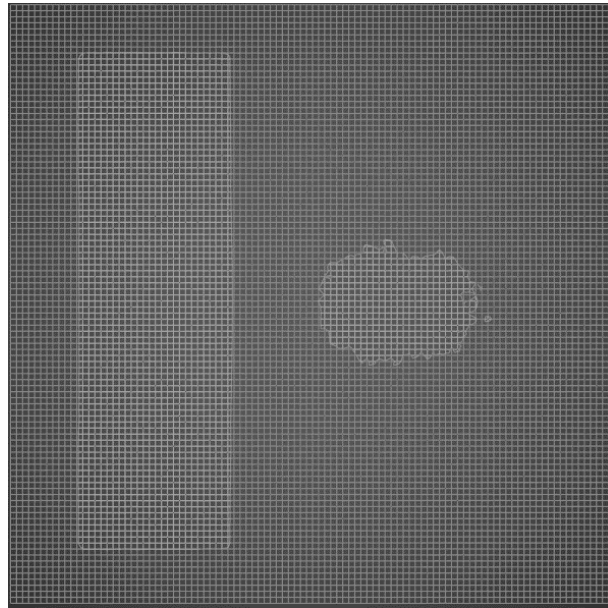
Figure 3-15: The constructed image of the test sample on sensor-2 plane
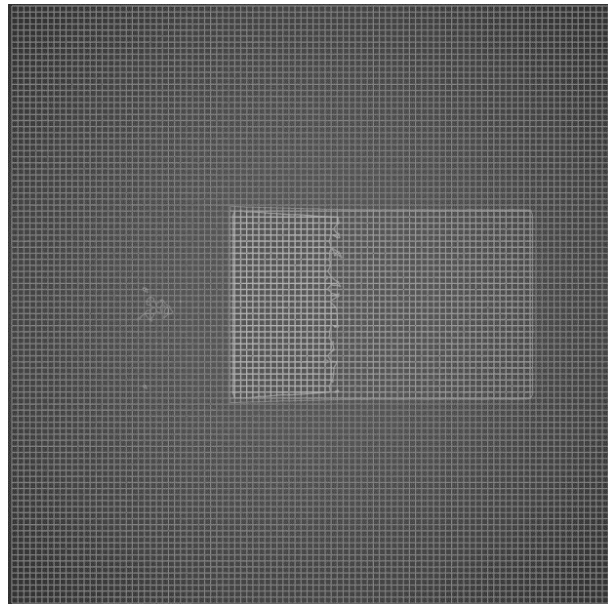
Figure 3-16: The constructed image of the test sample on sensor-3 plane

By combination of the images that constructed in sensor-1, sensor-2 and sensor-3 planes, the 3D image of the sample is achieved as given in Figure 3-17.
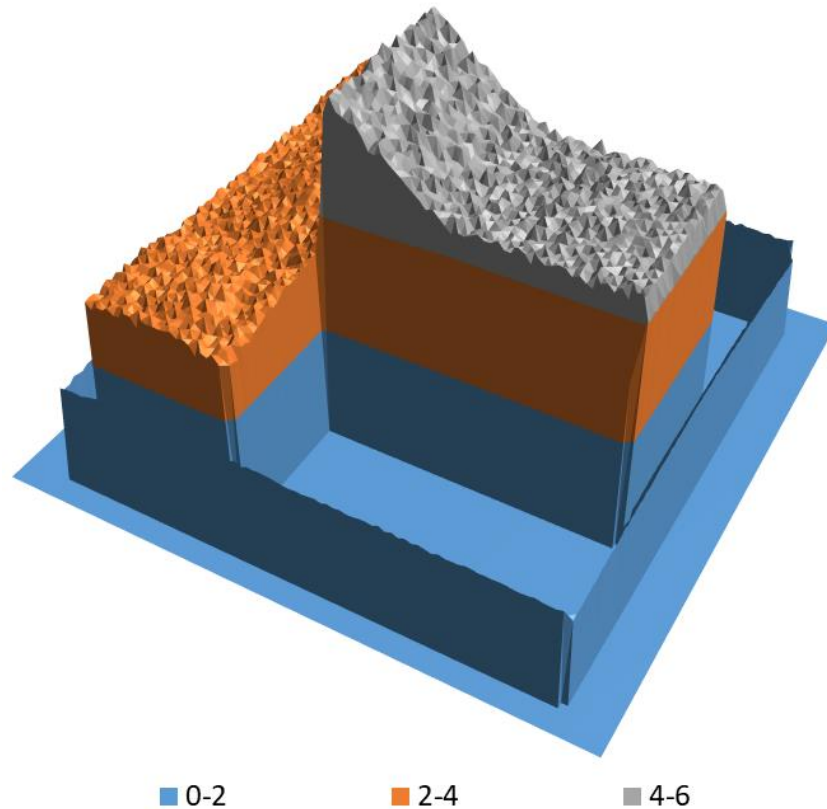
Figure 3-17: The constructed image of the test sample by Multifocal LIDAR Imaging System (Each color represents the points in corresponding 2 mm thickness)

In the conclusion of this chapter, the Multifocal LIDAR Imaging System basic design has been introduced, designed and the detailed analysis results are discussed. The results are showing that the concept of the Multifocal LIDAR Imaging System is working and introduce idea has been proven with the results of the sample images.

CHAPTER 4

USING CHROMATIC ABERRATION TO ENHANCE THE MULTIFOCAL LIDAR IMAGING SYSTEM PACKAGING

In chapter 3, the proof of concept has been shown for the newly introduced Multifocal LIDAR Imaging System. Although a relay lens system is designed with a high focal length, for proof of concept study, the distances between the sensor planes are found as 4.5 mm which brings packaging limitations to the system design. Especially for the lower focal length distances that can be discussed as an important limitation for the productibility. For enhancing the packaging and productibility of the system, a chromatic system is introduced to enlarge the distances between the sensor planes of the Multifocal LIDAR System and Chromatic Multifocal LIDAR System is developed.
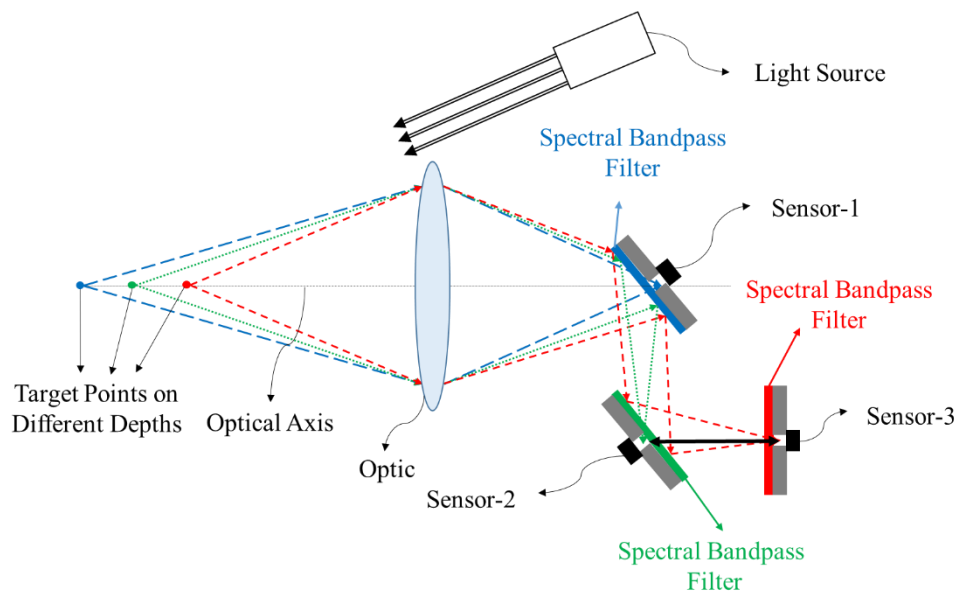
Figure 4-1: The schematic representation of the Chromatic Multifocal LIDAR Imaging system

As opposed to common optical designs, the optical design has been optimized for getting higher chromatic aberrations in the image plane in this study. The increased chromatic aberrations are used to enlarge the distances between the sensor planes. The basic schematic of the proposed enhancement is given in Figure 4-1.

Similarly, in chapter 3, the pulse is transmitted to the target with the help of the controlled light source and the time difference between the transmitted and received pulse is measured for calculation of the target distance D with the equation (1-6). After the reference target distance D is calculated by the direct ToF technique, the images taken by the sensor-1, sensor-2, and sensor-3 are used for the measurement of different depth layers on the Target plane by the multifocal technique. As described in Figure 4-1, the red layer (closer one) is getting focused on the sensor-3 plane where the green layer is getting focused on the sensor-2 layer and the blue layer (far one) is getting focused on the sensor-1 plane. The places of the sensors are fixed in the image plane, so the distances between the layers are known. The results are compared with the design in detailed chapter 3, to see the level of enhancement. For this purpose, again 50 cm target range is studied with a high focal distance objective relay system.

4.1   Design Criteria

For observing the enhancements, it is aimed at the same well-distinguished depth layers on the target plane with 2 mm depth differences with the same design parameters as chapter 3. During chromatic optimization of the optical design for getting a high chromatic aberration, the clear aperture of the new system has been decreased to 40 mm as a difference from chapter 3, which increases the depth of field slightly. The working wavelengths are selected as 450 nm (blue), 550 nm (green), and 650 nm (red). The 450 nm wavelength is assigned for the first target layer (500 mm distance), 550 nm wavelength is assigned for the second target layer (498 mm

distance) and 650 nm wavelength is assigned for the third target layer (496 mm distance). The basic design inputs of the system are given in Table 4.1.

Table 4.1 The Design Inputs for Chromatic Multifocal LIDAR Imaging Optic System

Parameter	Design Data
Target Distance	0.5 m
Clear Aperture	40 mm
Working wavelengths	450 nm, 550 nm and 650 nm

4.2   Optical Design

A basic relay optic is designed for chromatic concept study. The optical layout of the designed system is given in Figure 4-2.
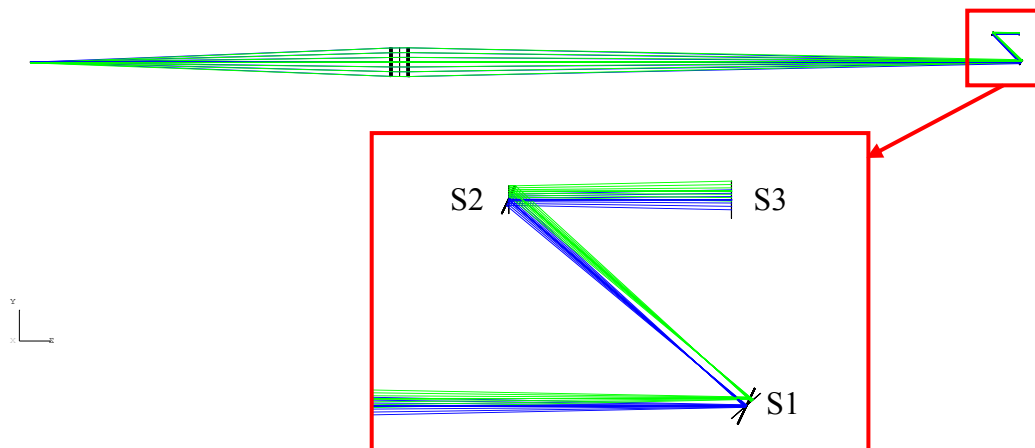
Figure 4-2: The optical design layout of Chromatic Multifocal LIDAR Imaging system.

3 sensors are located in the image plane with the help of reflective mirrors for different depth imaging as given in Figure 4-3 which is a zoomed part of the image plane. The relay system is designed and optimized for 500 mm target distance for 450 nm wavelength and better image quality in the image plane on sensor-1, and sensor-1 is placed on the optimized point in the image plane. The first reflective mirror is placed and then the relay system is optimized for 498 mm target distance for 550 nm wavelength and better image quality in the image plane on sensor-2, and sensor-2 is placed on the optimized point in the image plane. Finally, the second reflective mirror is placed and the relay system is optimized for 496 mm target distance for 650 nm wavelength and better image quality in the image plane on sensor-3, and sensor-3 is placed on the optimized point in the image plane. It is seen that the distances between the optimized points for sensor-1, sensor-2, and sensor-3 planes have been increased as aimed. The old distances and the new distances are given in Table 4.2
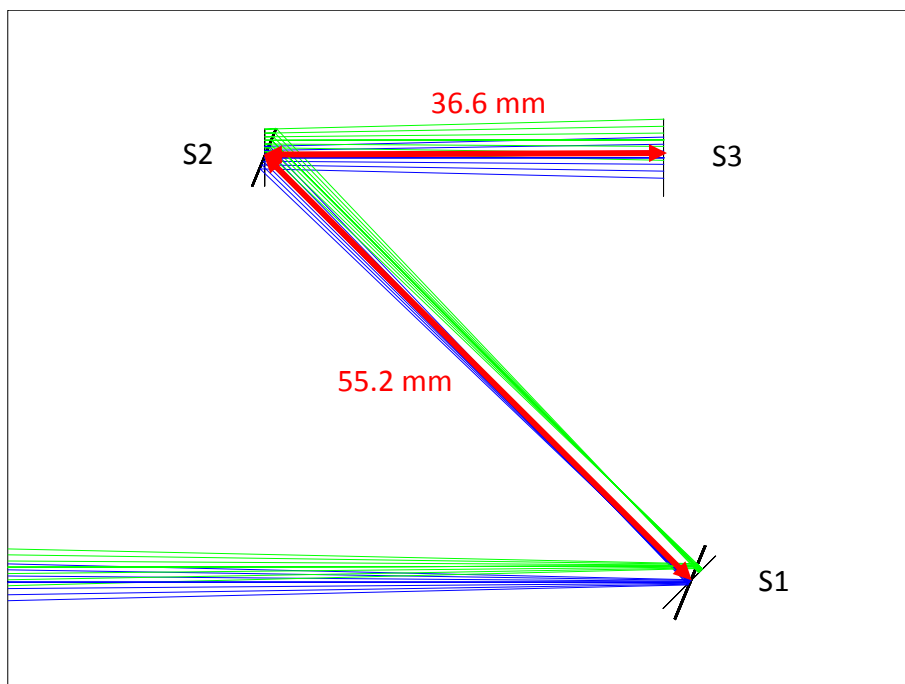
Figure 4-3: The sensor locations layout of new introduced Chromatic Multifocal LIDAR Imaging system.

Table 4.2 The Increased Sensor Plane Distances with the Chromatic Enhancement

Related Sensors Planes	Multifocal LIDAR Imaging System Distances	Chromatic Multifocal LIDAR Imaging System Distances
Distance between S1 and S2	4.5 mm	55.2 mm
Distance Between S2 and S3	4.5 mm	36.6 mm

The spot diagrams and encircled energies have been checked for each sensor plane and 496 mm, 498 mm, 500 mm target distances, to discuss the image quality of the system and further analysis. The design results of the system 496 mm target distance and for 650 nm wavelength condition are given in Table 4.3. The pinhole radius of the system is taken as the same in chapter 3 which is 10 µm. The IFOV is calculated by using equation (2-5) as,

$$\frac{IFOV}{2} = \tan^{-1}\frac{10 \ \mu m}{320mm} = 0.0018º \tag{4-1}$$

Table 4.3 The Design Outputs of Chromatic Multifocal LIDAR Imaging Optical System

Parameter	Design Data
Effective Focal Length (f)	320 mm
Pinhole Radius	10 µm
Calculated Depth of Field	~0.78 mm
Calculated Hyperfocal Distance	640 m
IFOV	0.0036º ~ 0.03 mm

4.3   Results

The optical layout results of different target layers for different wavelengths are given in Figure 4-4. In Figure 4-4, it is seen that:

- *For the first target layer at a distance of 500 mm*, the target image is constructed on Sensor-1. In this condition, the 450 nm rays are in a good in-focus condition on sensor-1, and the reflected parts of the 450 nm rays from the pinhole mirror of the sensor-1 continue their ways but they will not be able to be detected by sensor-2 and sensor-3 because of the spectral band filters on the sensor-2 and sensor 3 planes.

- *For the second target layer at a distance of 498 mm,* the target image is constructed on Sensor-2. In this condition the 550 nm rays are in the out-of-focus condition on sensor-1, they are also reflected by the spectral filter on the sensor-1 plane and so there will be no constructed image in the sensor-1 plane for 550 nm wavelength. Similarly, the 550 nm rays are in out-of-focus condition on sensor-3, there will be no constructed image in the sensor-3 plane for 550 nm wavelength because of the spectral bandpass filter.

- *For the third target layer at a distance of 496 mm,* the target image is constructed on Sensor-3. In this condition, the 650 nm rays are in a good in-focus condition on sensor-3, and 650 nm rays are in the out-of-focus condition on sensor-1 and sensor-2. 650 nm rays are also totally reflected by the spectral filters on sensor-1 and sensor-2 planes so there will be no constructed image in sensor-1 and sensor-2 planes for 650 nm wavelength.
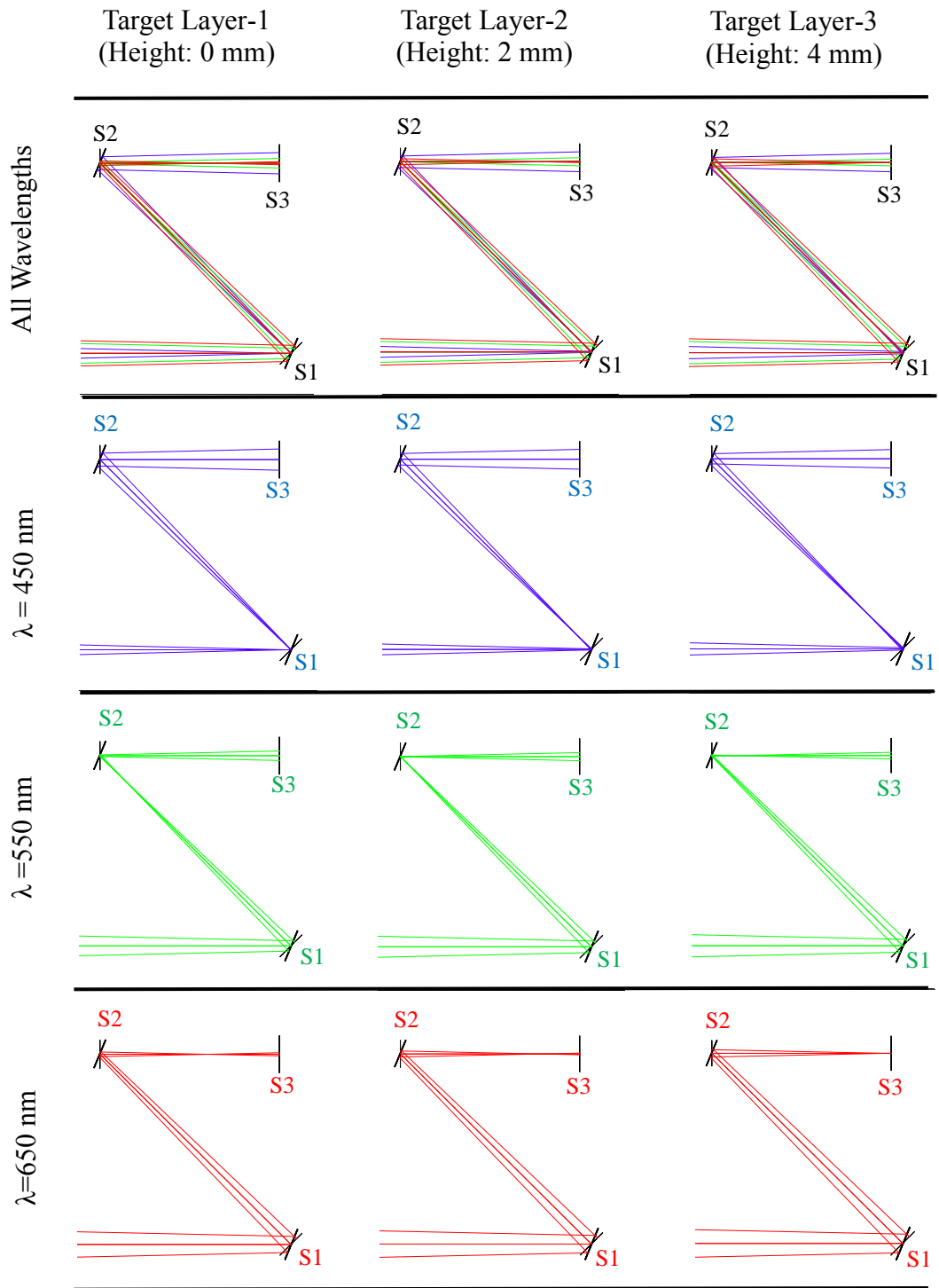
Figure 4-4: The optical layout results of target layers 1,2 and 3 for the 450 nm, 550 nm and 650 nm wavelengths

The spot diagrams on each sensor plane for each target layer are worked below for analyzing the results. Because of the spectral bandpass filters, only 450 nm wavelength is studied on Sensor-1, only 550 nm wavelength is studied on Sensor-2 and only 650 nm wavelength is studied on Sensor-3 planes. The spot diagram results on each sensor plane for each target layer are given in Figure 4-5. The scaling of the each spot diagram is given above the related one. In Figure 4-5, it is seen that;

- on the sensor plane-1
  - the spot size is close to the airy disk for Target Layer-1 which means that the optical design is close to the diffraction limit which is enough for us to construct a good image.
  - the spot sizes are bigger for Target Layer-2 and Target Layer-3 and far away from the airy disk which means that blurred images will be constructed with low intensity for Target Layer-2 and Target Layer-3.

- the spot size on the sensor plane-2
  - the spot size is close to the airy disk for Target Layer-2 which means that the optical design is close to the diffraction limit which is enough for us to construct a good image.
  - the spot sizes are bigger for Target Layer-1 and Target Layer-3 and far away from the airy disk which means that blurred images will be constructed with low intensity for Target Layer-1 and Target Layer-3.

- the spot size on the sensor plane-3
  - the spot size is close to the airy disk for Target Layer-3 which means that the optical design is close to the diffraction limit which is enough for us to construct a good image.
  - the spot sizes are bigger for Target Layer-1 and Target Layer-2 and far away from the airy disk which means that blurred images will be constructed with low intensity for Target Layer-1 and Target Layer-2.

Figure 4-5: The Spot Diagram results of target layers 1,2 and 3 for the Sensor-1 (450 nm), Sensor-2 (550 nm) and Sensor-3 (650 nm)

Spot diagram results of sensor-1 for all wavelengths are given in Figure 4-6 for the third first target layer at 500 mm distance It is seen that the spot size for 450 nm on the sensor plane is close to the airy disk where 550 nm and 650 nm spot sizes are much bigger which shows the chromatic effect on the sensor-1 plane.
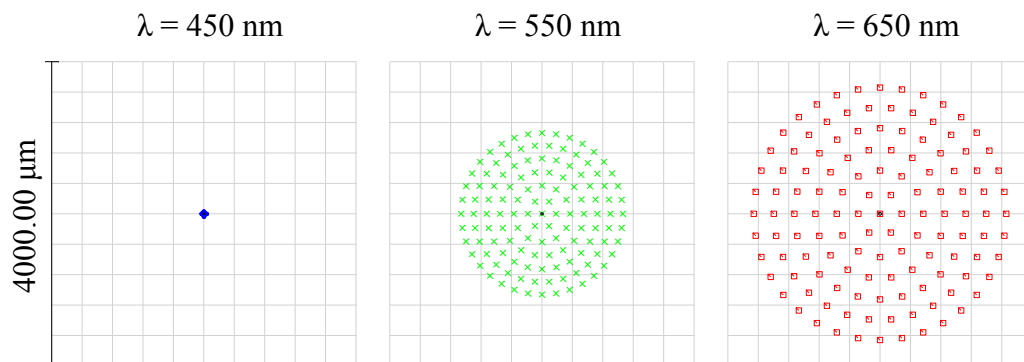
Figure 4-6: The Spot Diagram on Senor-1 plane for different wavelengths and for 500 mm target distance

Similarly, spot diagram results are given of sensor-2 plane for the second target layer in Figure 4-7 and sensor-3 plane for the third target layer in Figure 4-8. The sensor-2 plane and sensor-3 plane results also shows the chromatic effects clearly.
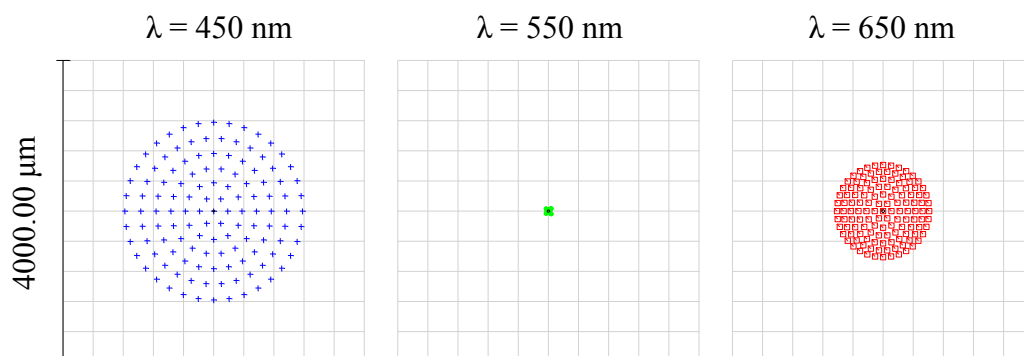
Figure 4-7: The Spot Diagram on Senor-2 plane for different wavelengths and for 498 mm target distance
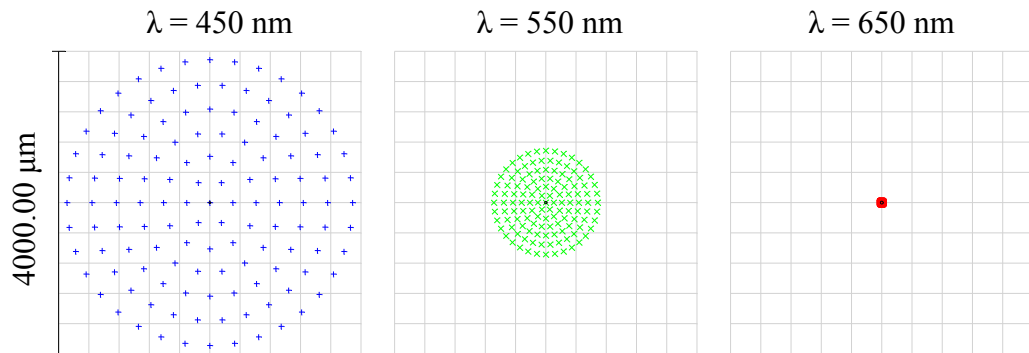
Figure 4-8: The Spot Diagram on Senor-3 plane for different wavelengths and for 496 mm target distance

4.4   Chapter Discussion

As discussed in chapter 4.2, the distance between the sensor-1 and sensor-2 planes has been increased from 4.5 mm to 55.2 mm, and the distance between the sensor-2 and sensor-3 planes has been increased from 4.5 mm to 36.6 mm by using chromatic aberrations as a design tool. The chromatic optical design and multifocal imaging cases results are also checked and discussed in chapter 4.3 for Chromatic Multifocal LIDAR System, and shows that Multifocal LIDAR Technique is also working well with chromatic enhancement.

The chromatic aberration is also checked via the optical design program's analysis tools and it is found that chromatic focal shift on the sensor-3 plane is around 55 mm between 450 nm and 550 nm rays and around 35 mm between 550 and 650 nm rays as expected from the distance enhancements that measured in chapter 4.2. The chromatic focal shift on the sensor-3 plane is given in Figure 4-9
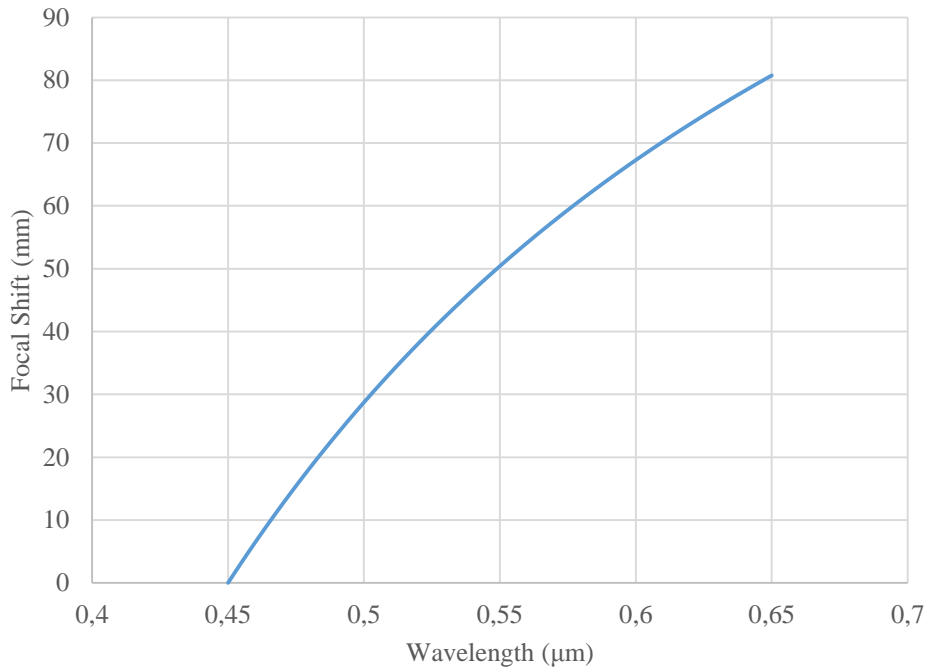
Figure 4-9: The Chromatic Focal Shift Diagram on Sensor-3 plane

In the results, it is seen that for the first target layer at 500 mm spot sizes are good enough for a clear image construction on sensor-1 plane where spot sizes are not good sensor-2 and sensor-3 planes which means that blurred images are expected on sensor-2 and sensor-3 planes.

Similarly, results show that for the second target layer at 498 mm and spot sizes are good enough for a clear image construction on sensor-2, and spot sizes are good enough for a clear image construction on sensor-3 for the third target layer at 496 mm. Spot sizes are not good on sensor-1 and sensor-2 planes for the second target layer and not good on sensor-2 and sensor-3 planes for the third target layer.

Also for better representation of the constructed images on different sensor layers for different target layers, geometric image analysis tools are used for further analysis, and the results are given in Figure 4-9 for the first target layer,

As expected from the Spot diagram results of sensor-1, sensor-2, and sensor-3 planes, it is clearly seen that a good image is constructed in the sensor-1 plane for the first target plane at 450 nm wavelength where there are only optical noises, which will be reflected by the spectral Bandpass filter, for the 550 nm and 650 nm wavelengths. Also, there are only optical noises on sensor-2 and sensor-3 planes for all wavelengths as given in Figure 4-10.

Similarly, a good image is constructed in the sensor-2 plane for the second target plane and 550 nm wavelength where there are only optical noises, which will be reflected by the spectral Bandpass filter, for the 450 nm and 650 nm wavelengths. Also, there are only optical noises on sensor-1 and sensor-3 planes for all wavelengths as given in Figure 4-11.

And finally, a good image is constructed in the sensor-3 plane for the third target plane and 650 nm wavelength where there are only optical noises, which will be reflected by the spectral Bandpass filter, for the 450 nm and 550 nm wavelengths. It is seen that there are only optical noises on sensor-1 and sensor-2 planes for all wavelengths as given in Figure 4-12.

Image diagram at
Sensor-1 Plane
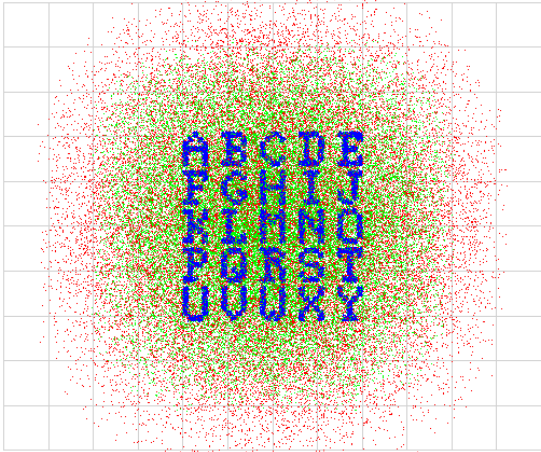
Image diagram at
Sensor-2 Plane
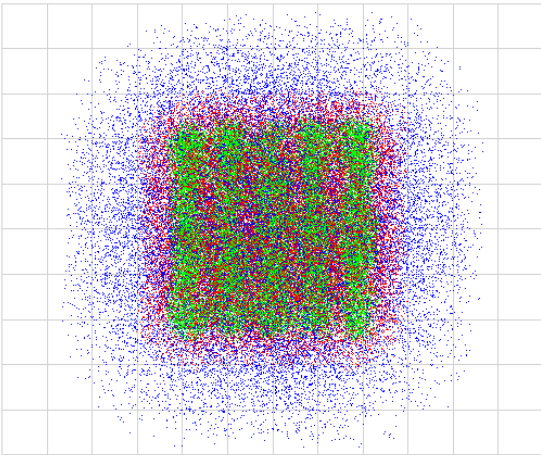
Image diagram at
Sensor-3 Plane
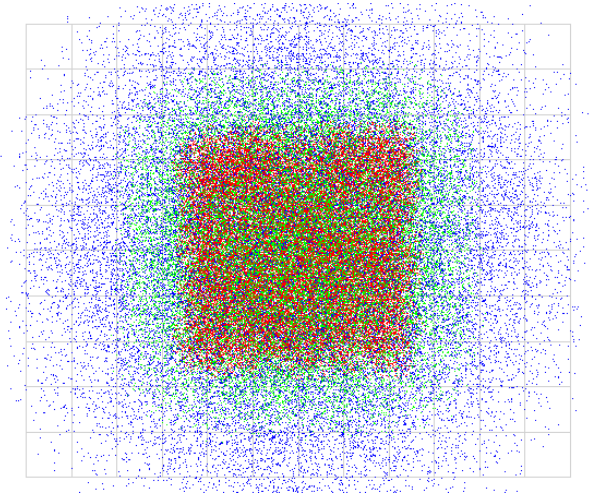
Figure 4-10: The Image Diagrams on Sensors for all wavelengths and 500 mm
target distance

Image diagram at
Sensor-1 Plane
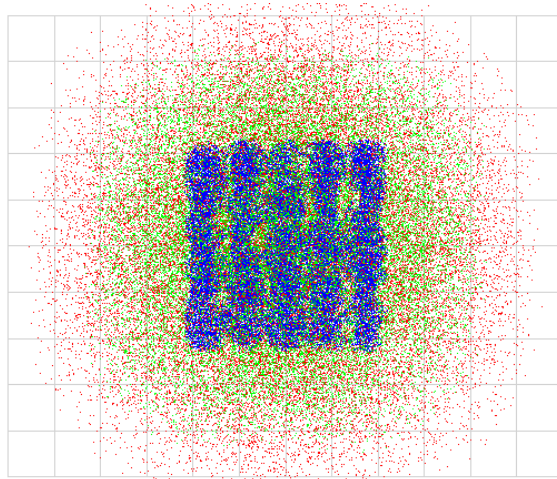
Image diagram at
Sensor-2 Plane
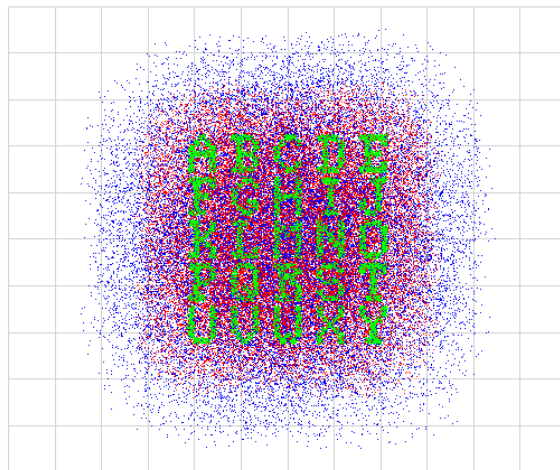
Image diagram at
Sensor-3 Plane
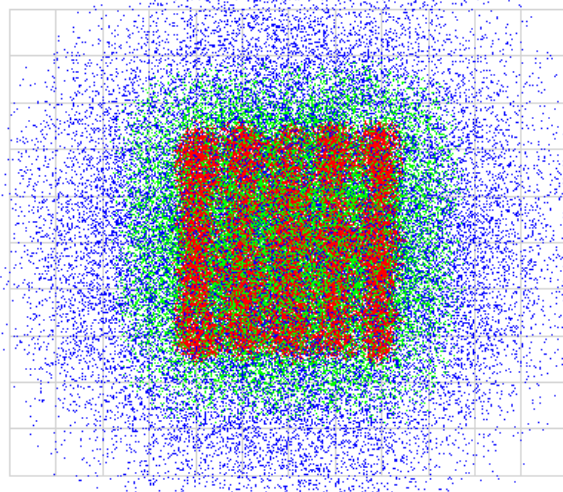
Figure 4-11: The Image Diagrams on Sensors for all wavelengths and 498 mm
target distance

Image diagram at
Sensor-1 Plane
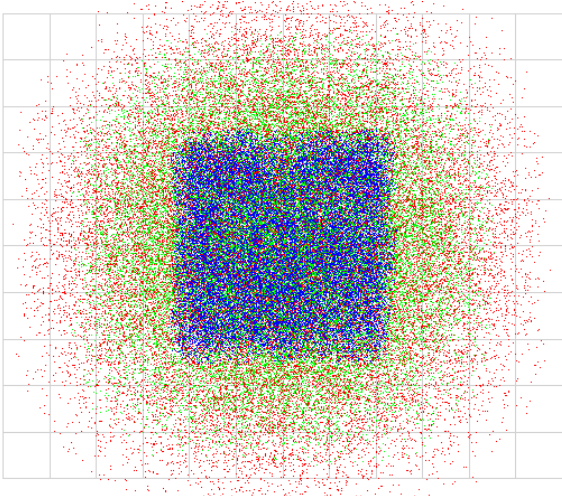
Image diagram at
Sensor-2 Plane
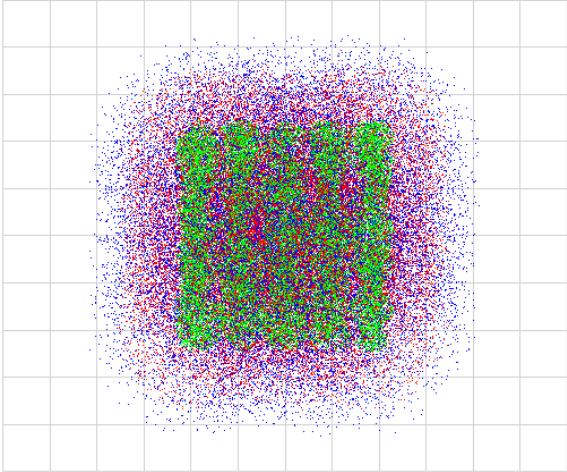
Image diagram at
Sensor-3 Plane
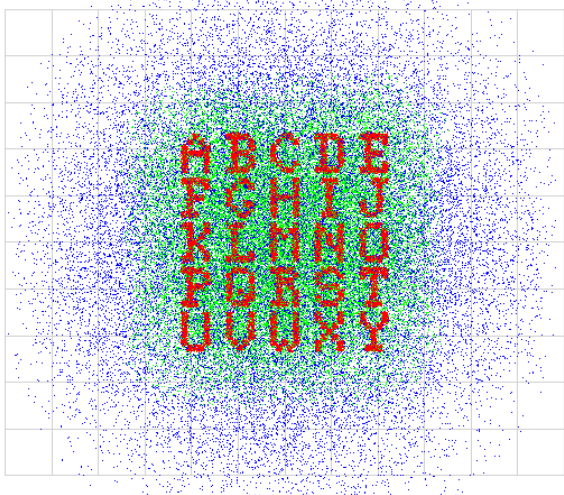
Figure 4-12: The Image Diagrams on Sensors for all wavelengths and 496 mm
target distance

For further analysis, the normalized energy levels for the relevant wavelength, regarding the spectral filters that are placed in front of the sensors (such as 450 nm on sensor-1, 550 nm on sensor-2, and 650 nm on sensor-3), on the sensor planes are measured by the encircled energy analysis tool of the optical program, for observing the energy changes on the sensor planes regarding different object heights on the target plane. The results of the normalized energy diagram are given in Figure 4-13. It is seen that the concept still works for the determined target layers and the energy is collected on the corresponding sensor planes for each 2mm separated target layer after packaging enhancement by the chromatic aberrations.
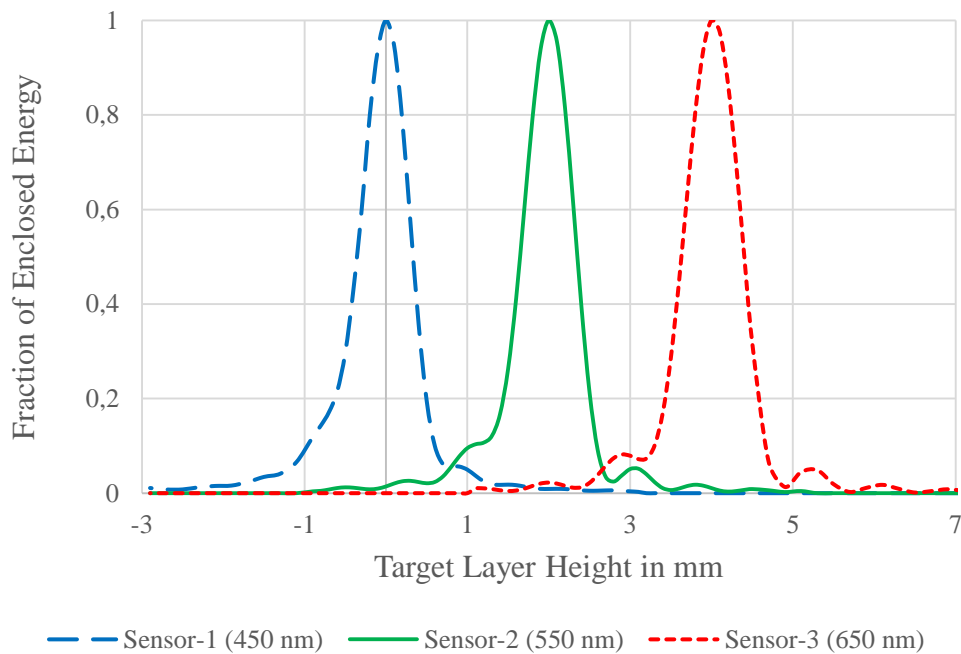
Figure 4-13: The Encircled Energy change on 10 µm Pinholes of Sensor-1 (for 450 nm), Sensor-2 (for 550 nm) and Sensor-3 (for 650 nm) via target point heights on the target plane

As the final step of the analysis, the 3D sample is used (Figure 3-13) to analyze corresponding images on sensor-1, sensor-2, and sensor-3 planes, for an ideal

detector system. In this work, also the constructed optical noise levels on sensor-1 for the second and third target layers are added to the constructed image of the first target layer on sensor-1 to see the effect of the noise levels caused by the other target layers. Similarly, the same work was done for the constructed images on sensor-2 and sensor-3 planes. The constructed images for sensor-1, sensor-2, and sensor-3 planes are given in Figure 4-14, Figure 4-15, and Figure 4-16 respectively.
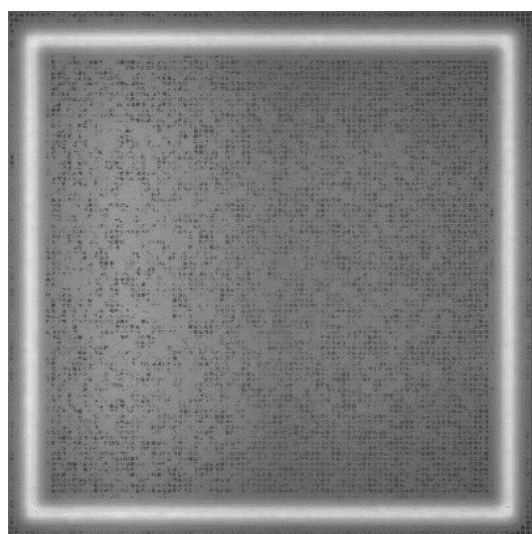
Figure 4-14: The constructed image of the test sample on sensor-1 plane
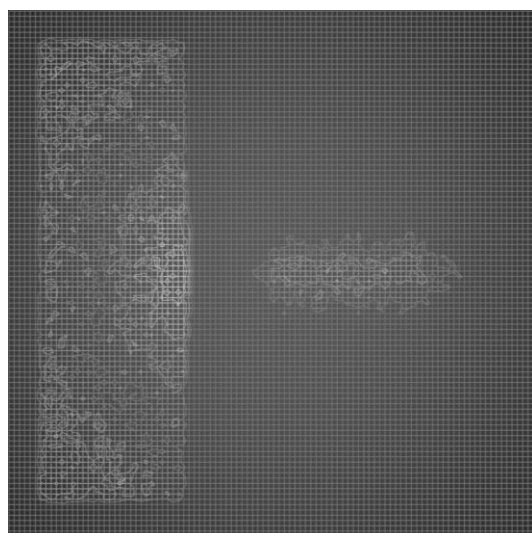
Figure 4-15: The constructed image of the test sample on sensor-2 plane
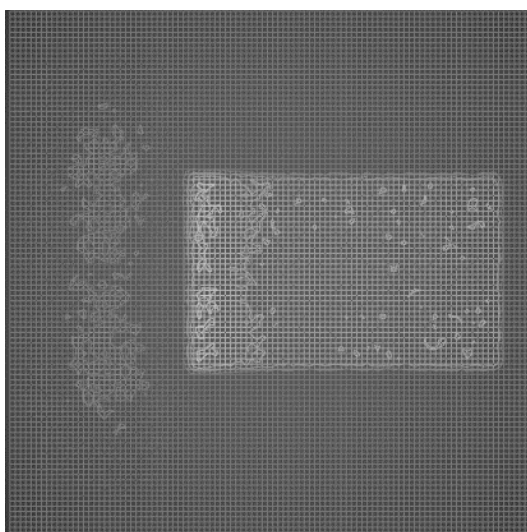
Figure 4-16: The constructed image of the test sample on sensor-3 plane

By combination of the images that constructed in sensor-1, sensor-2 and sensor-3 planes, the 3D image of the sample is achieved as given in Figure 4-17.
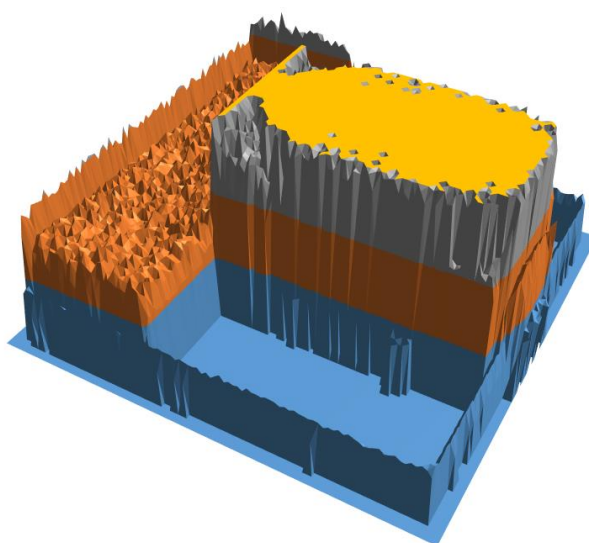
■ 0-2   ■ 2-4   ■ 4-6

Figure 4-17: The constructed image of the test sample (Each color represents the points in corresponding 2 mm thickness)

In the conclusion of this chapter, the Chromatic Multifocal LIDAR Imaging System basic design has been introduced, designed and the detailed analysis results are discussed. The results are showing that the concept of the Chromatic Multifocal LIDAR Imaging System is working and can be used for enlarging the distances between the sensors for enhancing the packaging.

CHAPTER 5

USING DISPERSIVE MEDIA TO ENHANCE THE SYSTEM

In chapter 4, it has also been proven that chromatic aberration can be used as a tool to enhance the packaging by increasing the distances between the sensors for Multifocal LIDAR Imaging System. Although the distances between the sensor planes are increased by the chromatic aberration in chapter 4, there is still a good alignment requirement for the detectors that are placed on the same optical axis. In this chapter, we aimed to separate the optical axis's for the different wavelengths to enable using a linear array in a single plane to distinguish the different wavelengths and so different depth layers on the target plane.
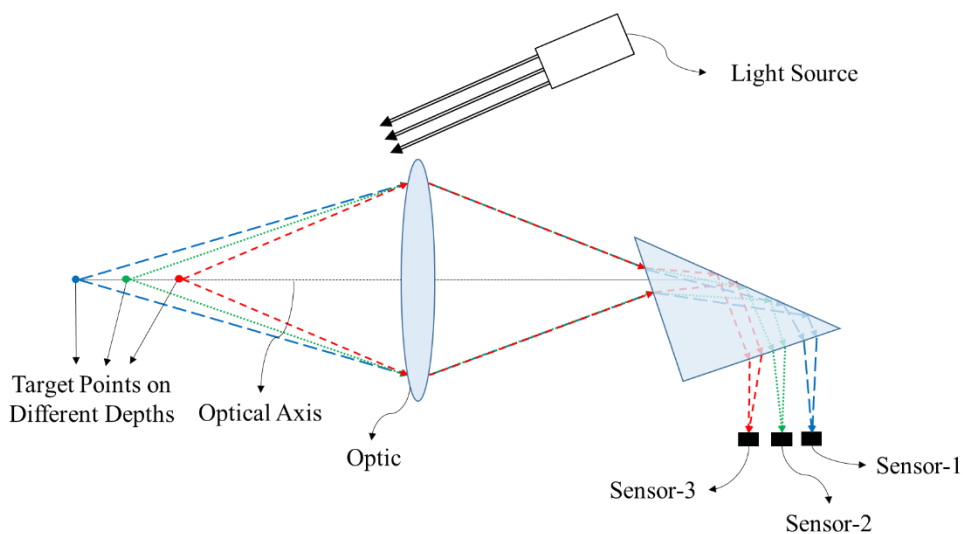
Figure 5-1: The schematic representation of the Chromatic Multifocal LIDAR Imaging system with dispersion prism

Again, similar to in chapter 4, the optical design has been optimized for getting higher chromatic aberrations in the image plane and these chromatic aberrations are used to enlarge the distances between the sensors on the linear array. The basic schematic of the proposed enhancement of the introduced Chromatic Multifocal LIDAR Imaging system with dispersion prism is given in Figure 5-1.

Similarly in chapter 3 and chapter 4, the pulse is transmitted to the target with the help of the controlled light source and the time difference between the transmitted and received pulse is measured for calculation of the target distance D with the equation (1-6). After the reference target distance D is calculated by the direct ToF technique, the images taken by the sensor-1, sensor-2, and sensor-3 are used for the measurement of different depth layers on the Target plane by the multifocal technique. As described in Figure 5-1, the red layer (closer one) is getting focused on the sensor-3 plane where the green layer is getting focused on the sensor-2 layer and the blue layer (far one) is getting focused on the sensor-1 plane. The sensors are at the same height on the linear array, so the distances between the layers are known.

5.1   Design Criteria

The basic design inputs of the system is given in Table 5.1.

Table 5.1 The Design Inputs for Chromatic Multifocal LIDAR Imaging System with Dispersion Prism

Parameter	Design Data
Target Distance	0.5 m
Clear Aperture	35 mm
Working wavelengths	450 nm, 550 nm and 650 nm

For proof of concept, it is aimed to have well-distinguished depth layers on the target plane. The working wavelengths are selected as 450 nm (blue), 550 nm (green), and 650 nm (red). The 450 nm wavelength is assigned for the first target layer, 550 nm wavelength is assigned for the second target layer and 650 nm wavelength is assigned for the third target layer.

5.2   Optical Design

A basic relay optical system with a dispersion prism is designed. The optical layout of the designed system is given in Figure 5-2.
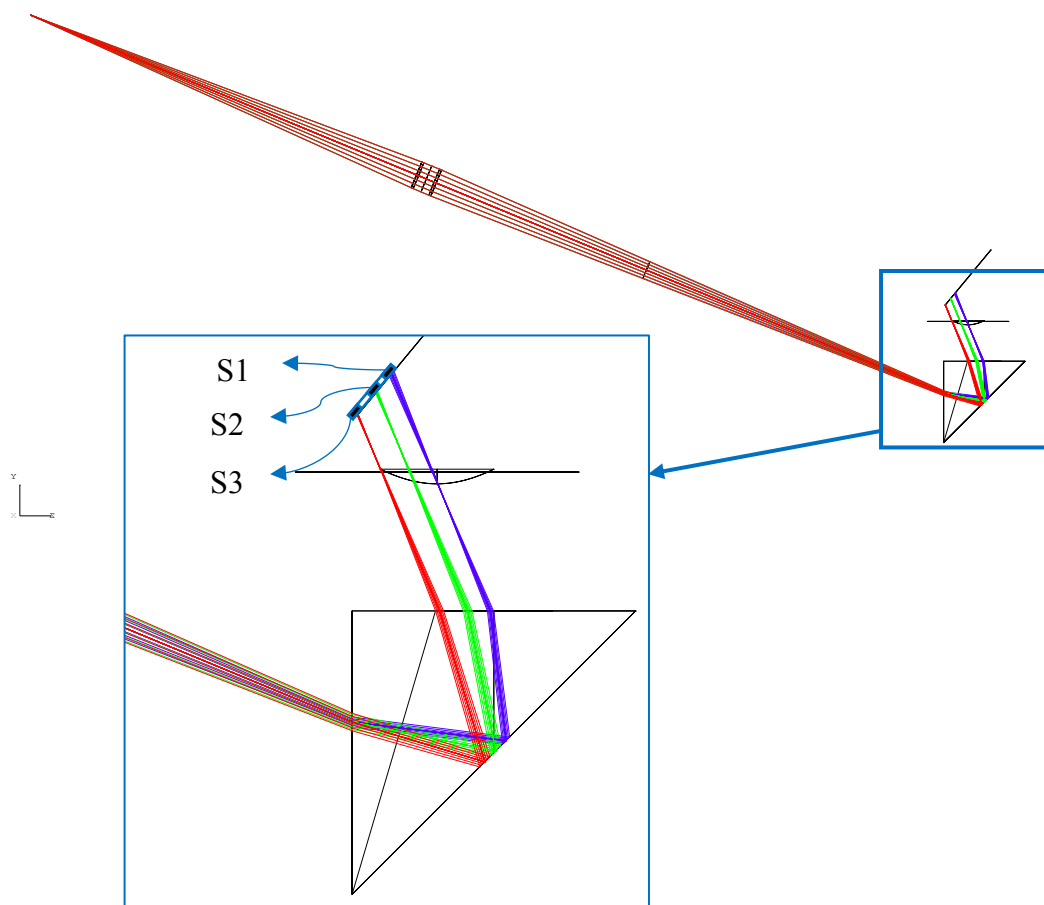
Figure 5-2: The optical design layout of Chromatic Multifocal LIDAR Imaging System with dispersion prism.

The optical paths of rays are dispersed for the 450 nm, 550 nm, and 650 nm wavelengths, with the help of a dispersion prism, and collected on 3 sensors which are located on a linear array. The sensor locations are given in Figure 5-3 with a detailed optical layout dispersing prism.
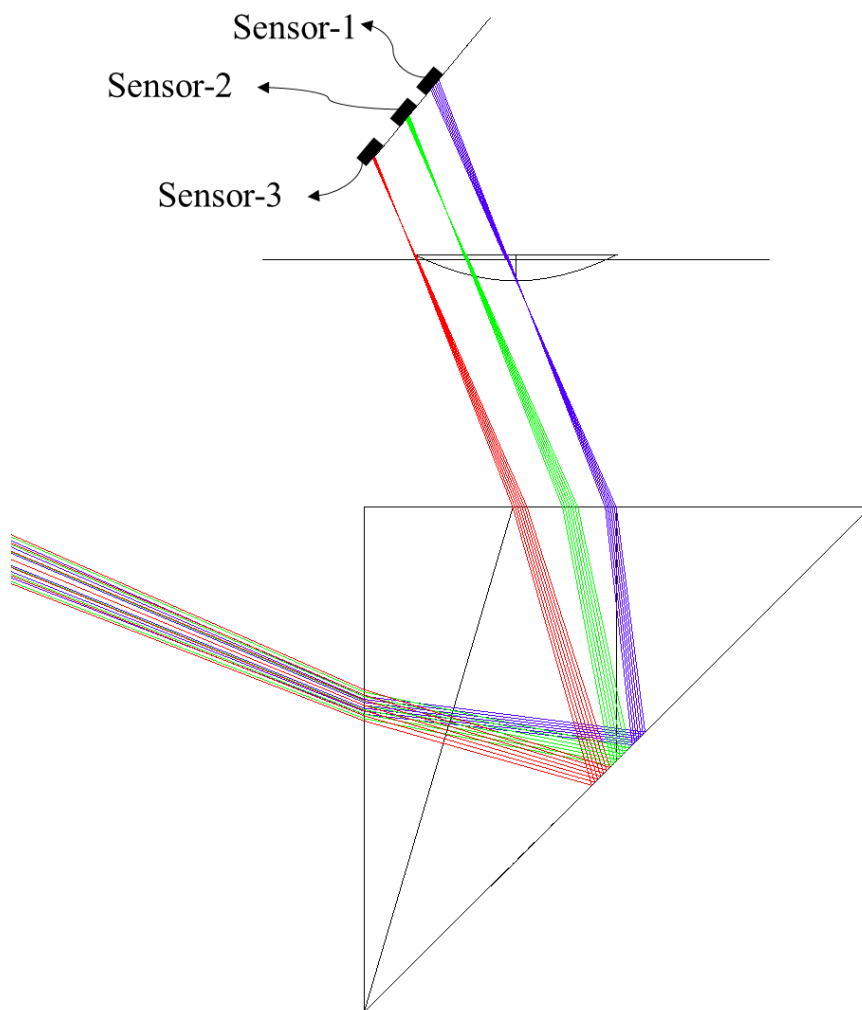
Figure 5-3: The sensor locations layout of new introduced Chromatic Multifocal LIDAR Imaging System with dispersion prism.

The relay system is designed and optimized for 500 mm target distance for 450 nm wavelength and better image quality in the image plane on sensor-1. Sensor-2 and Sensor-3 are placed on the optical paths of 550 nm and 650 nm rays respectively. For the in-focus condition of sensor-2, the corresponding target layer-2 distance is measured as 511.480 mm. Similarly, for the in-focus condition of sensor-3, the corresponding target layer-3 distance is measured as 513.730 mm.

The spot diagrams and encircled energies have been checked for each target layer, and to discuss the image quality of the system and further analysis. The design results of the system for 500 mm target distance and for 450 nm wavelength conditions are given in Table 5.2. The pinhole radius of the system is taken as 15 μm for 450 nm wavelength and 35 μm for 450 and 550 nm wavelengths regarding encircled energy results of the system. The IFOV is calculated by using equation (2-5) as,

$$\frac{IFOV}{2} = \tan^{-1}\frac{15\mu m}{310mm} \approx 0.0027º \tag{5-1}$$

$$\frac{IFOV}{2} = \tan^{-1}\frac{35\mu m}{310mm} \approx 0.0064º \tag{5-2}$$

Table 5.2 The Design Outputs of Chromatic Multifocal LIDAR Imaging System with Dispersion Prism

Parameter	Design Data
Effective Focal Length (f)	310 mm
Pinhole Radius	15 μm for 450 nm,
	35 μm for 550nm and 650nm
Calculated Depth of Field	~1.38 mm for 450 nm
	~3.22 mm for 550nm and 650nm
Calculated Hyperfocal Distance	155 m
IFOV	$0.0055º \sim 0.05$ mm for 450nm
	$0.0128º \sim 0.11$ mm for 550nm and
	650nm

5.3   Results

The optical layout results of different target layers for different wavelengths are given in Figure 5-4. In Figure 5-4, it is seen that:

- ***For the first target layer at a distance of 500 mm****, the target image is constructed on sensor-1 for 450 nm wavelength, on sensor-2 for 550 nm wavelength, and on sensor-3 for 650 nm wavelength. In this condition, the 450 nm rays are in a good in-focus condition on sensor-1 with a spot size around 8.3 μm. The spot size of 550 nm wavelength is measured around 437 μm and the spot size of 650 nm wavelength is measured around 495 μm which are much bigger than the airy-disks. Regarding to these measured values, the 550 nm and 650 nm rays are out-of-focus conditions on sensor-2 and sensor-3 planes respectively which also means lower intensities on on sensor-2 and sensor-3 planes. So it is expected to have a good image quality on sensor-1 plane where it is expected poor and blurred image quality in sensor-2 and sensor-3 planes with low intensities.

- *For the second target layer at a distance of 511.480 mm,* the target image is constructed on sensor-1 for 450 nm wavelength, on sensor-2 for 550 nm wavelength, and on sensor-3 for 650 nm wavelength. In this condition, the 550 nm rays are in a good in-focus condition on sensor-2 with a spot size around 30 μm. The spot size of 450 nm wavelength is measured around 458 μm and the spot size of 650 nm wavelength is measured around 84 μm which are much bigger than the airy-disks. Regarding to these measured values, the 450 nm and 650 nm rays are out-of-focus conditions on sensor-1 and sensor-3 planes respectively which also means lower intensities on on sensor-1 and sensor-3 planes. So it is expected to have a good image quality on sensor-2 plane where it is expected poor and blurred image quality in sensor-1 and sensor-3 planes with low intensities.

- *For the third target layer at a distance of 513.710 mm,* the target image is constructed on Sensor-3. the target image is constructed on sensor-1 for 450 nm wavelength, on sensor-2 for 550 nm wavelength, and on sensor-3 for 650 nm wavelength. In this condition, the 650 nm rays are in a good in-focus condition on sensor-3 with a spot size around 36 μm. The spot size of 450 nm wavelength is measured around 546 μm and the spot size of 550 nm wavelength is measured around 96 μm which are much bigger than the airy-disks. Regarding to these measured values, the 450 nm and 550 nm rays are out-of-focus conditions on sensor-1 and sensor-2 planes respectively which also means lower intensities on on sensor-1 and sensor-2 planes. So it is expected to have a good image quality on sensor-3 plane where it is expected poor and blurred image quality in sensor-1 and sensor-2 planes with low intensities.

	Sensor-1	**Sensor-2**	**Sensor-3**
Target Layer-3 (Height: 13,73 mm)	2000.00 µm	400.00 µm	100.00 µm
Target Layer-2 (Height: 11.48 mm)	2000.00 µm	200.00 µm	400.00 µm
Target Layer-1 (Height: 0 mm)	100.00 µm	2000.00 µm	2000.00 µm
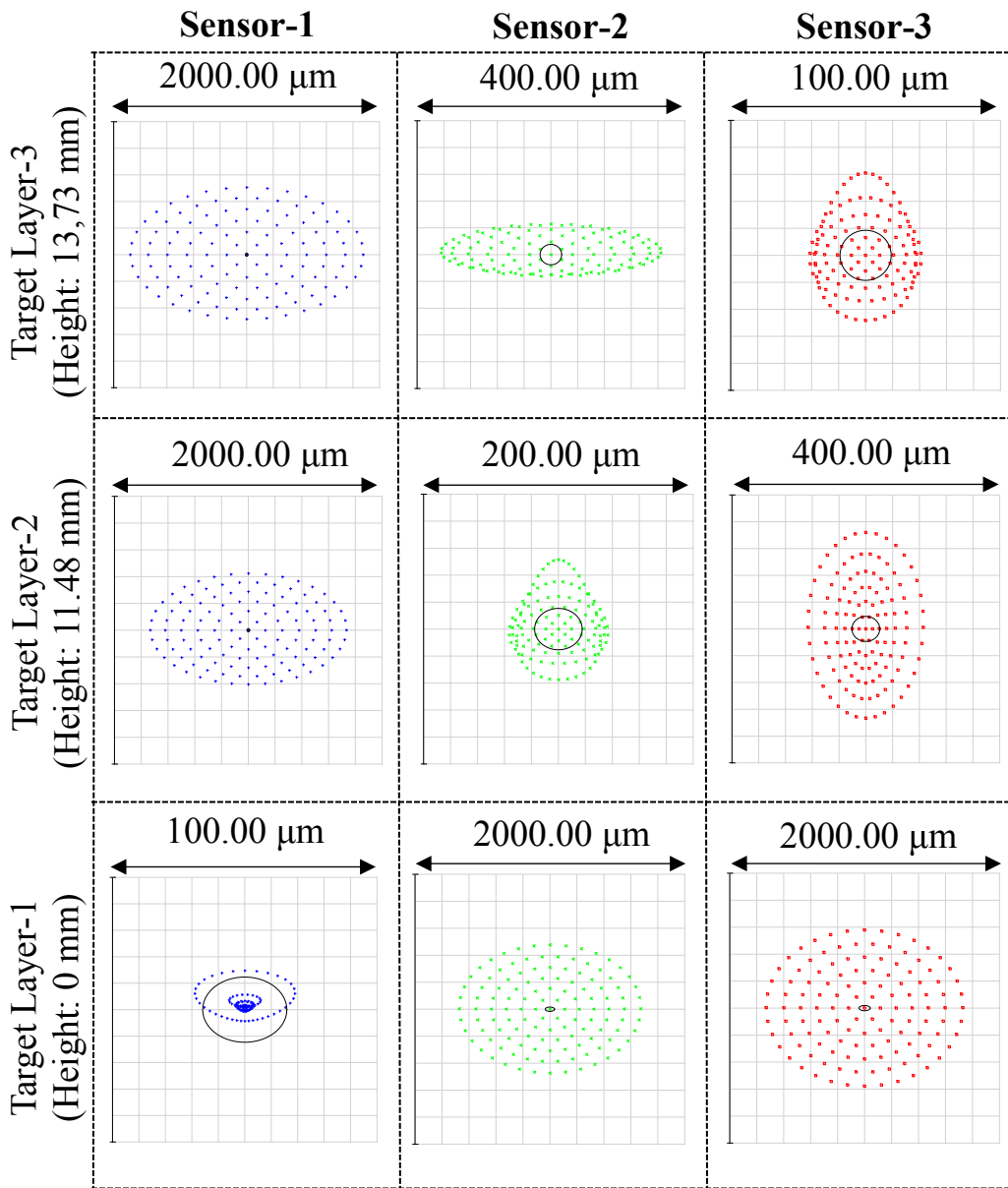
Figure 5-4: The Spot Diagram on Senor-1 plane for the first target layer at 500 mm
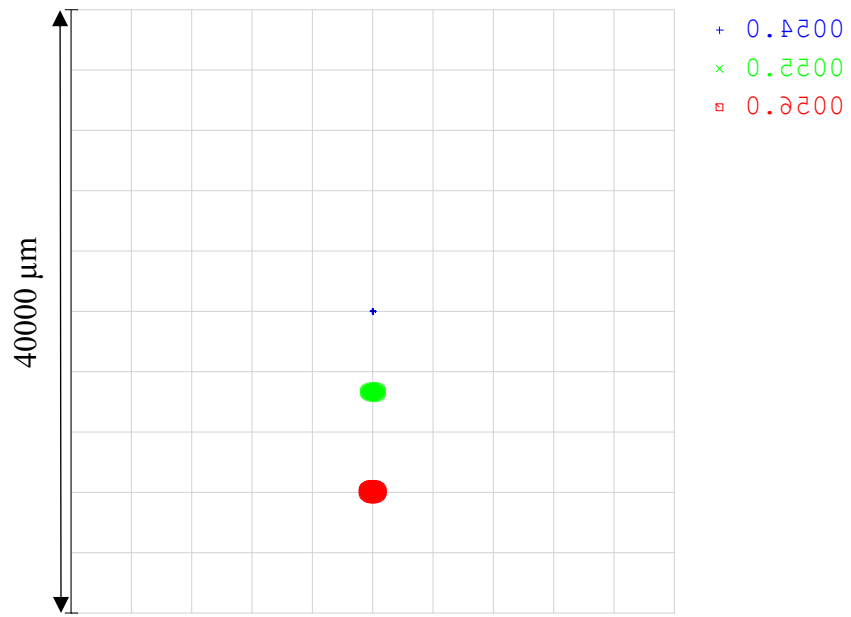
Figure 5-5: The Spot Diagram of first target plane on Image Plane for 450 nm, 550 nm and 650 nm wavelengths
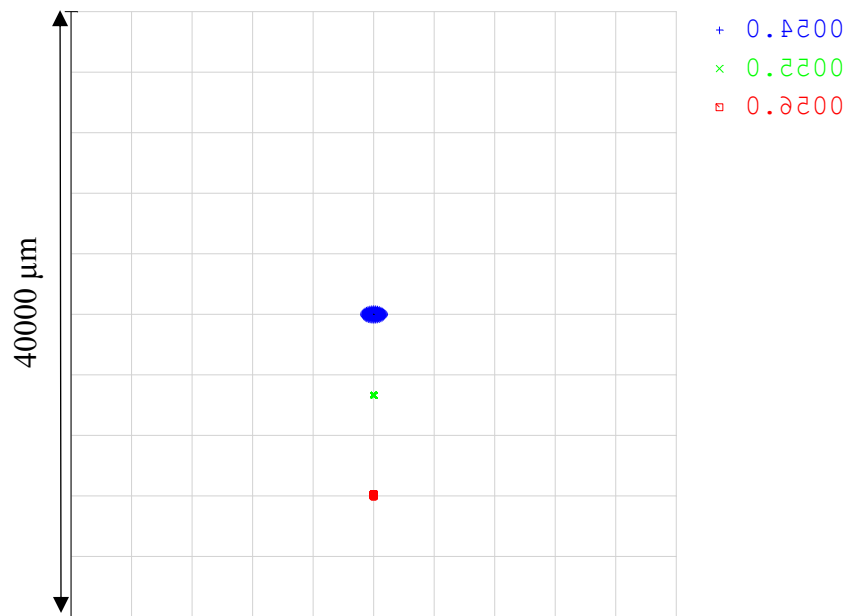
Figure 5-6: The Spot Diagram of second target plane on Image Plane for 450 nm, 550 nm and 650 nm wavelengths
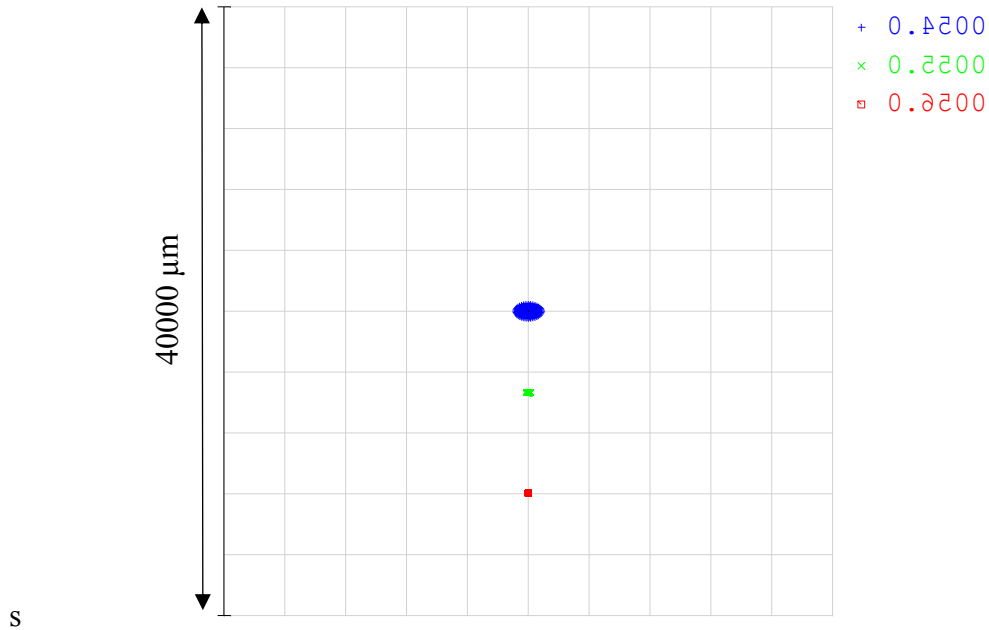
Figure 5-7: The Spot Diagram of third target plane on Image Plane for 450 nm, 550 nm and 650 nm wavelengths

In Figure 5-5, Figure 5-6 and Figure 5-7 it is clearly seen that spots are completely dispersed and located on the lateral plane which enables us to use a linear array. The distances between the 450 nm and 550 nm spots are measured as 5.32 mm and The distances between the 550 nm and 650 nm spots are measured as 6.62 mm.

5.4   Chapter Discussion

Also for better representation of the constructed images on different sensor layers for different target layers, geometric image analysis tools are used for further analysis, and the results are given in Figure 5-8.

	Sensor-1	Sensor-2	Sensor-3

Images of
Target Layer -1
(500 mm)

Images of
Target Layer -2
(511.480 mm)

Images of
Target Layer -3
(513.730 mm)
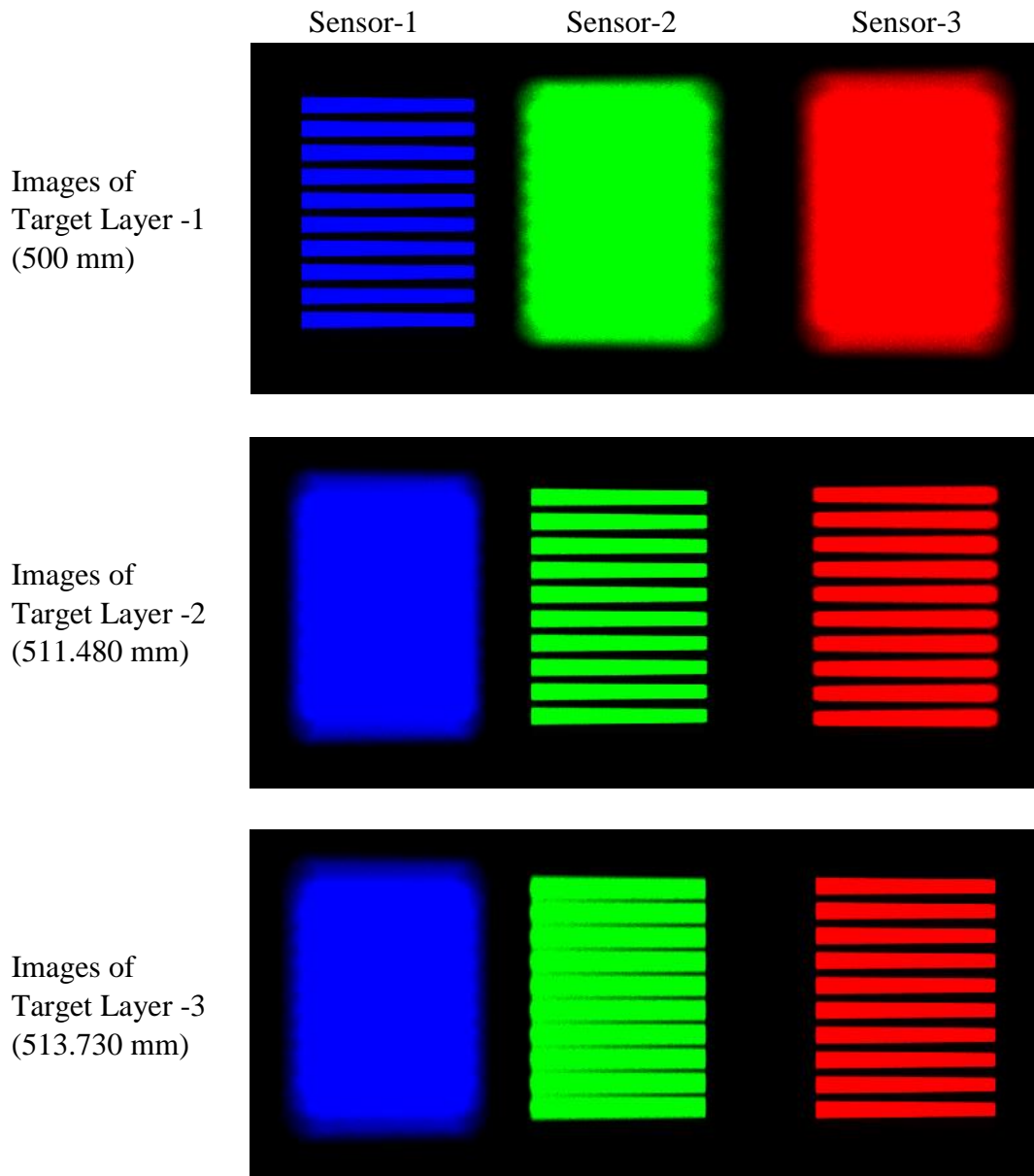
Figure 5-8: The Image Diagrams on Sensors for all wavelengths and 500 mm target
distance

As expected from the Spot diagram results of sensor-1, sensor-2, and sensor-3 planes, it is clearly seen that a good image is constructed in sensor-1 for the first target plane with blurred images on sensor-2 and sensor-3. Similarly, a good image is constructed in the sensor-2 plane for the second target plane with blurred images on sensor-2 and sensor-3. And, finally, a good image is constructed in the sensor-3 plane for the third target plane with blurred images on sensor-2 and sensor-3.

As the final step of the analysis, the 3D sample is used (Figure 3-13) to analyze corresponding images on sensor-1, sensor-2, and sensor-3 planes, for an ideal detector system. To achieve 2mm resolution, the wavelength has been selected as 450 nm, 461 nm and 473 nm. In this analysis, also the constructed optical noise levels on sensor-1 for the second and third target layers are added to the constructed image of the first target layer on sensor-1 to see the effect of the noise levels caused by the other target layers. Similarly, the same work was done for the constructed images on sensor-2 and sensor-3 planes. By combination of the images that constructed in sensor-1, sensor-2 and sensor-3 planes, the 3D image of the sample is achieved as given in Figure 5-9.
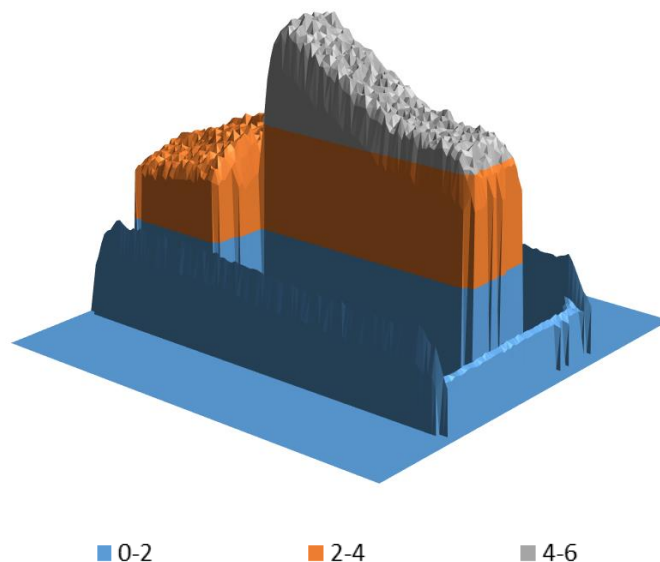
Figure 5-9: The constructed image of the test sample (Each color represents the points in corresponding 2 mm thickness)

In the conclusion of this chapter, the Chromatic Multifocal LIDAR Imaging System with Dispersion Prism has been introduced, designed and the detailed analysis results are discussed. The results are showing that the concept of the Chromatic Multifocal LIDAR Imaging System with Dispersion Prism is working and can be used for enhanced packaging. Because dispersion prism separates the optical axis's for the different wavelengths to enable using a linear array in a single plane also it is possible to observe much more than three wavelengths at the same time.

CHAPTER 6

ADVANCED DESIGN FOR MULTIFOCAL IMAGING LIDAR SYSTEM

By the Advanced Multifocal LIDAR Imaging system, it is aimed to observe the intensity changes on the detector for different detector positions in the image plane instead of well-distinguished depth layers for increasing the target ranges and measurement ranges. The schematic diagram of the proposed Advanced Multifocal LIDAR Imaging system is given in Figure 6-1.
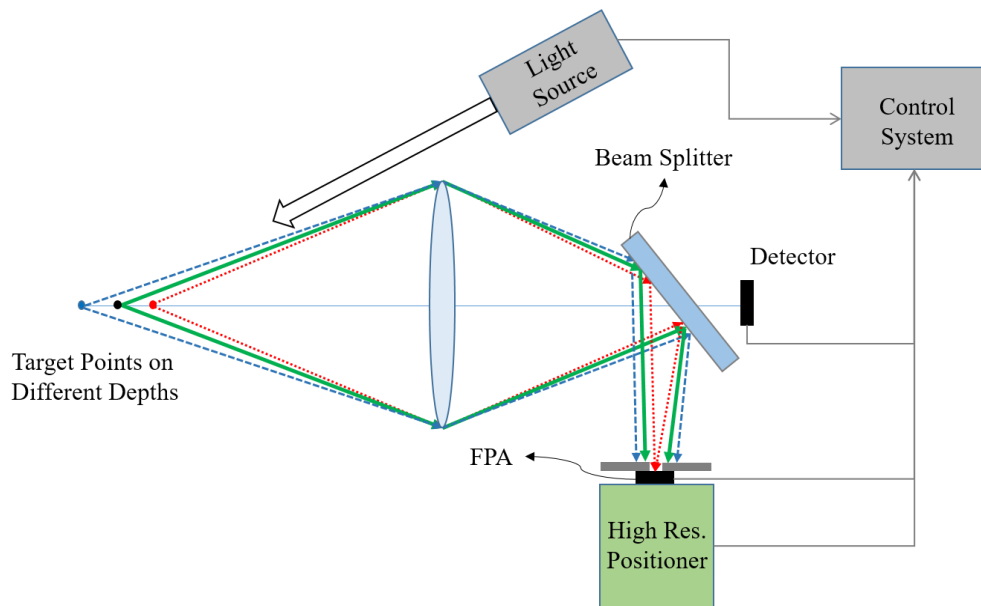
Figure 6-1: The schematic representation of the Advanced Multifocal Imaging LIDAR System

In this method, the pulse is transmitted to the target with the help of the controlled light source and the time difference between the transmitted and pulse is measured for calculation of the target distance D with the equation (1-6). A beam splitter or folding mirror can be used for steering the light between the ToF measurement

detector and FPA. After the reference target distance D is calculated by the direct ToF technique, the images are taken by the FPA for different positions on the image plane with the help of the high-resolution positioner. A high-resolution positioner can be a piezoelectric driver or micro screw motor. The main aim of the high-resolution positioner is scanning a predefined linear distance in the image plane to get different depth layer images by the FPA similar to the proposed Multifocal LIDAR System. Because, high magnification is required for getting a narrow depth of field to achieve distinguishable layers, and it is extremely difficult to get high magnification for long ranges, this method is aimed to work on slightly distinguishable layers. As it is known and also shown in chapters 3 and 4, the intensity on the pinhole or pixel gets maximum for in-focus conditions and get lowers proportionally to the power of out-of-focus conditions. So the main idea of this method is to measure the pixel intensities for different positions in the image plane during the scan of the high positioner system and find the maximum pixel intensity image plane locations for each pixel by the post-processing to achieve depth layer information on the target plane.

6.1   Design Criteria

It is aimed to imaging slightly distinguished depth layers on the target plane within mm depth differences, where such a depth resolution requires picosecond pulse rise time in direct ToF measurement technique, with a moderate clear aperture. So as the main design criterion, it is aimed to get a slightly narrow depth of field in cm scale for distinguishing the target layers. Also, it is aimed to have a moderate measurement range of 8m with commercial FPA's. A commercial FPA with 4.2 µm and 12 MP resolution, which is used in commercial cameras successfully, is selected for a cheaper and producible design. The main design parameters are defined in Table 6.1.

86

Table 6.1 The Design Inputs for Advanced Multifocal LIDAR Imaging Optical System

Parameter	Design Data
Target Distance	8 m
Clear Aperture	55 mm
Pixel Pitch	4.2 µm
FPA Size	12.6 MP (4.352 x 2.904 Pixels)
FPA Dynamic Range	14 bit
Working wavelength	850 nm (NIR)

6.2   Optical Design

A Double Gauss objective system is designed for 8 m range and high optical image quality where a commercial type FPA is selected with a 4.2 µm pixel pitch. The optical layout of the designed system is given in Figure 6-2.
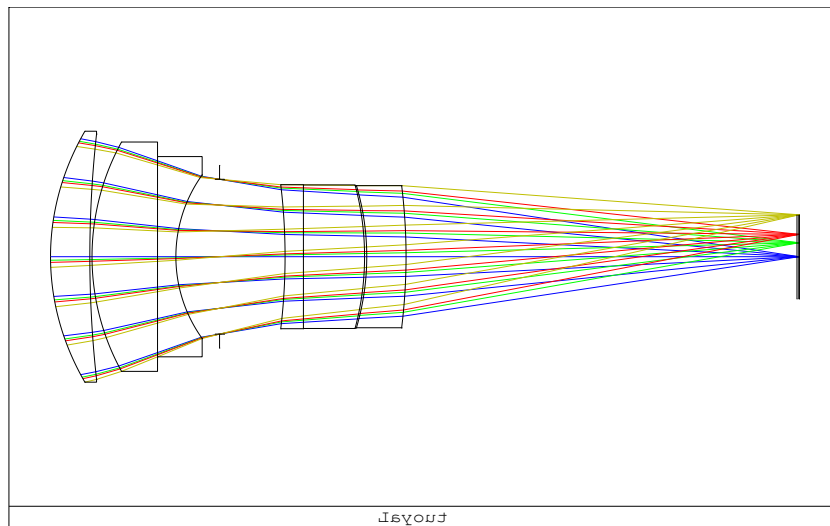
Figure 6-2: The optical design layout of advanced design for Multifocal Imaging LIDAR System.

The Double Gauss objective system is designed and optimized for 8 m target distance and 850 nm (Near Infrared) wavelength. The spot diagrams, MTF graphs, and ensquared energy diagrams have been checked for image quality and the results are given in the following chapters. The IFOV is calculated by using equation (2-5), FOVHorizontal is calculated by using equation (2-6) and FOVVertical is calculated by using equation (2-7) as,

$$\frac{IFOV}{2} = \tan^{-1}\frac{4.2\mu m}{176mm} = 0.0014^{\circ} \tag{6-1}$$

$$FOV_{Horizontal} = 4352 \cdot 0.0014^{\circ} \approx 5.9^{\circ} \tag{6-2}$$

$$FOV_{Vertical} = 2904 \cdot 0.0014^{\circ} \approx 4^{\circ} \tag{6-3}$$

Regarding FOVHorizontal and FOVVertical results of the optical system, the working fields have been selected as 0°, 1°, 1.6°, and 3° which cover all the FPA area. All analyses and results have been discussed for all fields to ensure the same image quality in the all FPA area.

The magnification can be calculated by using equation (2-4) as

$$M = \frac{176}{8000} = 0.022 \tag{6-4}$$

The output parameters of the optimized design are given in Table 6.2.

Table 6.2 The Design Outputs of Advanced Multifocal LIDAR Imaging System

Parameter	Design Data
Effective Focal Length (f)	176 mm
Calculated Depth of Field	~5.5 cm
Calculated Hyperfocal Distance	2,305 m
IFOV	0.0014º ~ 0.2 mm
Horizontal FOV	5.9º
Vertical FOV	4º
Magnification	0.022

6.3   Results

The optical design is optimized for 8 m target distance and all variables have been fixed except the image plane distance. For the target layer at a distance of 8 m and in the original position of the image plane, the rays are perfectly in-focus condition on FPA. The MTF graphs and spot diagrams on the image plane in its original position are worked below for analyzing the imaging quality of the design.

Spot diagram results on the image plane in its original location are given in Figure 6-3. In the spot diagram, it is seen that the spot sizes on the sensor plane are smaller than the airy disk for each field which means that optical design is diffraction limited. MTF Graph on the image plane for its original location is given in Figure 6-4. For 4.2 µm pixel pitch the required spatial frequency in cycles per mm can be calculated as,

$$\# \ of \ Cycles = \frac{1mm}{2.pixel \ pitch} = \frac{1mm}{2.4.2\mu m} = 119 \qquad (6\text{-}5)$$
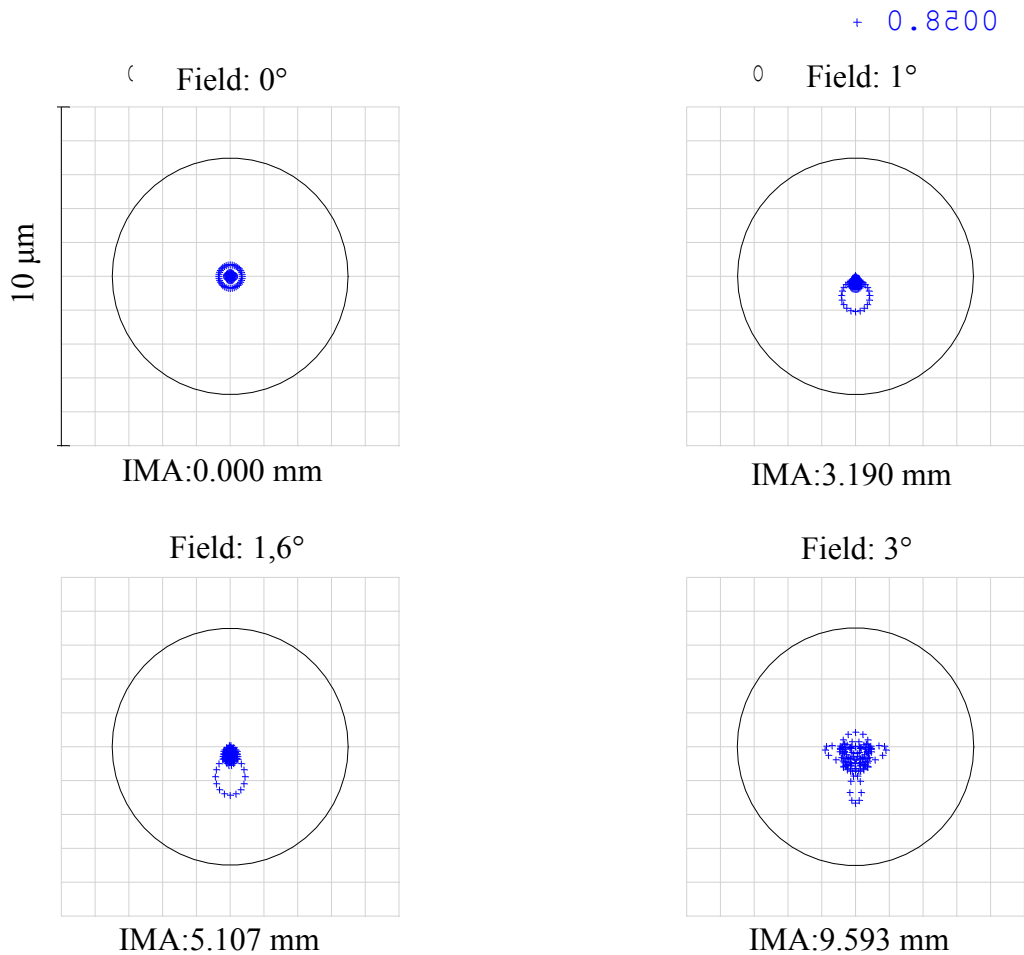
Figure 6-3: The Spot Diagram for in focus condition

As a rule of thumb in industry, the required OTF value for the spatial frequency of the FPA shall be higher than 0.5 for good imaging. In Figure 6-4, it is seen that the OTF value for 119 cycles is around 0.58 which means that good imaging result is expected from the optical design.
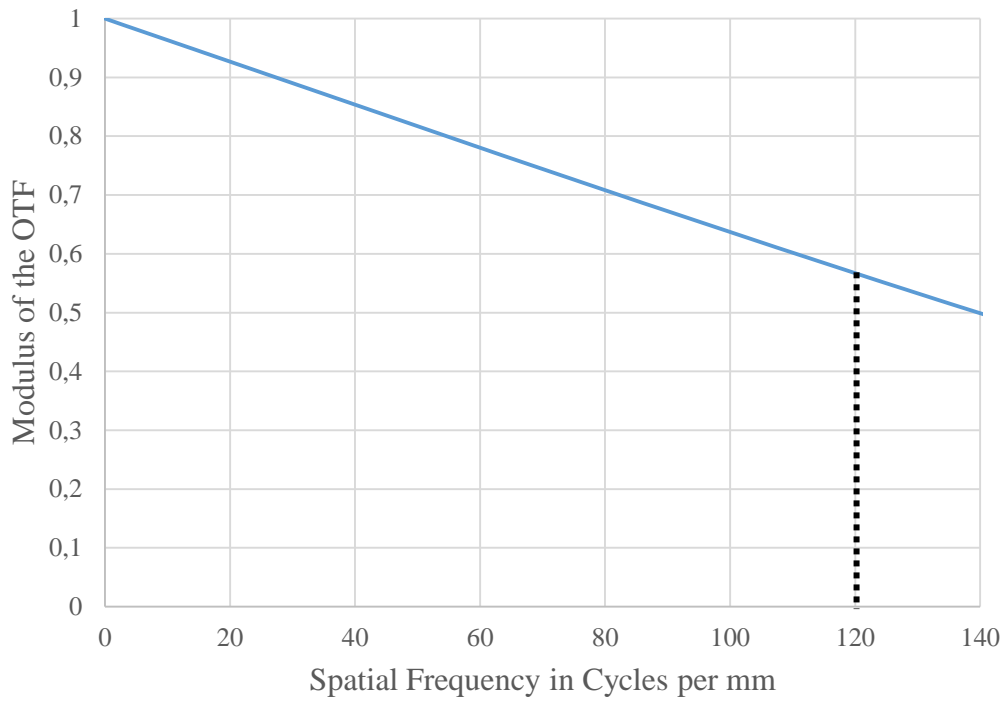
Figure 6-4: The MTF graph for in focus condition
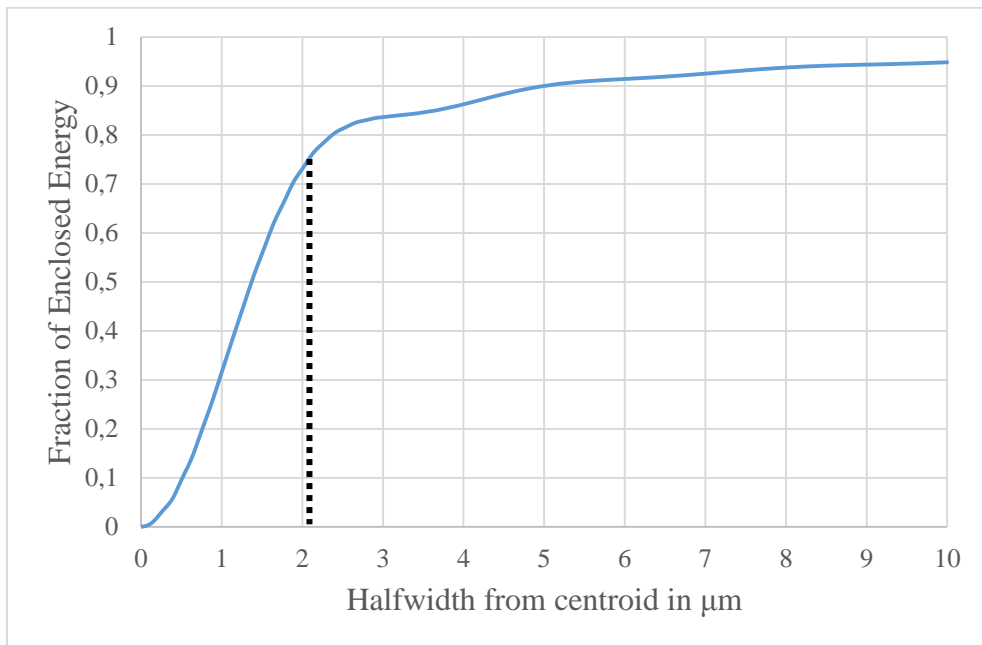
Figure 6-5: The Diffraction Limited Ensquared Energy Diagram for in focus
condition

The ensquared energies have been measured with the help of the optical design program. The ensquared energy is found around %78 on a 4.2 μm pixel in all fields.
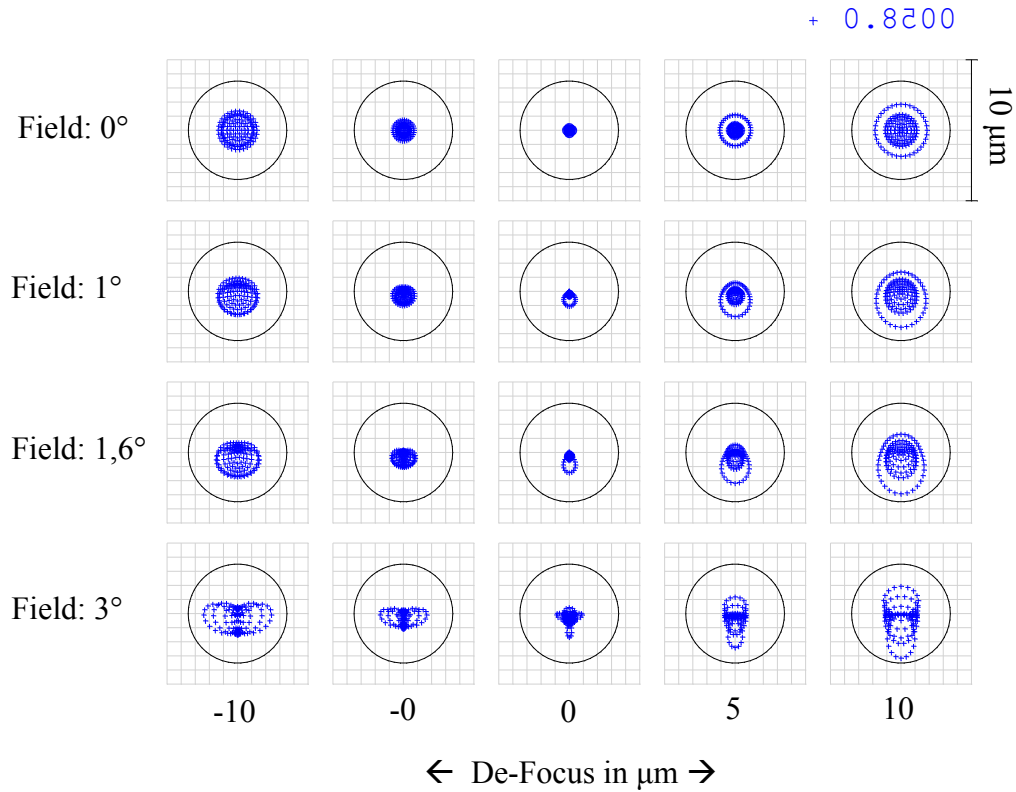
Figure 6-6: Through Spot Diagram for in focus condition.

The Through Spot Diagram is checked for spot size changes for the different image plane locations. In Figure 6-6 it is seen that, as expected the spot sizes are getting bigger by the small image plane displacements in units of microns, because of the narrow depth of field. Also, diffraction through focus diagram (Figure 6-7) shows the sharp OTF value changes by the small image plane location changes in micrometers.
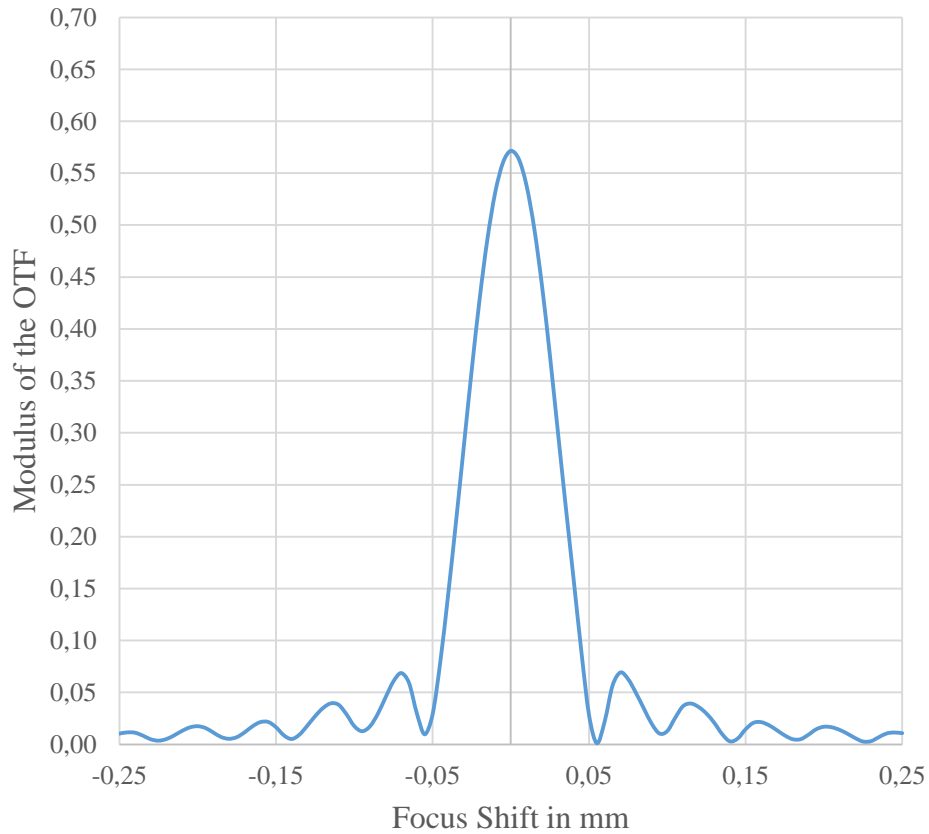
Figure 6-7: Diffraction Through Focus MTF graph for in focus condition.

6.4   Chapter Discussion

The results of the optical design show that a good spatial resolution is achieved for 8 m target range with a small depth of focus value as aimed. To show that the main aim of the design is working, we measured the optimized image plane locations for different depth layers on the target plane with 1 mm resolution. The results of the measurements are given in Figure 6-8. The results show that any 1 μm focus shift in the image plane corresponds to 2.184 mm distance change in the target plane. Or in another word, any1 mm change in target distance corresponds approximately 0.459 μm focus shift in the image plane.
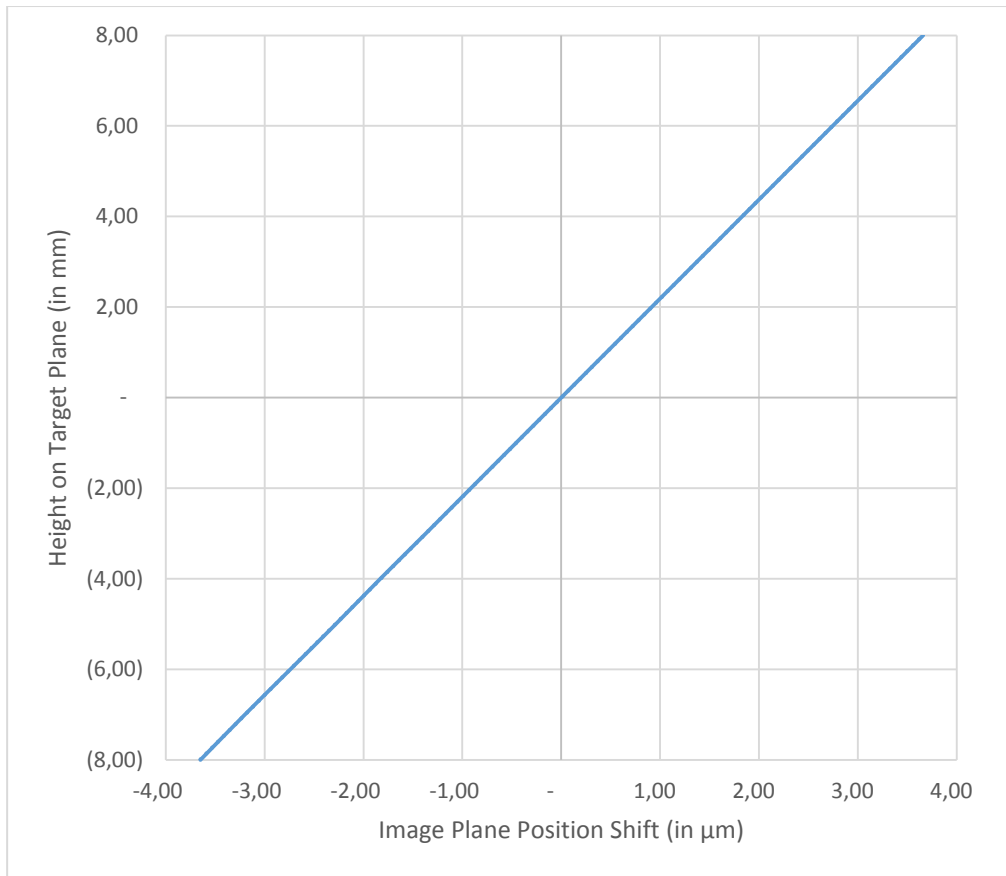
Figure 6-8: Responded height levels (in mm) on Target Plane corresponding to different image plane locations (in µm).

The image plane region is scanned with 1µm steps between -1 µm and 1 µm for different target heights between -100 mm and 100 mm on the target plane. The corresponding diffraction ensquared energies are measured for each image plane and target height combinations to see the ensquared energy changes regarding different target heights and the peak point shift of the ensquared energy graphs for different image plane locations. The Encircled Energy Diagrams for different target point heights and different image plane displacements are given in Figure 6-9. It is seen that the ensquared energy change curve is Gaussian-like and the peak point of each diagram is shifting with the image plane displacement.
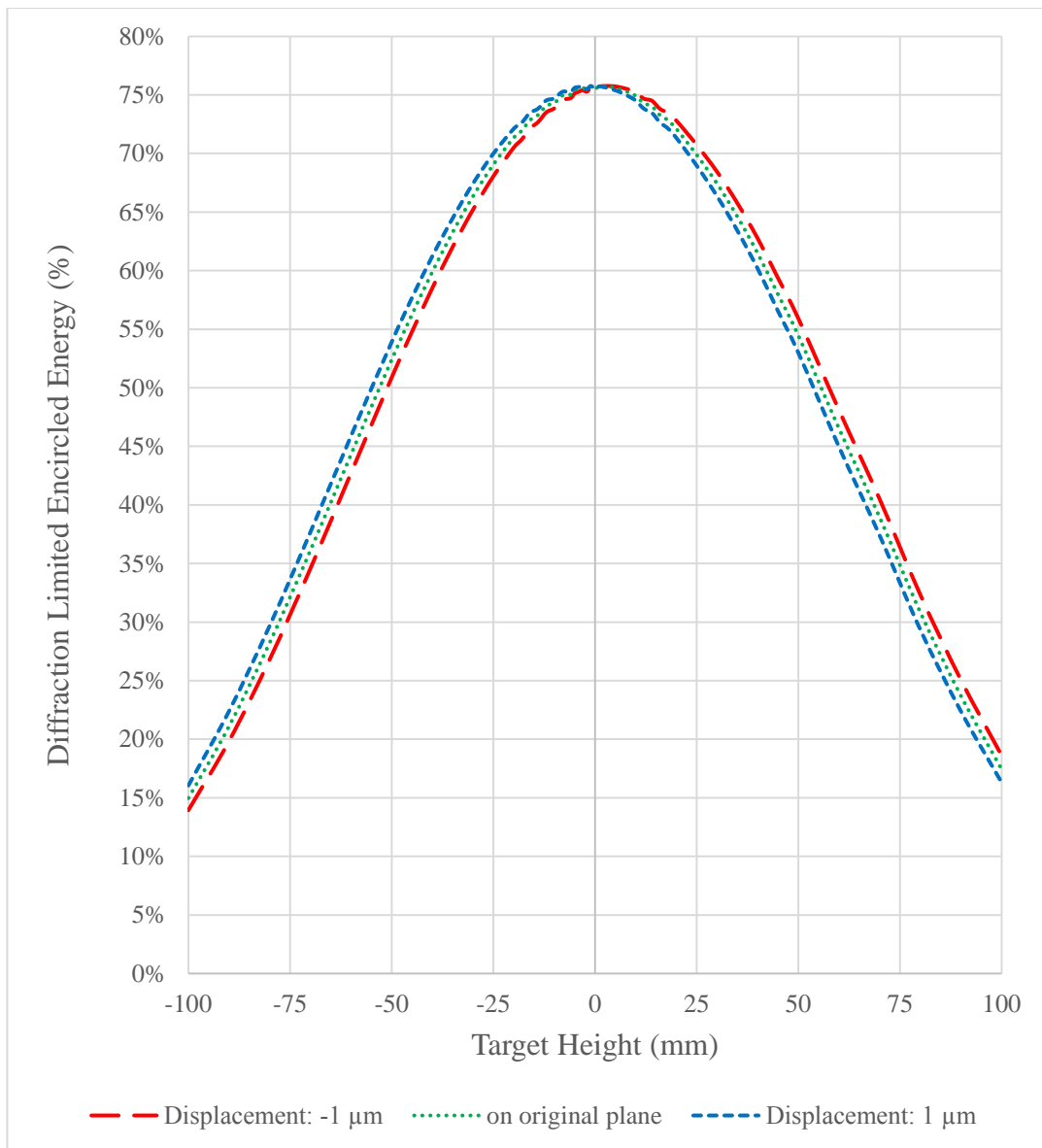
Figure 6-9: The Encircled Energy Diagrams for different target point heights and different image plane displacements.

If the diagram is zoomed between -25 mm and 25 mm target height values as given in Figure 6-10, the relation between the shift in the peak points of the encircled energy with the image plane displacement. The exact peak point positions are given in Table 6.3.
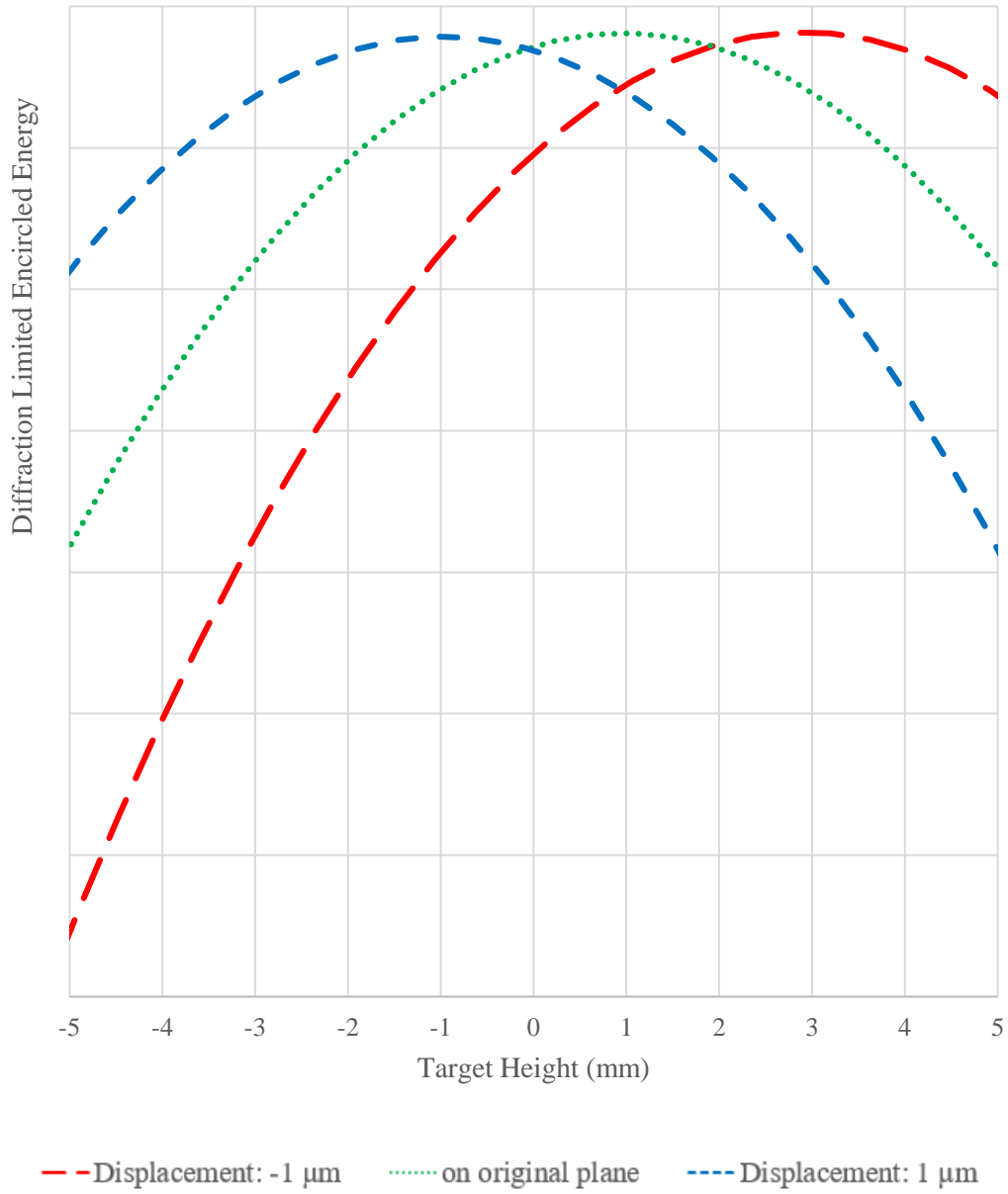
Figure 6-10: The Detailed Encircled Energy Diagrams for different target point height on the target plane.

Table 6.3 The Ensquared Energy Diagram Peak Points regarding to different
Image Plane Displacements

Image Plane Displacement (μm)	Peak Point Position (mm)
-2	4-5
-1	3
0	1
1	-1
2	-3

In Table 6.3, it is seen that there is 1 mm constant measurement error in the + height position direction and the corresponding peak point shifts for each 1 μm image plane displacement is ~2 mm. The result is also consistent with Figure 6-9, where 1 mm changes in target distance correspond approximately 0.459 μm focus shift.

For a better understanding of ensquared energy change with the image plane displacement, the image plane region is scanned with 40 nm steps between -50 μm and 50 μm for -2 mm, 0, and 2 mm target heights on the target plane. The corresponding diffraction ensquared energies are measured for each image plane and target height combinations to see the ensquared energy changes regarding image plane displacement and the peak point shift of the ensquared energy graphs in detail. The normalized encircled energy diagrams for different target point heights are given in Figure 6-11. It is seen that the ensquared energy graph is Gaussian-like and the peak point of each diagram is shifting with the image plane displacement.
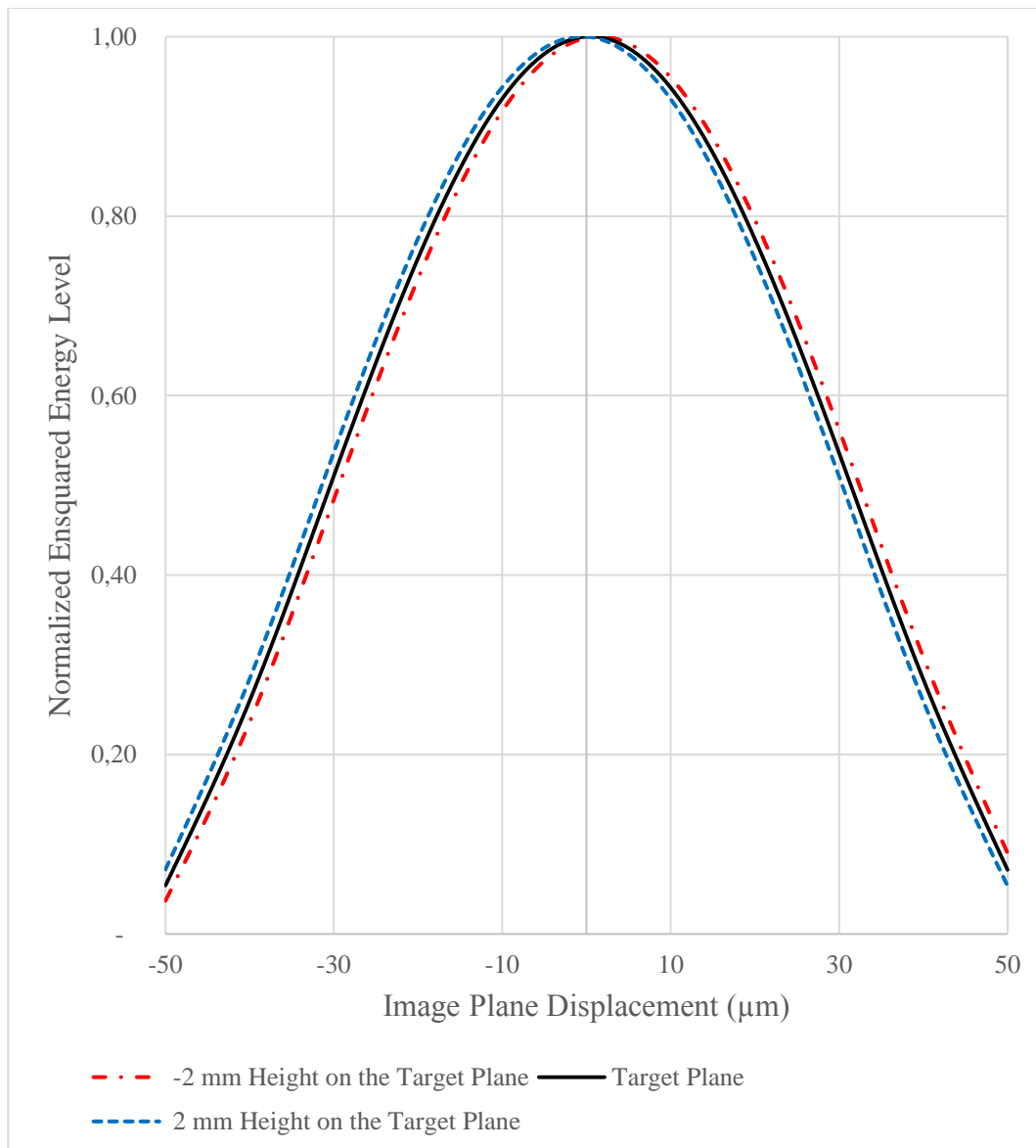
Figure 6-11: The Normalized Encircled Energy Diagrams for different target point heights and different image plane displacements.

Figure 6-11 has been zoomed between -10 µm and 10 µm image plane displacements in Figure 6-12, and zoomed between -2 µm and 2 µm image plane displacements in Figure 6-13. In Figure 6-12, the peak point shift of the normalized ensquared energy level seems more clear.
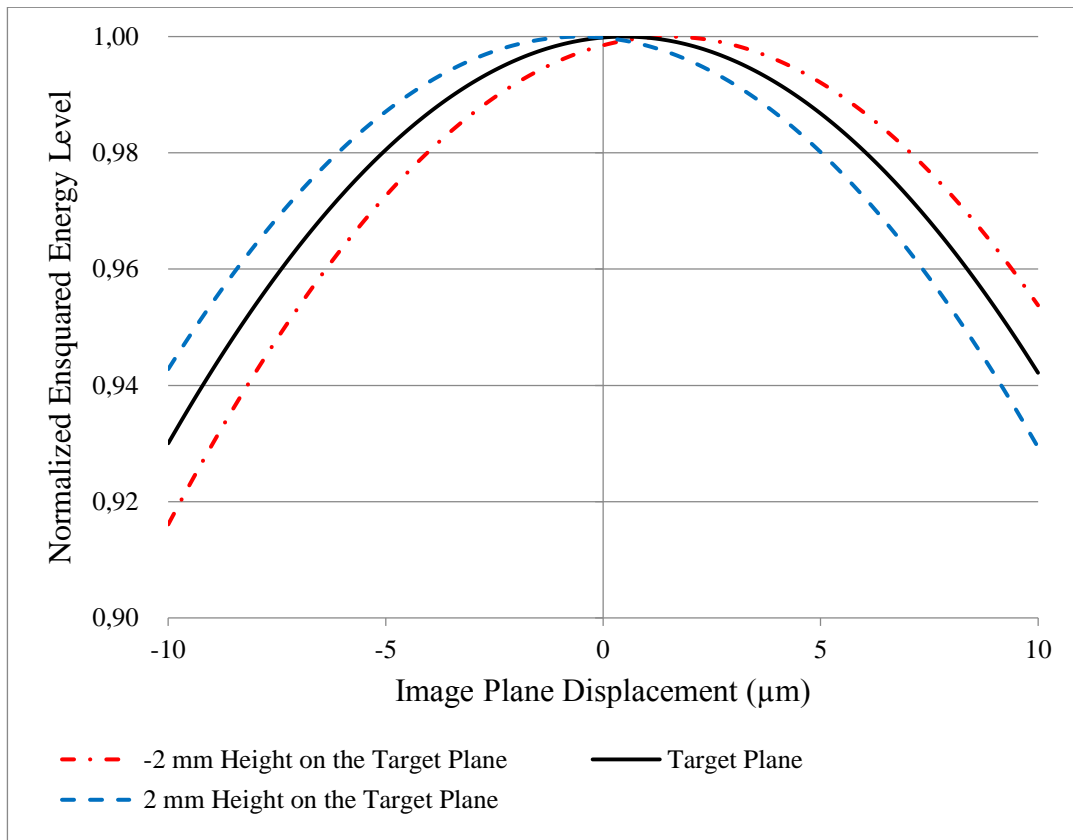
Figure 6-12: The Detailed Normalized Encircled Energy Diagrams for different target point heights and different image plane displacements between -10 µm and 10 µm.

In Figure 6-13, the distances between the peaks seem easier and the peak points are observed at -0.54 µm high-resolution positioner position for the target point with 2 mm height, at -0.54 µm high-resolution positioner position for the target point with 2 mm height; 0.48 µm high-resolution positioner position for the target point that on the target plane; and 1.52 µm high-resolution positioner position for the target point with -2 mm height (2 mm depth) on the target plane. So the distances between the peak point locations are calculated as 1.02 µm between the signals for + 2mm and 0 mm layer on the target plane and 1.04 µm between the signals for 0 mm and -2 mm layers on the target plane.
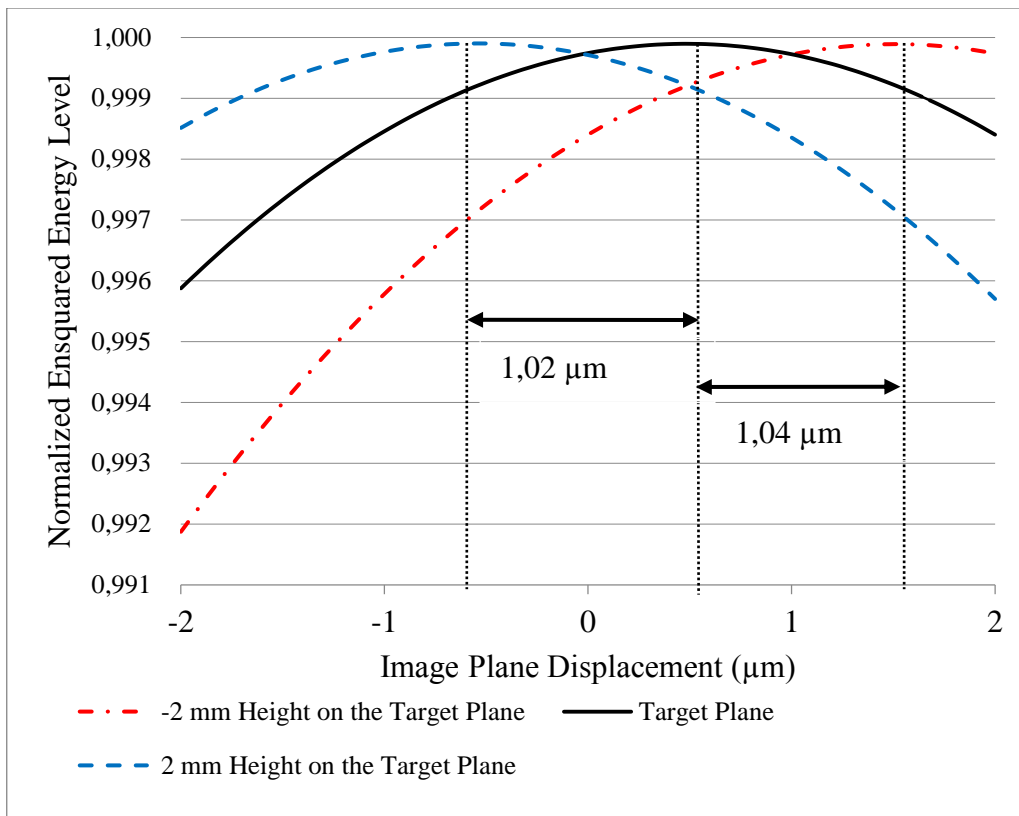
Figure 6-13: The Detailed Normalized Encircled Energy Diagrams for different target point heights and different image plane displacements between -2 µm and 2 µm.

The calculated peak point distance results are consistent with Figure 6-9 and Table 6.3. The minimum signal level difference between the signal on the peak point and the signal on a point that is 1µm far away from the peak point, is measured as 0.0066 which is almost 11 times higher than the resolution of a 14-bit detector.

In the conclusion of this chapter, the results show that it is possible to detect the peak point shifts in the image plane that are caused by the different heights on the target plane by scanning the image plane with a high-resolution positioner. And also, it is possible to estimate the height differences on the image plane within mm resolution by using the peak point shifts in the image plane.

CHAPTER 7

**AM MODULATED MULTIFOCAL IMAGING LIDAR SYSTEM FOR
ENHANCED DEPTH RESOLUTION AT LONGER RANGES**

For AM Multifocal LIDAR Imaging system, it is aimed to use multifocal imaging and depth of field as an optical gating tool to increase the measurement range while keeping the wavelength of modulation small, for better depth resolution. The schematic diagram of the proposed AM Multifocal LIDAR Imaging system is given in Figure 7-1.
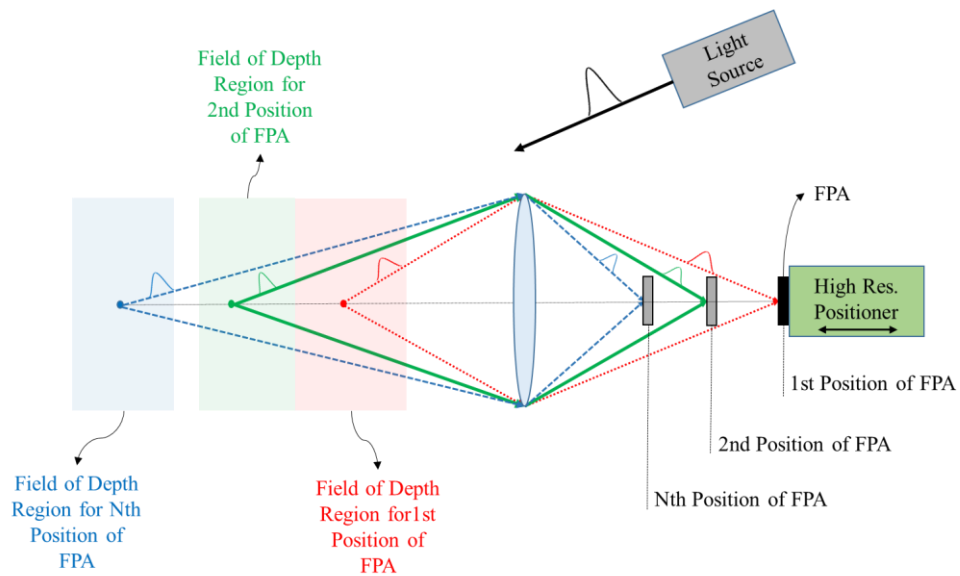
Figure 7-1: The schematic representation of the AMCW Multifocal Imaging
LIDAR System

In this method, amplitude modulated light is transmitted to the target and the phase difference between transmitted and received AM signal is measured for calculation

of the target distance D with the equation (1-15). Because of the ambiguity of the modulation, the maximum range, that can be measured, is limited by the wavelength of the AM modulation. The main idea of this technique is to divide the measurement range into different layers (named gating layers) where each layer's width is equal to the wavelength of the AM modulation. So it will be possible to increase the maximum measurement range as proportional to the number of the gating layers. As it is known and also shown in chapters 3 and 6, the intensity on the pinhole or pixel gets maximum for in-focus conditions and get lowers proportionally to the power of out-of-focus conditions. So the main idea of this method is to compare the measured pixel intensity for different gating layers for different positions of the high-resolution positioner system. Then it is aimed to find the gating layer for each pixel for finding that targets gating layer information.

With gating layer information of the target, the exact depth calculation can be done over the ambiguity range.

With this technique, the high-resolution depth measurement capability of the AMCW LIDAR techniques can be saved when the measurement range limitation of the AMCW LIDAR technique is exceeded. Similar to the proposed Advanced Multifocal LIDAR technique in Chapter 6, a high-resolution positioner, which can be a piezoelectric driver or micro screw motor, can be used for changing the image plane position to predefined coordinated for creating gating layers. Another advantage of this technique is measuring a branch of depth layers with the help of the AMCW LIDAR technique at the same time with a single capture, so the number of the captured images decreased significantly regarding Advanced Multifocal LIDAR technique.

The proposed techniques also eliminated the narrow depth of field problem [22] of the AMCW LIDAR's that is seen especially for low-frequency modulation that is used for extended ranges. This introduced technique avoids narrow depth of field

problem because the depth of field is controlled by gating function and ambiguity limitation of the high frequencies is getting solved by this technique.

7.1   Design Criteria

The main aim is to keep the width of the gating layer the same as the modulation wavelength by using controlled depth of field as a gating function. So the required depth of field is units of meters and much higher than the ones described in chapters 3 and 6, but also it shall be narrow regarding common imaging optics. For proving the concept, an AMCW LIDAR FPA structure is selected with 320 x 216 Pixels spatial resolution, 10 μm pixel pitch, 100 MHz operating frequency, 850 nm working wavelength, and 5.9 mm depth measurement resolution [19]. A higher maximum measurement range is aimed at regarding chapters 3 and 6. The design inputs of the system are described in Table 7.1.

Table 7.1 The Design Inputs of the AMCW Multifocal Imaging Optical System

Parameter	Design Data
Measurement Range	7 – 18 m
Clear Aperture	15 mm
Pixel Pitch	10 μm
FPA Size	320 x 240 Pixels
AM modulation Frequency	100 MHz
Depth Resolution	5.9 mm
Working wavelength	850 nm (NIR)

It is aimed to use the maximum working frequency of the AMCW LIDAR FPA to achieve maximum depth resolution as 5.9 mm. So, the ambiguity range of the AMCW LIDAR can be calculated as;

$$Modulation\ Time = \frac{1}{Modulation\ Frequency} \qquad (7\text{-}1)$$

$$Modulation\ Time\ of\ AMCW = \frac{1}{100.000.000\ Hz} \qquad (7\text{-}2)$$

$$Modulation\ Time\ of\ AMCW = 10\ nano\ seconds \qquad (7\text{-}3)$$

$$Ambiguity\ Range = Modulation\ Time\ of\ AMCW\ .c \qquad (7\text{-}4)$$

$$Ambiguity\ Range \approx 3m \qquad (7\text{-}5)$$

This means that 5.9 mm depth resolution can be measured for up to 3 m with a 100 MHz AMCW LIDAR system, where the measurements for the larger distances that the ambiguity range, 3m, will not be distinguished. For example, measurement results of both 8m and 11m range measurements will give the phase difference because of the ambiguity. So we aimed to divide the measurement area into gating layers with a width of 3m by using depth of focus as a tool to distinguish the range measurements over the ambiguity range.

7.2   Optical Design

A Double Gauss objective system is designed for high optical image quality for the selected AMCW LIDAR FPA with 10.0 μm pixel pitch. The optical layout of the designed system is given in Figure 7-2.
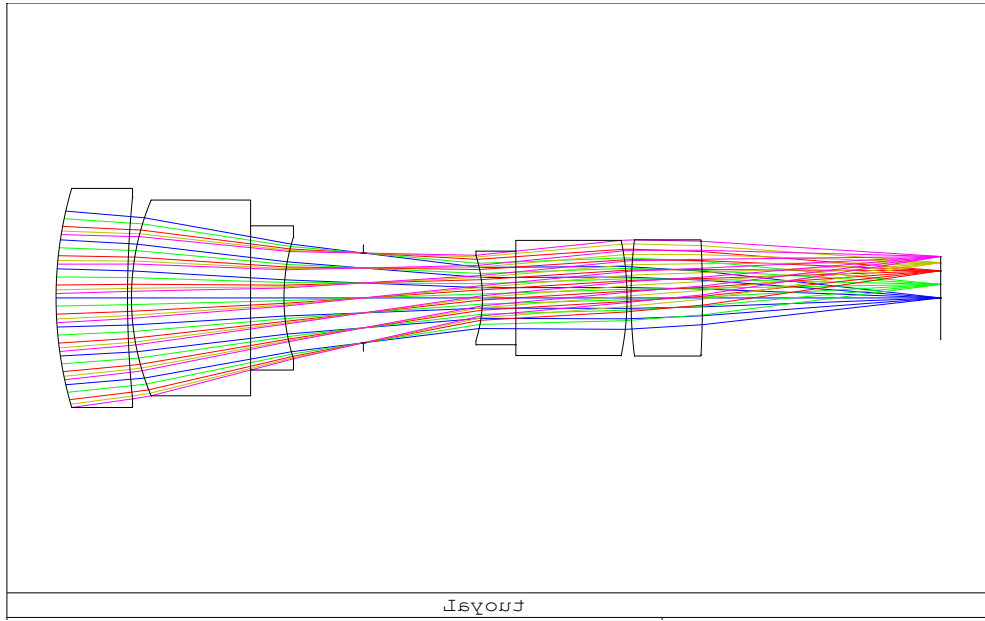
Figure 7-2: The optical design layout of AMCW Multifocal Imaging LIDAR
System.

The Double Gauss objective system is designed and optimized for 850 nm (Near
Infrared) wavelength. The spot diagrams, MTF graphs, and ensquared energy
diagrams have been checked for image quality and the results are given in below.
The IFOV is calculated by using equation (2-5), FOV$_{Horizontal}$ is calculated by using
equation (2-6) and FOV$_{Vertical}$ is calculated by using equation (2-7) as,

$$\frac{IFOV}{2} = \tan^{-1}\frac{10\mu m}{100mm} = 0.0057º \tag{7-6}$$

$$FOV_{Horizontal} = 320 \cdot 0.0057º \approx 1.8º \tag{7-7}$$

$$FOV_{Vertical} = 240 \cdot 0.0057^{\circ} \approx 1.4^{\circ} \qquad (7\text{-}8)$$

Regarding FOV$_{Horizontal}$ and FOV$_{Vertical}$ results of the optical system, the working fields have been selected as 0°, 0.5°, and 0.9° which cover all the FPA area. All analyses and results have been discussed for all fields to ensure the same image quality in the all FPA area.

The minimum and maximum magnifications can be calculated by using equation (2-4) as

$$M_{Minimum} = \frac{100}{7000} = 0.014 \qquad (7\text{-}9)$$

$$M_{Maximum} = \frac{100}{18000} = 0.006 \qquad (7\text{-}10)$$

The output parameters of the optimized design are given in Table 7.2.

Table 7.2 The Design Outputs of the AMCW Multifocal Imaging Optical System

Parameter	Design Data
Effective Focal Length (f)	100 mm
Calculated Depth of Fields	1.1 m for first gating layer
	4.4 m for 4th gating layer
Calculated Hyperfocal Distance	150 m
IFOV	0.0057º
	~ 0.9 mm for 1st gating layer
	~ 1.8 mm 4th for gating layer
Horizontal FOV	1.8º
Vertical FOV	1.5º
Magnification	0.014 for 7 m Target Distance
	0.006 for 18 m Target Distance
Image Plane Location for 9m Target Distance	30.273 mm
Image Plane Location for 12m Target Distance	29.995 mm
Image Plane Location for 15m Target Distance	29.829 mm
Image Plane Location for 18m Target Distance	29.719 mm

7.3   Results

The optical design is optimized for 850 nm wavelength for the first gating layer with the best focus condition at 9 m, and all variables have been fixed except the image plane distance.

7.3.1 Results for Target Plane at 9m

For the target layer at a distance of 9 m and in the original position of the image plane (30.273 mm), the rays are perfectly in-focus condition on FPA. The MTF graphs and spot diagrams on the image plane in its original position are worked below for analyzing the imaging quality of the design.

Spot diagram results on the image plane in its original location are given in Figure 7-3. In the spot diagram, it is seen that the spot sizes on the sensor plane are much smaller than the airy disk for each field which means that optical design is diffraction limited.

Figure 7-3: The Spot Diagram for the 1st gating layer at 9 m target plane distance

MTF Graph on the image plane for its original location is given in Figure 7-4. For 10 μm pixel pitch, the required spatial frequency in cycles per mm can be calculated as,

$$\# \ of \ Cycles = \frac{1mm}{2 \cdot pixel \ pitch} = \frac{1mm}{2 \cdot 10\mu m} = 50 \qquad (7\text{-}11)$$

Figure 7-4, it is seen that the OTF value for 50 cycles is around 0.64 which means that a perfect imaging result is expected from the optical design.

Figure 7-4: The MTF Diagram for the 1st gating layer at 9 m target plane distance

The ensquared energies have been measured with help of the optical design program. The ensquared energy is found around %82 on a 10 μm pixel in all fields.

Figure 7-5: The Ensquared Energy Diagram for the 1st gating layer at 9 m target plane distance

Figure 7-6: The Through Spot Diagram for the 1st gating layer at 9 m target plane distance

he Through Spot Diagram is checked for spot size changes for the different image plane locations and given in Figure 7-6. As expected the spot sizes are getting bigger by the image plane displacements in units of microns, because of the controlled depth of field. Regarding image plane locations for other gating layers that are given in Table 7.2, the second gating layer is located at -278 µm away, and the third gating layer is located at -444 µm away. In Figure 7-6, it is clearly seen that the spot sizes exceed the airy disk for the -150 µm location and get very big at the -300 µm location which means a totally blurred image will be contracted in the second and third gating layers for this image plane location.

Figure 7-7: The Diffraction Through Focus Diagram for the 1st gating layer at 9 m target plane distance

Also, diffraction through focus diagram (Figure 7-7) shows the smoother OTF value changes regarding design in chapter 6, because the depth of field is wider than it. On the other hand, it is clearly seen that the OTF values will be decreased down to approximately %12 for the second gating layer image position at -278 µm and OTF values will be decreased down to approximately %6 for the third gating layer image position at -444 µm.

7.3.2   Results for Target Plane at 12 m

The new image plane location is found for the second gating layer as 29.995 mm for the target distance of 12 m. The results for 29.995 mm image plane location and 12 m target distance show that the rays are perfectly in-focus condition on FPA. The MTF graphs and spot diagrams on the image plane are worked below for analyzing the imaging quality of the design.

Spot diagram results on the image plane in its original location are given in

Figure 7-8. In the spot diagram, it is seen that the spot sizes on the sensor plane are much smaller than the airy disk for each field which means that optical design is diffraction limited.
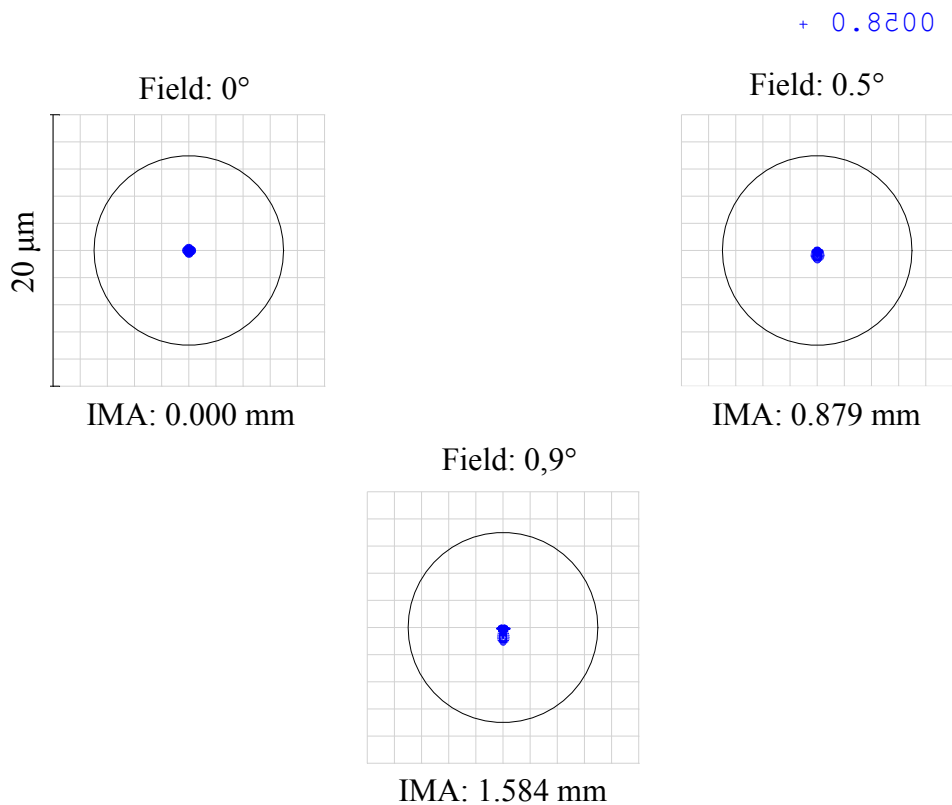

Figure 7-8: The Spot Diagram for the 2nd gating layer at 12 m target plane distance

In Figure 7-9, it is seen that the OTF value for 50 cycles is around 0.64 which means that a perfect imaging result is expected from the optical design.
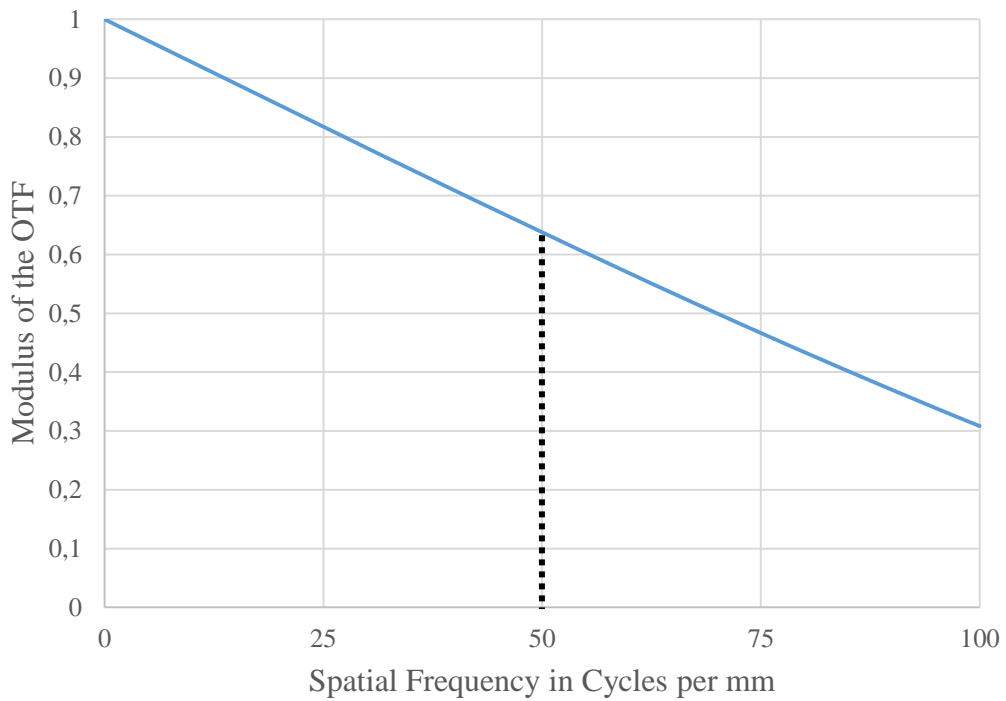

Figure 7-9: The MTF Diagram for the 2nd gating layer at 12 m target plane distance

113

Figure 7-10: The Ensquared Energy Diagram for the 2nd gating layer at 12 m
target plane distance

The ensquared energies have been measured with help of the optical design program
analysis tooling as ~ %82 on a 10 µm pixel in all fields.
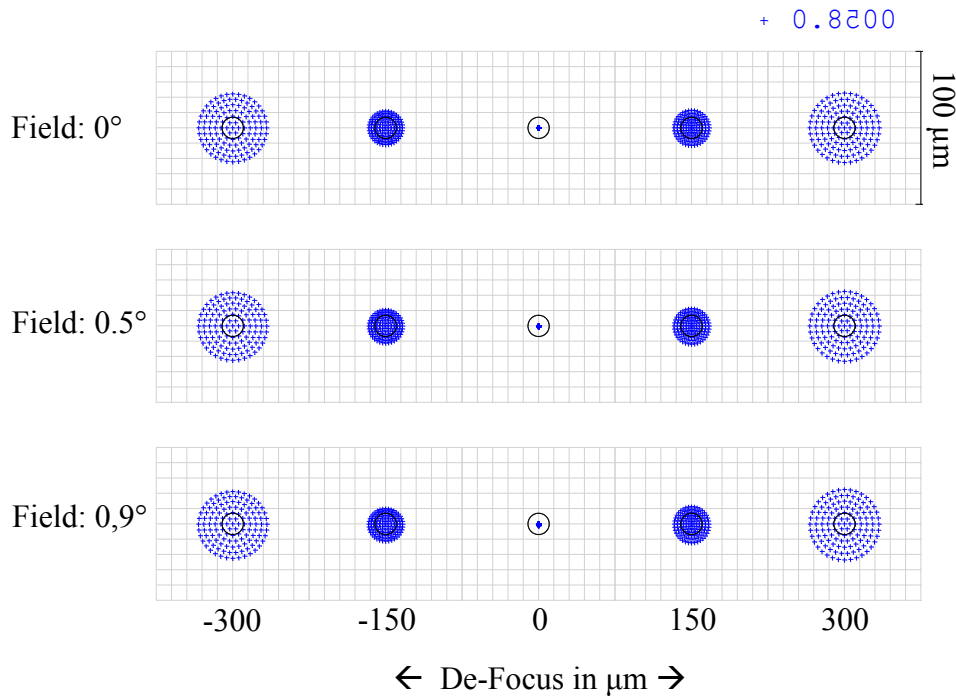
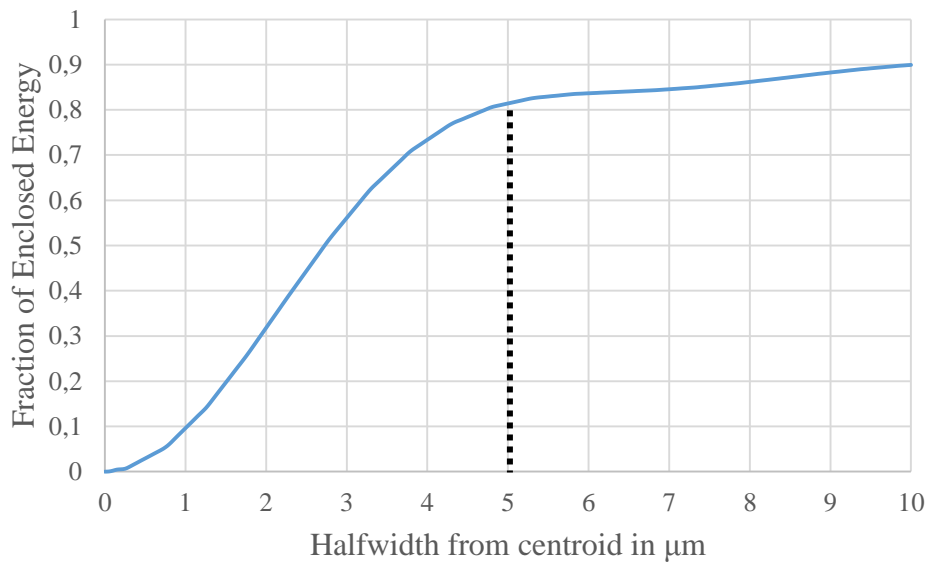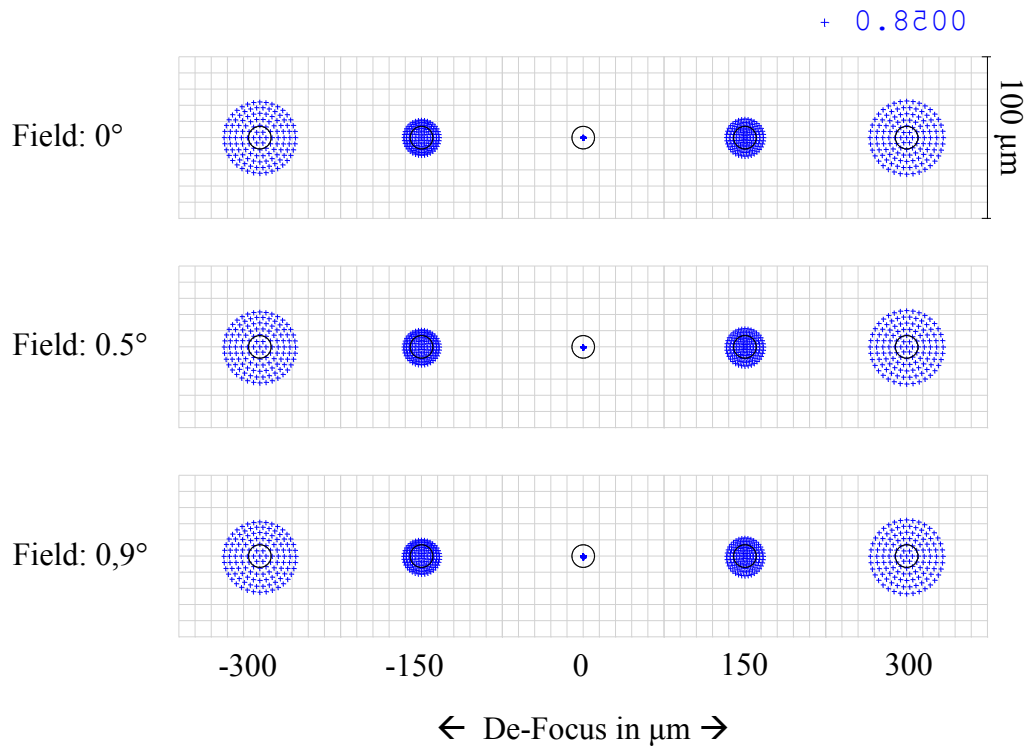Figure 7-11: The Through Spot Diagram for the 2nd gating layer at 12 m target
plane distance

The Through Spot Diagram is checked for spot size changes for the different image
plane locations and is given in Figure 7-11. As expected the spot sizes are getting
bigger by the image plane displacements in units of microns, because of the
controlled depth of field. Regarding image plane locations for other gating layers
that are given in Table 7.2, the first gating layer is located at +278 µm away, the
third gating layer is located at -166 µm away and the fourth gating layer is located at
-276 µm away. In Figure 7-11, it is clearly seen that the spot sizes exceed the airy

disk for -150 μm location and get very big at -300 μm and +300 μm locations which mean a blurred image will be contracted at the third layer and totally blurred image will be contracted in first and fourth gating layers for this image plane location.
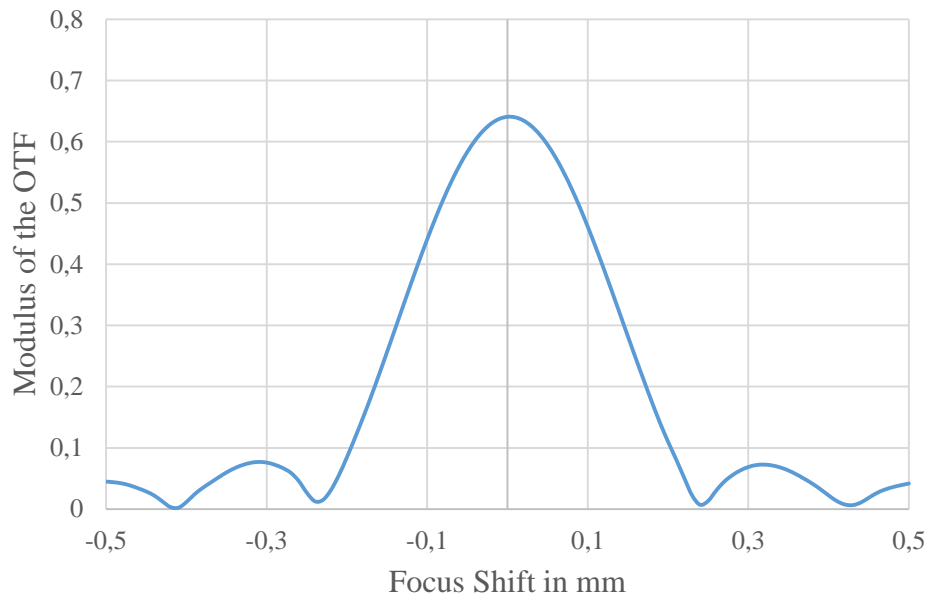

Figure 7-12: The Diffraction Through Focus Diagram for the 2nd gating layer at 12 m target plane distance

Also, diffraction through focus diagram (Figure 7-12) shows that OTF values will be decreased down to approximately %12 for the first gating layer image position at +278 μm, approximately %31 for the third gating layer image position at -166 μm and OTF values will be decreased down to approximately %12 for the third gating layer image position at -276 μm.

7.3.3 Results for Target Plane at 15 m

The third image plane location is found for the third gating layer as 29.829 mm for the target distance of 15 m. The results for 29.829 mm image plane location and 15

m target distance show that the rays are perfectly in-focus condition on FPA. The MTF graphs and spot diagrams on the image plane are worked below for analyzing the imaging quality of the design.

Spot diagram results on the image plane in its original location are given in Figure 7-13. In the spot diagram, it is seen that the spot sizes on the sensor plane are much smaller than the airy disk for each field which means that optical design is diffraction limited.
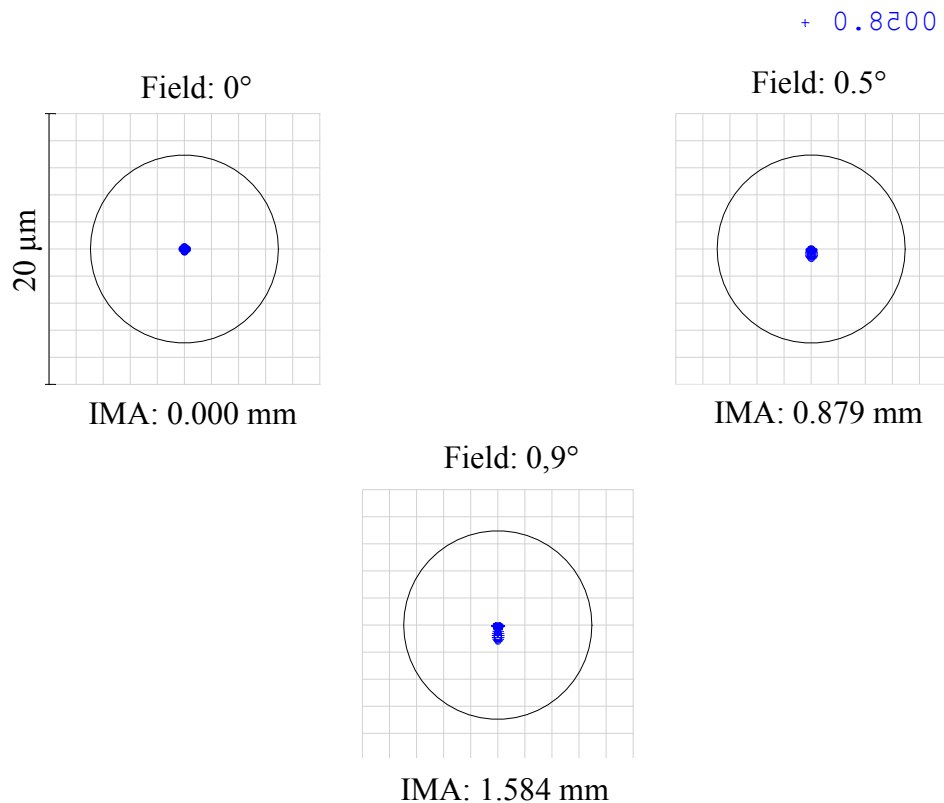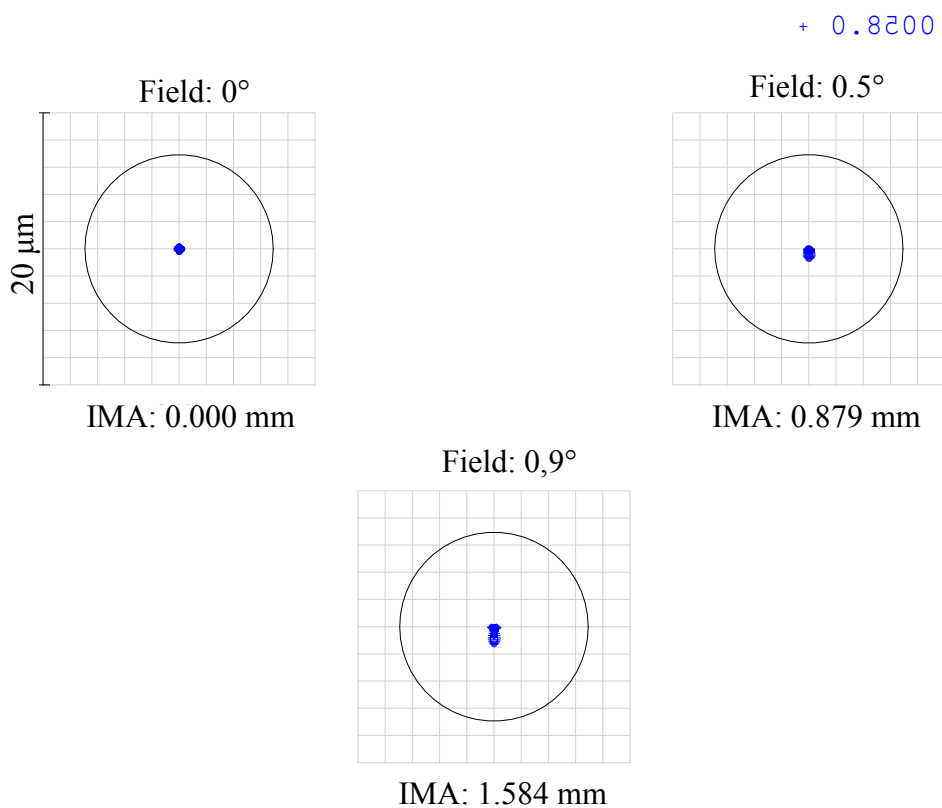

Figure 7-13: The Spot Diagram for the 3rd gating layer at 15 m target plane distance

Figure 7-14, it is seen that the OTF value for 50 cycles is around 0.65 which means that a perfect imaging result is expected from the optical design.
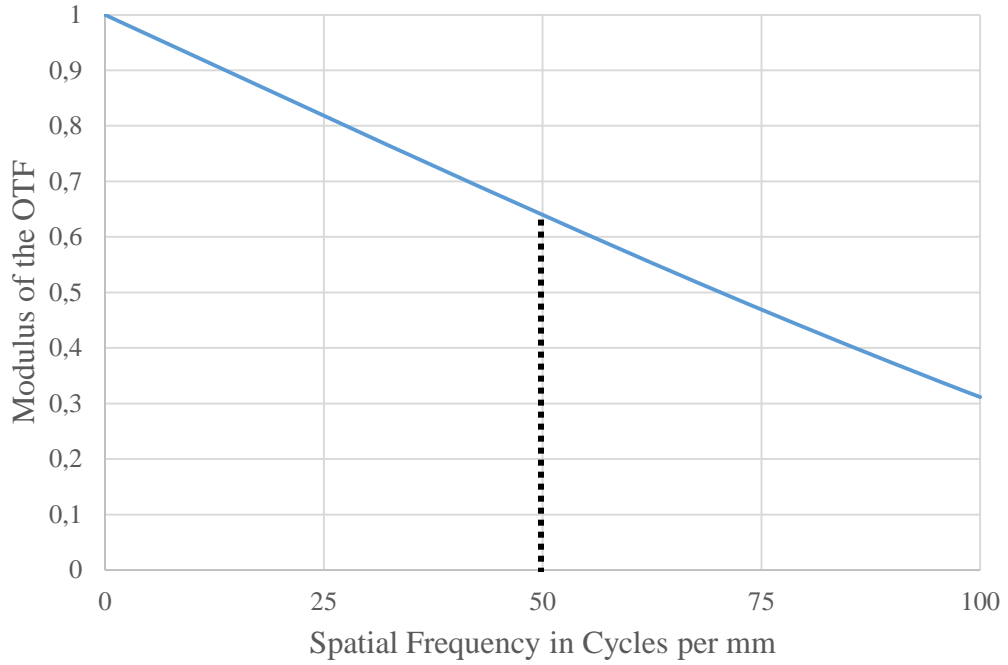
Figure 7-14: The MTF Diagram for the 3rd gating layer at 15 m target plane
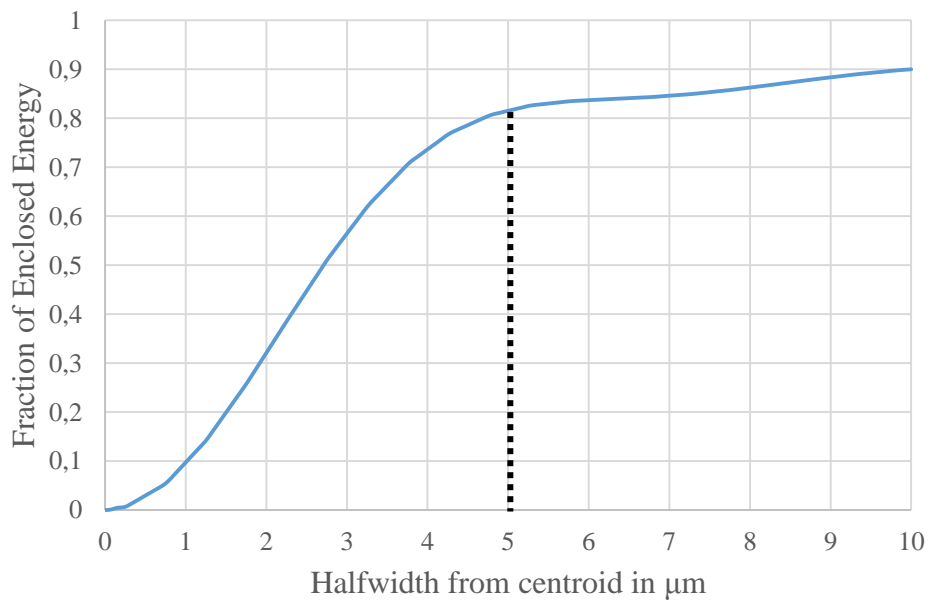distance

Figure 7-15: The Ensquared Energy Diagram for the 3rd gating layer at 15 m target plane distance
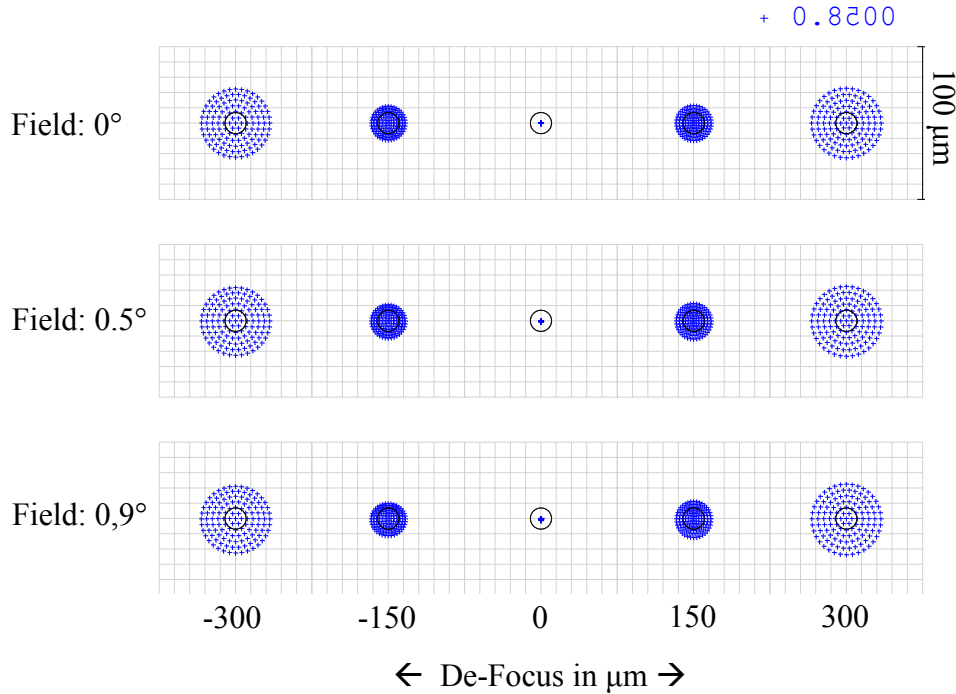
Figure 7-16: The Through Spot Diagram for the 3rd gating layer at 15 m target plane distance

The ensquared energies have been measured with help of the optical design program. The ensquared energy is found around %82 on a 10 µm pixel in all fields.

The Through Spot Diagram is checked for spot size changes for the different image plane locations and is given in Figure 7-16. Regarding image plane locations for other gating layers that are given in Table 7.2 the first gating layer is located at +444 µm away, the second gating layer is located at +166 µm away and the fourth gating layer is located at -110 µm away. In Figure 7-16, it is clearly seen that the spot sizes exceed the airy disk for -150 µm and +150 µm locations and get very big at +300 µm which means a blurred image will be contracted at the second and fourth layers

118

and the totally blurred image will be contracted in first gating layer for this image plane location.
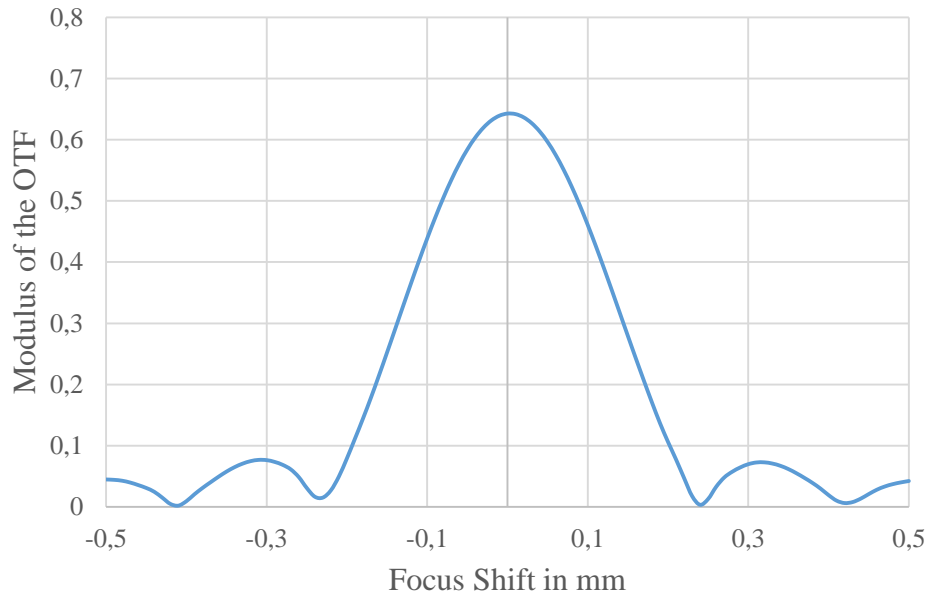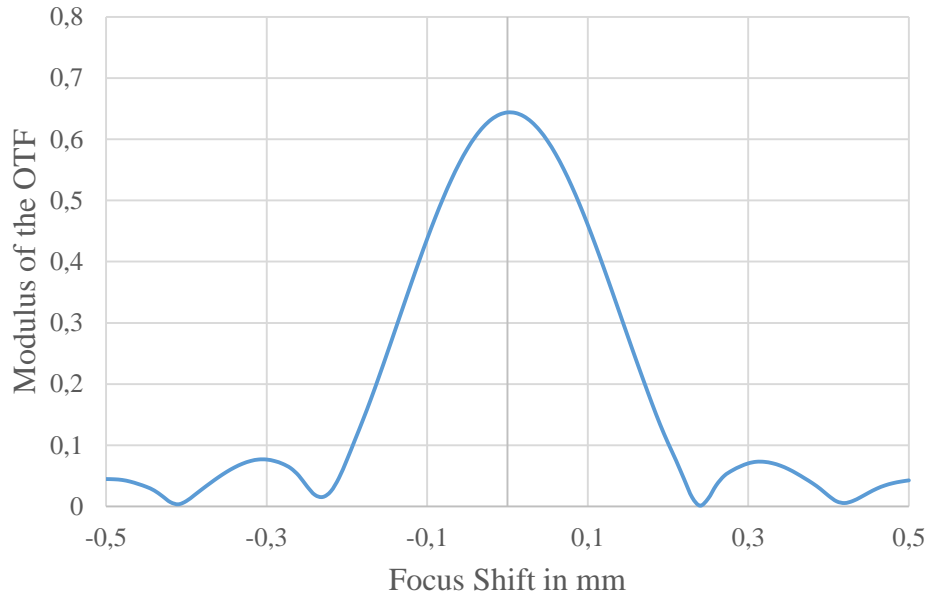

Figure 7-17: The Diffraction Through Focus Diagram for the 3rd gating layer at 15 m target plane distance

Also, diffraction through focus diagram (Figure 7-17) shows that OTF values will be decreased down to approximately %6 for the first gating layer image position at +444 μm, approximately %31 for the second gating layer image position at +166 μm and OTF values will be decreased down to approximately %58 for the third gating layer image position at -110 μm.

7.3.4   Results for Target Plane at 18 m

The final image plane location is found for the fourth gating layer as 29.719 mm for the target distance of 18 m. The results for 29.719 mm image plane location and 18 m target distance show that the rays are perfectly in-focus condition on FPA. The

MTF graphs and spot diagrams on the image plane are worked below for analyzing the imaging quality of the design.

Spot diagram results on the image plane in its original location are given in Figure 7-18. In the spot diagram, it is seen that the spot sizes on the sensor plane are much smaller than the airy disk for each field which means that optical design is diffraction limited.
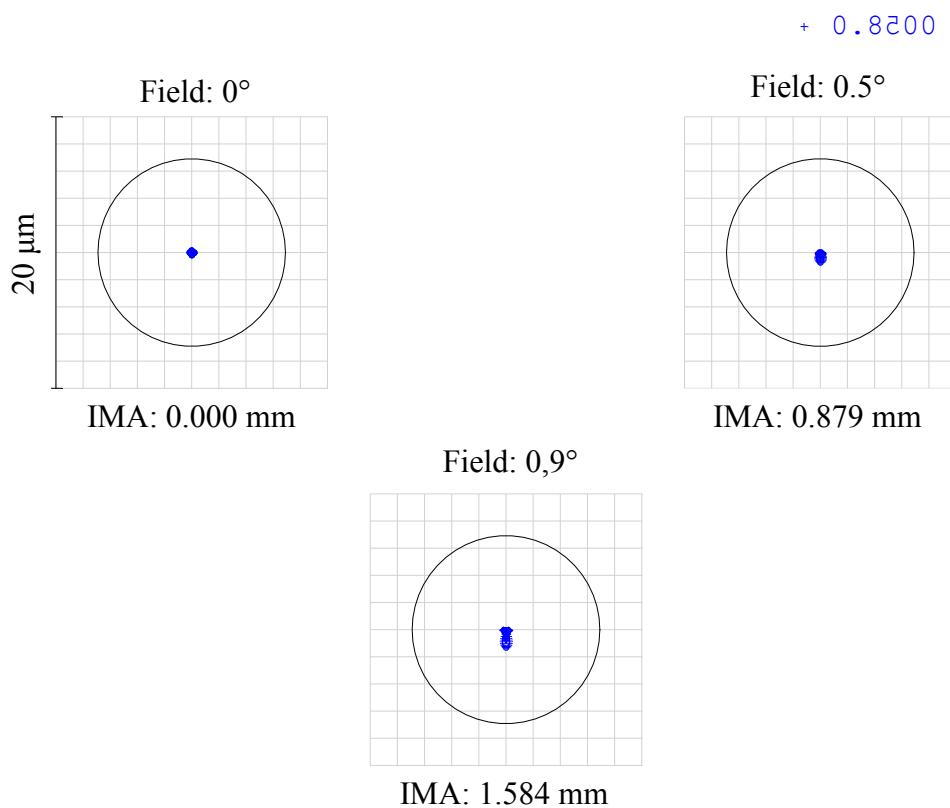
Figure 7-18: The Spot Diagram for the 4th gating layer at 18 m target plane distance

In
Figure 7-19, it is seen that OTF value for 50 cycles is around 0.65 which means that a perfect imaging result is expected from the optical design.
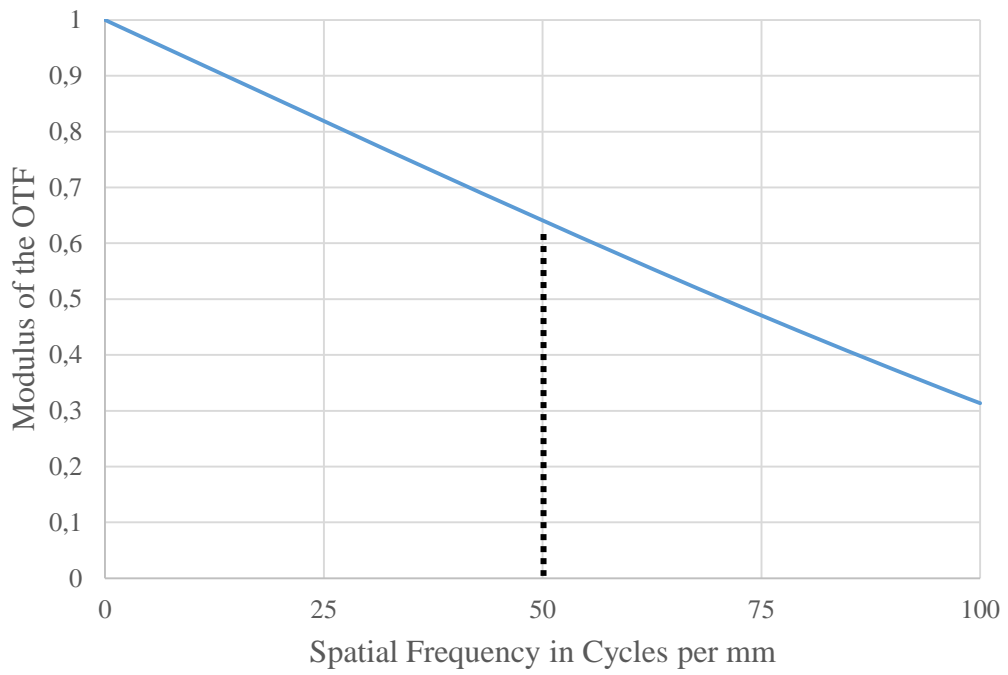
120

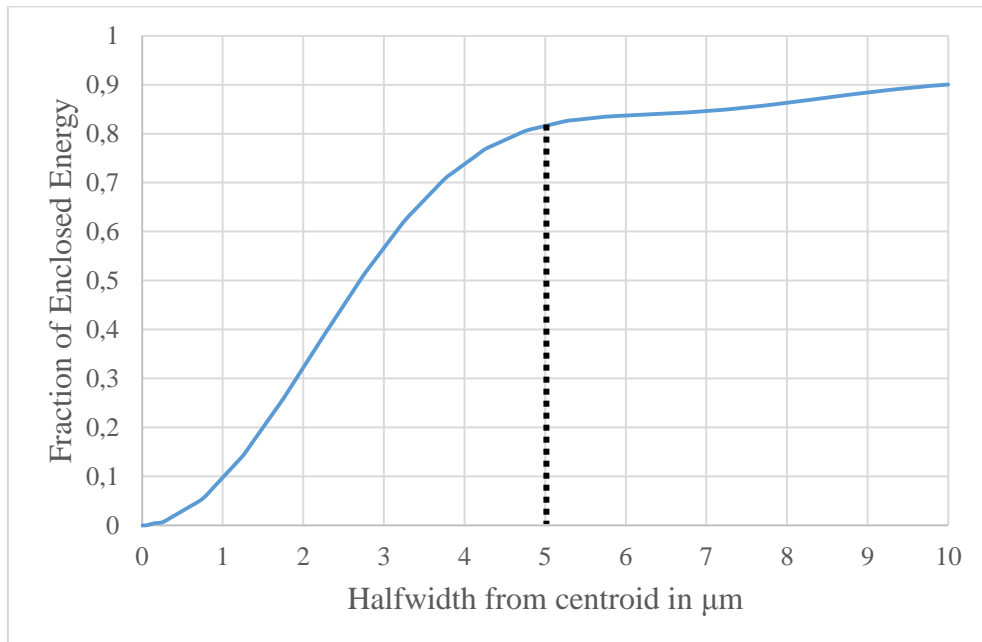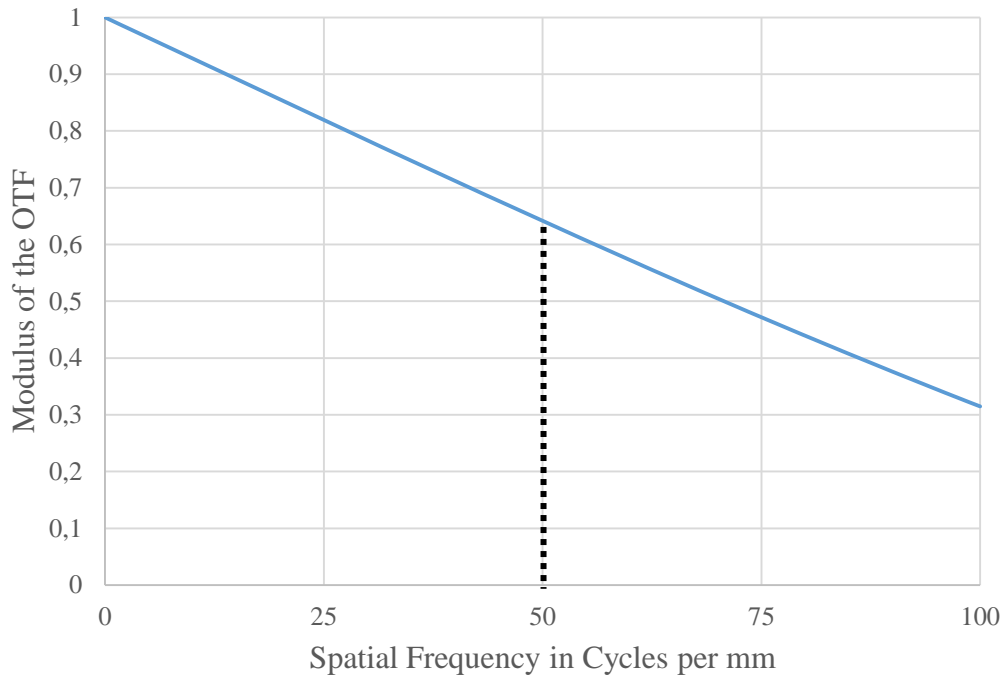Figure 7-19: The MTF Diagram for the 4th gating layer at 18 m target plane
distance
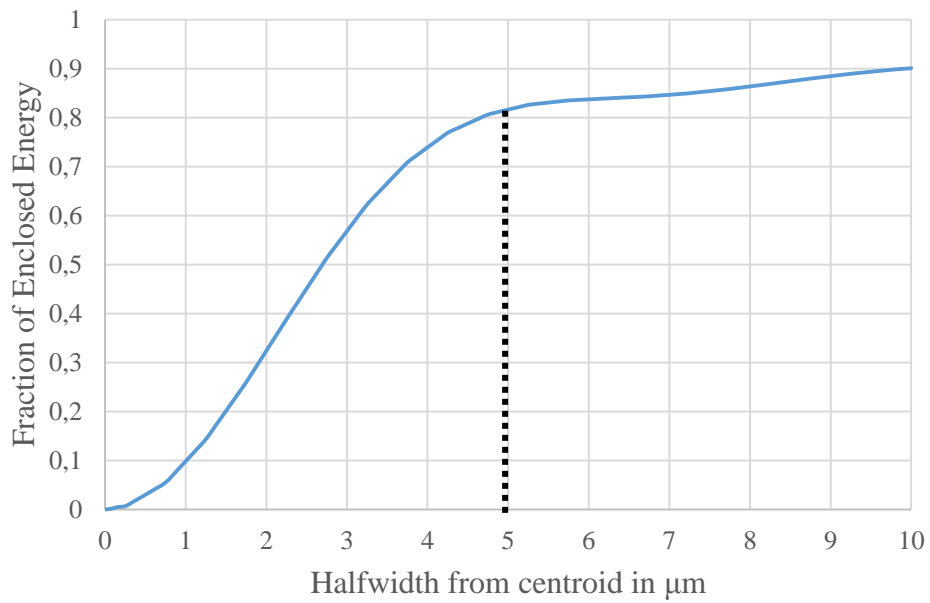
Figure 7-20: The Ensquared Energy Diagram for the 4th gating layer at 18 m target
plane distance

The ensquared energies have been measured with help of the optical design program. The ensquared energy is found around %82 on a 10 μm pixel in all fields.
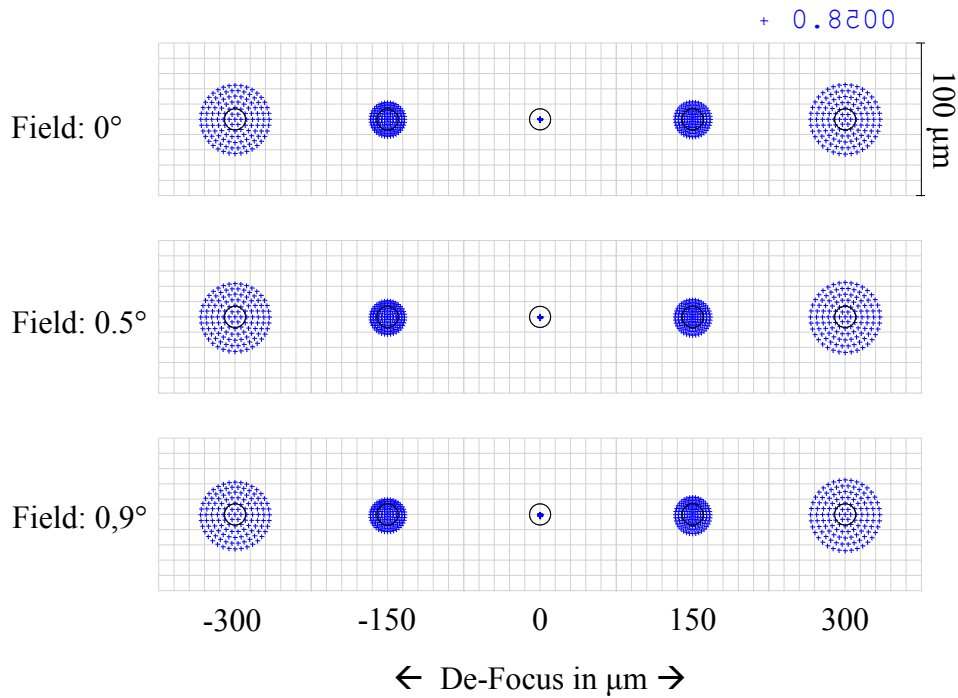
Figure 7-21: The Through Spot Diagram for the 4th gating layer at 18 m target plane distance

The Through Spot Diagram is checked for spot size changes for the different image plane locations and given in Figure 7-21. Regarding image plane locations for other gating layers that are given in Table 7.2, the first gating layer is located at +554 μm away, the second gating layer is located at +276 μm away and the third gating layer is located at +110 μm away. In Figure 7-21, it is clearly seen that the spot sizes exceed the airy disk for +150 μm location and get very big at +300 μm which means a blurred image will be contracted at the third gating layer and totally blurred image will be contracted in first and second gating layers for this image plane location.
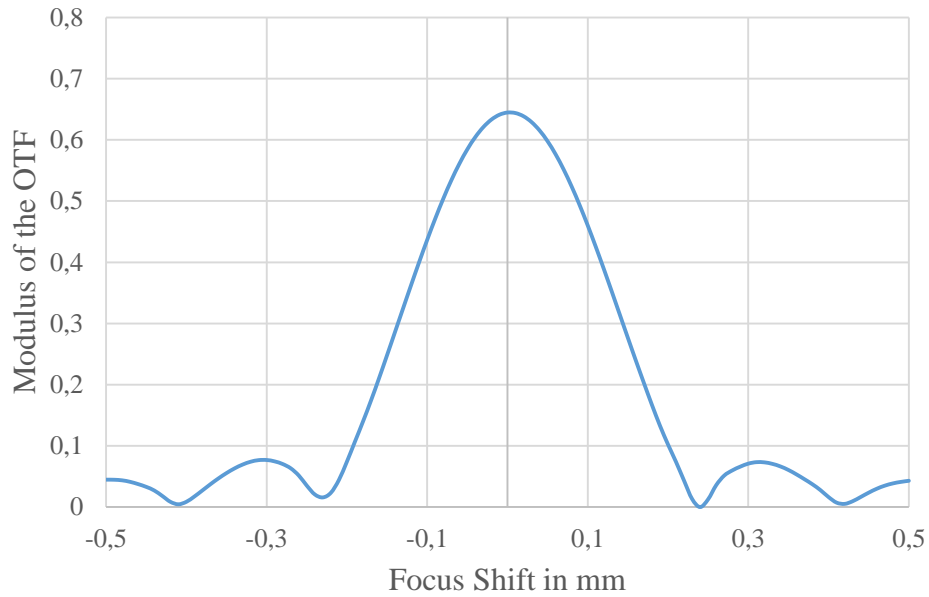
Figure 7-22: The Diffraction Through Focus Diagram for the 4th gating layer at 18 m target plane distance

Finally, diffraction through focus diagram (Figure 7-22) shows that OTF values will be decreased down to approximately %6 for the first gating layer image position at +554 μm, approximately %12 for the second gating layer image position at +266 μm and OTF values will be decreased down to approximately %58 for the third gating layer image position at +110 μm.

7.4 Chapter Discussion

The results of the optical design show that a good spatial resolution is achieved for all predefined FPA locations in the image plane with a controlled depth of focus values as aimed. In the results, it is seen that for the first gating layer, OTF values and spot sizes are good enough for a clear image construction for the FPA location on 30.273 mm where OTF values are very low and spot sizes are very big for the FPA locations on 29.995 mm, 29.829 mm and 29.719 mm, which means that totally

blurred images and very low signal levels are expected for FPA positions at 29.995 mm, 29.829 mm and 29.719 mm.

For the second gating layer, results show that OTF values and spot sizes are very good for a clear image construction for the FPA location on 29.995 mm where OTF values are very low and spot sizes are very big for the FPA locations on 30.273 mm, 29.829 mm and 29.719 mm, which means that blurred images and very low signal levels are expected for FPA positions at 30.273 mm, 29.829 mm and 29.719 mm. For the third gating layer, results show that OTF values and spot sizes are very good for a clear image construction for the FPA location on 29.829 mm where OTF values are very low and spot sizes are very big for the FPA locations on 30.273 mm, and OTF values are low and spot sizes are big for 29.995 mm and 29.719 mm. So blurred images and low signal intensities are expected for FPA positions at 29.995 mm and 29.719 mm, and totally blurred images with very low signal levels are expected for FPA position 30.273 mm.

Finally, for the third gating layer, results show that OTF values and spot sizes are very good for a clear image construction for the FPA location on 29.719 mm where OTF values are very low and spot sizes are very big for the FPA locations on 30.273 mm, and OTF values are low and spot sizes are big for 29.995 mm and OTF values are lower and spot sizes are bigger, but close to values at 29.719 mm, for 29.829 mm. So little blurred images with lower signal intensities are expected for the FPA position 29.829 mm. Blurred images with lower signal intensities are expected for the FPA position at 29.995 mm, and totally blurred images with very low signal levels are expected for FPA position 30.273 mm.

For further analysis, the normalized energy levels on each sensor plane are measured by the encircled energy analysis tool of the optical design program, for observing the energy changes on the different gating layers for the target distances 9 m, 12 m, 15 m, and 18 m. The results of the normalized energy diagram are given in Figure 3-12.

It is seen that the concept works for the determined target layers and the energy is collected on the corresponding sensor planes for each 2mm separated target layer. Figure 7-23 shows that not only a totally clear (not blurred) image is constructed on the corresponding gating layer, but also there will be very low-intensity noise levels on the other FPA locations.
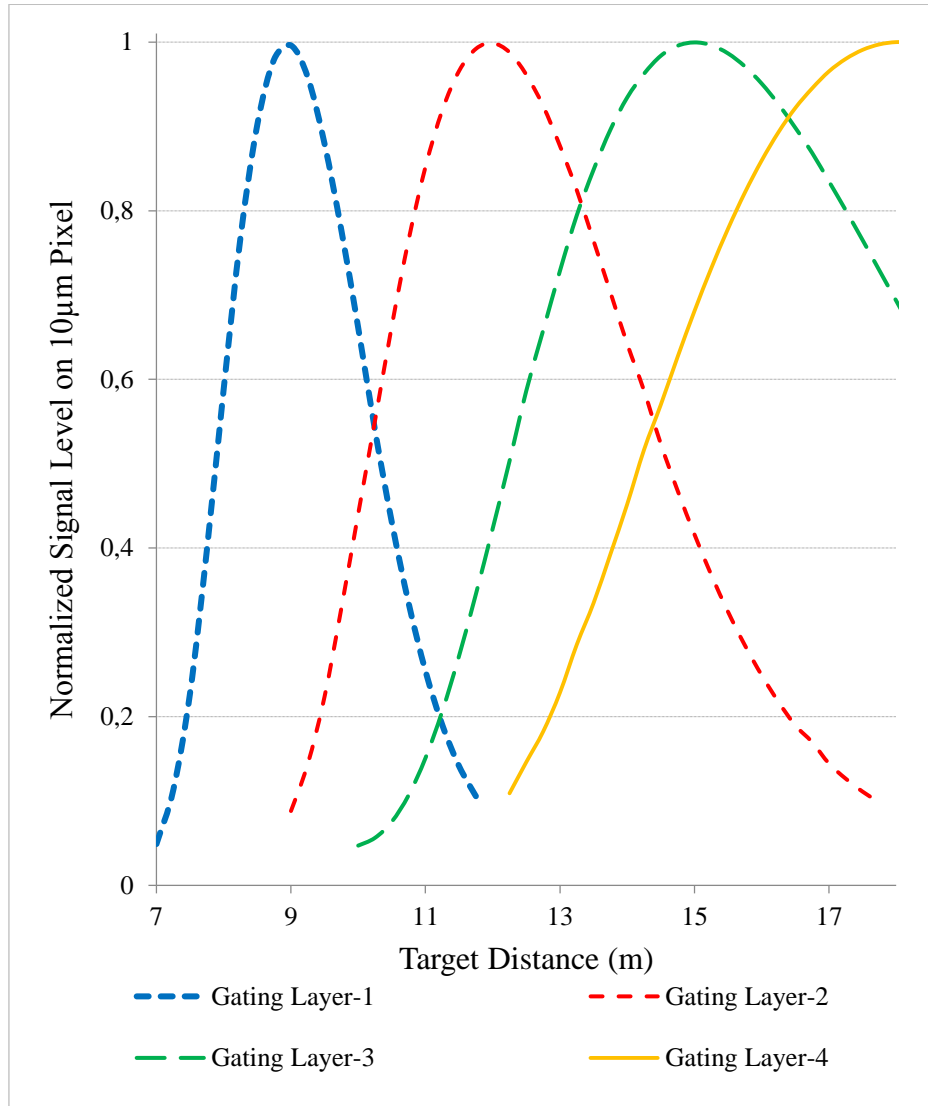
Figure 7-23: The Normalized Encircled Energy Diagrams on 10 µm Pixel of AMCW LIDAR FPA for different target point heights and different image plane displacements.

Figure 7-23 has been zoomed to aimed measurement range which is between 7 m and 16 m in Figure 7-24, and also gating layer regions are shown in the figure for a better representation of the gating layers.
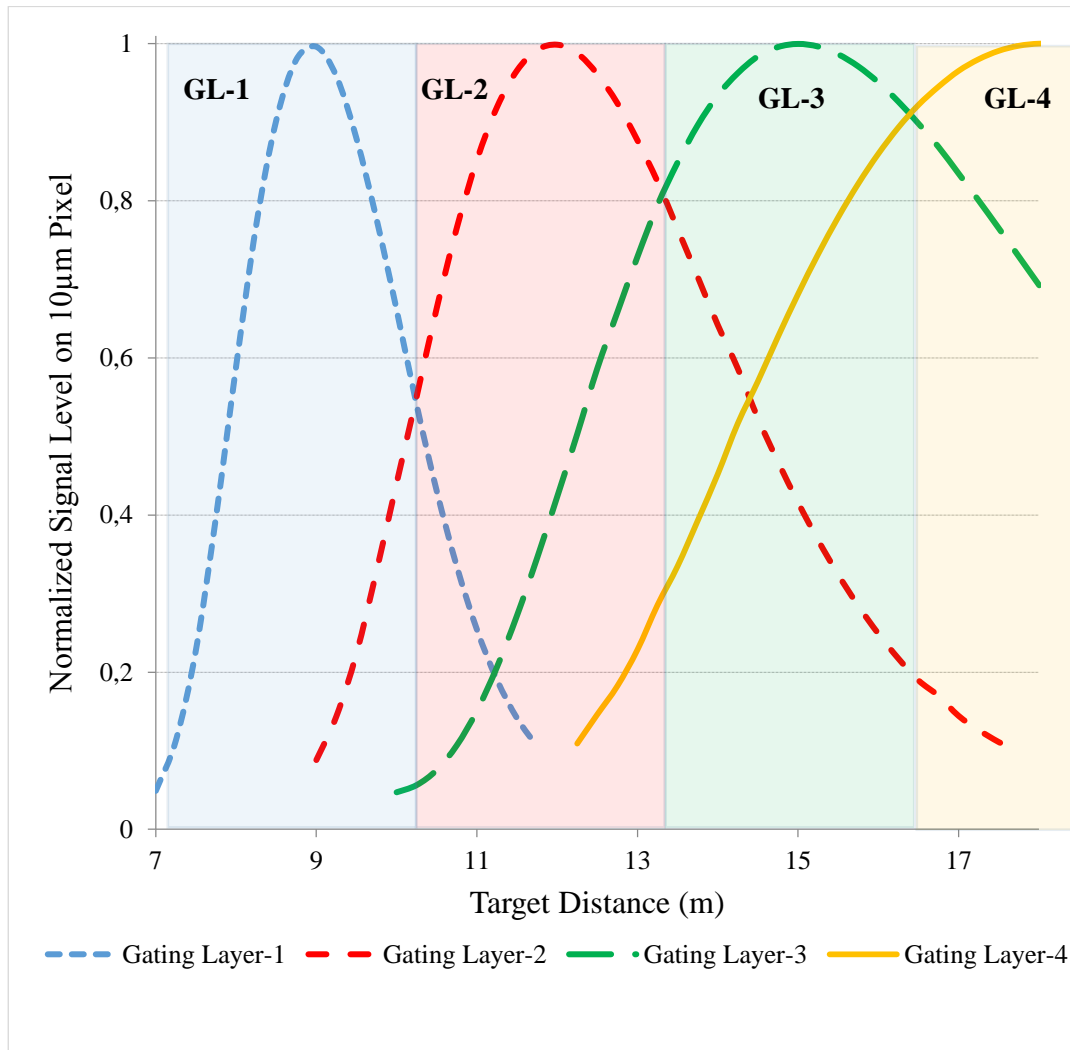
Figure 7-24: The Detailed Normalized Encircled Energy Diagrams on 10 µm Pixel of AMCW LIDAR FPA for different target point heights and different image plane displacements.

126
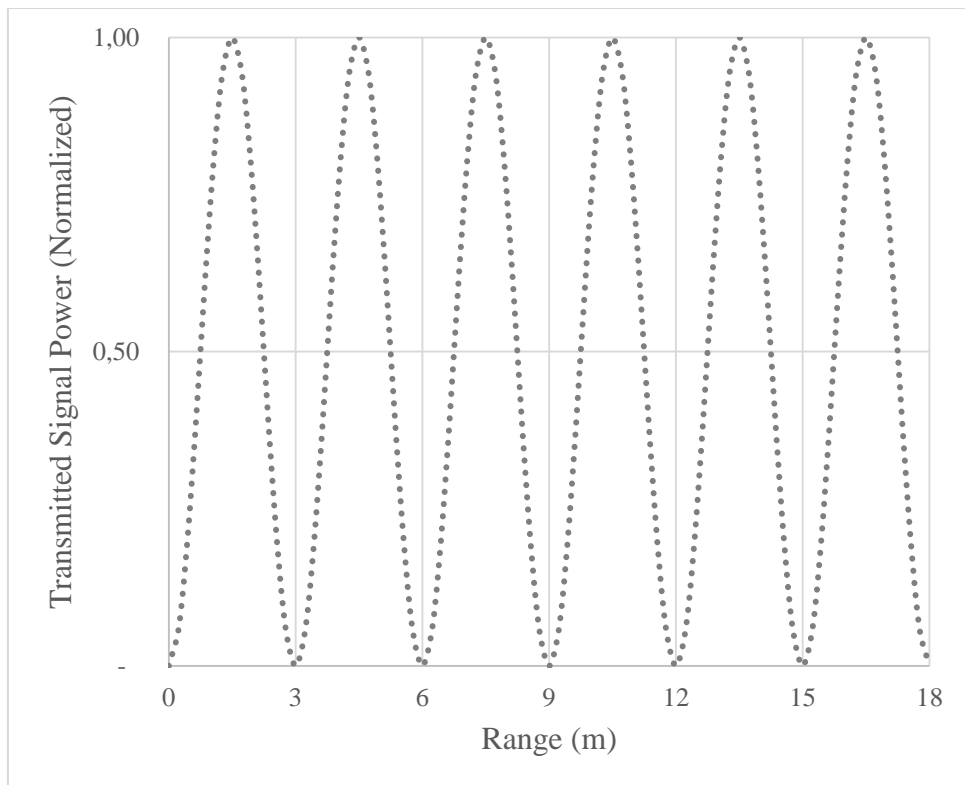
Figure 7-25: The amplitude modulated signal that used for illumination of the targets.

For further analysis, the AMCW signal is modeled as given in Figure 7-25 and the received signals, which will be created by the reflected signal from the target surface, are modeled and the results are given below.

As the first step, the received signals have been modeled for a standard AMCW LIDAR measurement case which is not using any gating layers. The target distances are selected as 8.25 m, 11.25 m, 14.25 m, and 17.25 m which shows the ambiguity problem for a standard AMCW LIDAR range measurement method. In Figure 7-26, it is seen that the received signals have exactly the same phase difference as the transmitted signal for the target distances 8.25 m, 11.25 m, 14.25 m, and 17.25 m. So it is impossible to distinguish the right distances of the objects which are at longer

distances than the 3 m ambiguity range, because of the ambiguity problem shown in Figure 7-26.

Transmitted and Collected Signals for Tatgets at 8,25 m, 11,25 m, 14,25 m and 17,25 m
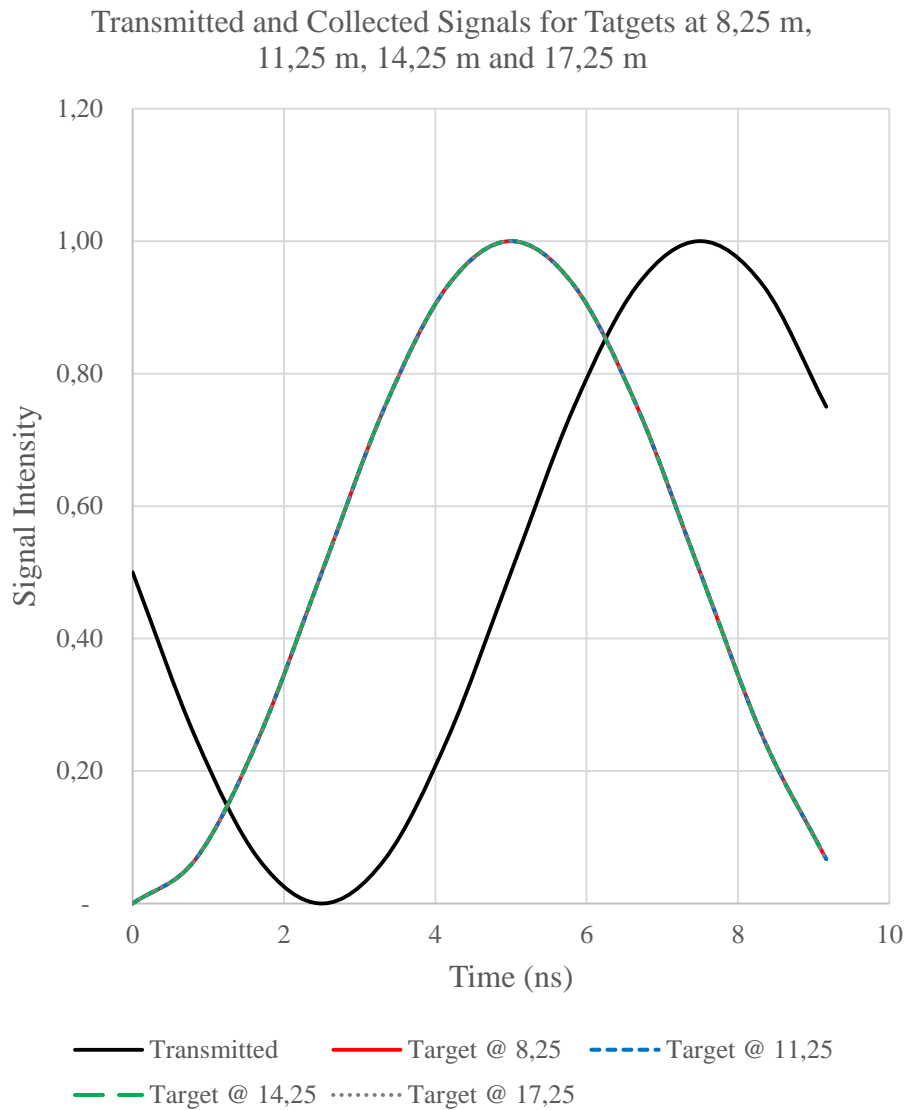
Figure 7-26: The Transmitted and Received signals of AMCW range measurement for the target distances 8.25 m, 11.25 m, 14.25 m and 17.25 m.
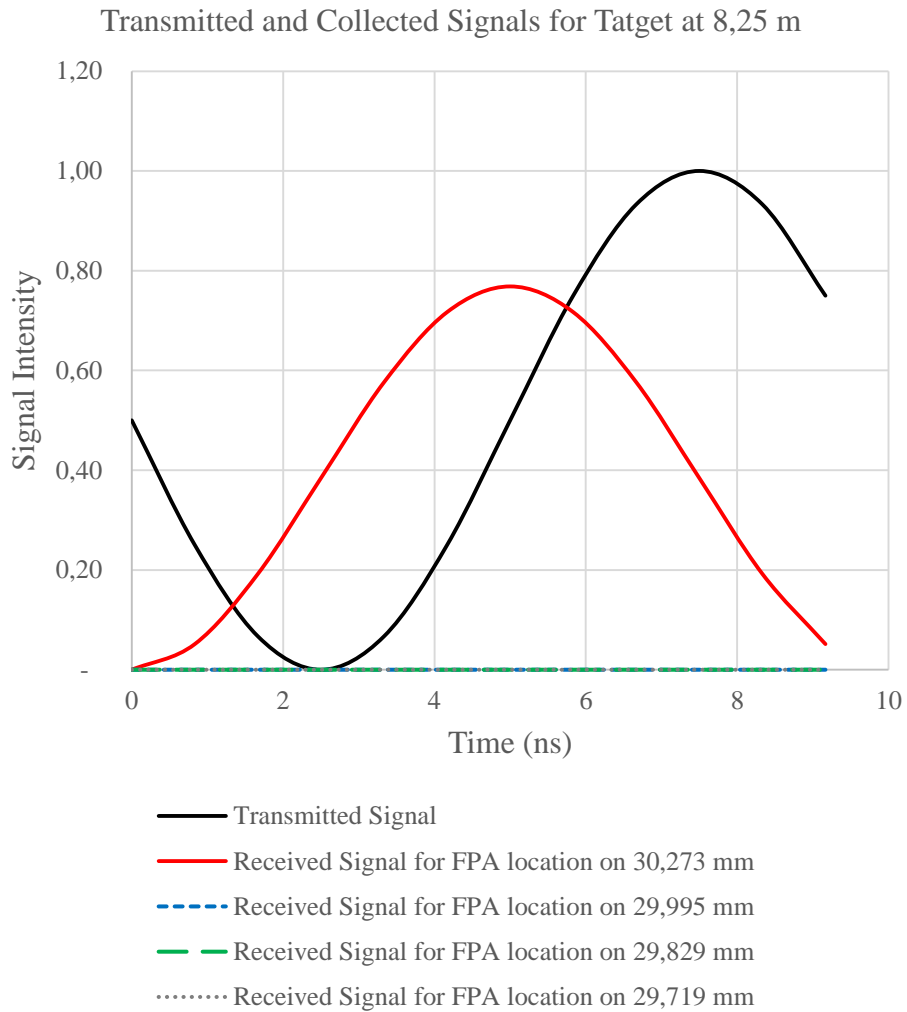
Figure 7-27: The Transmitted and Received signal Levels of AMCW Multifocal
LIDAR System for 8.25 m target distance

In Figure 7-27, the received signals have been modeled for an AMCW Multifocal
LIDAR Imaging System for a target at a distance of 8.25 m. It is easily seen that
there is a meaningful signal only for 30.273 mm FPA location with a phase
difference that gives the displacement between the nearest $N2\pi$ phase shift point
which is 9 m for the first gating layer.
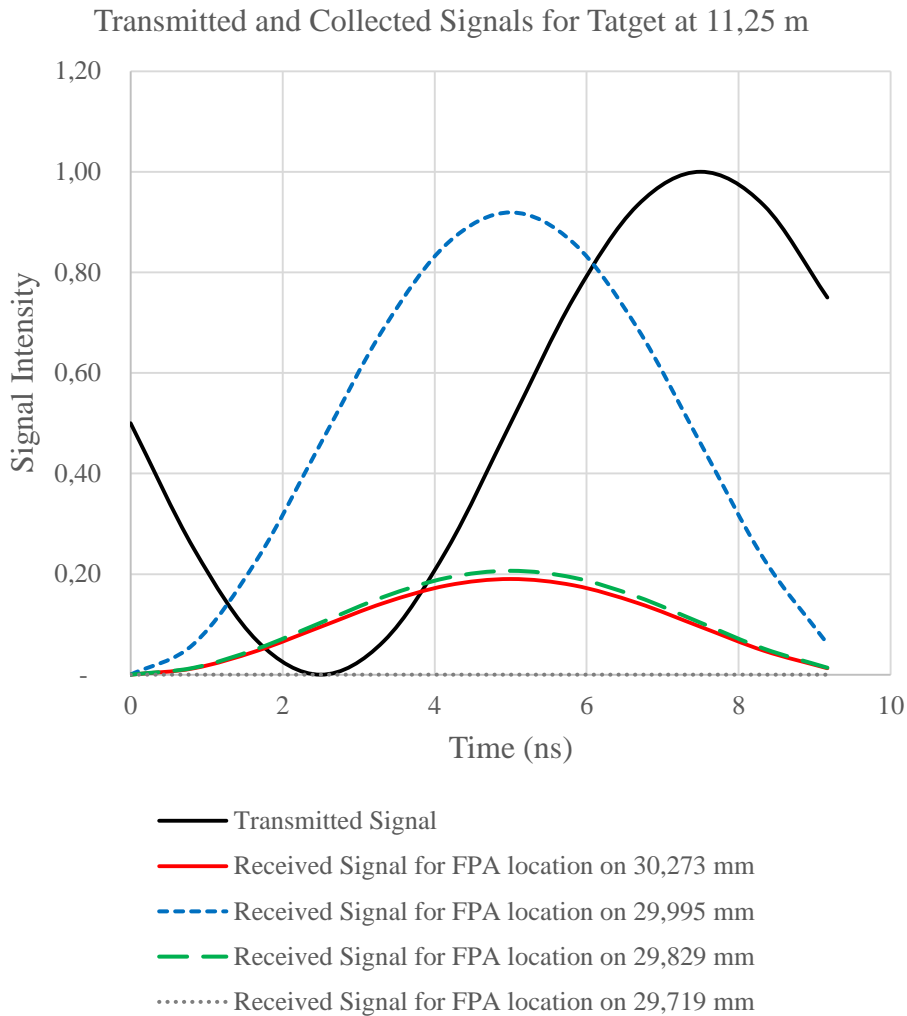
Figure 7-28: The Transmitted and Received signal Levels of AMCW Multifocal LIDAR System for 11.25 m target distance

In Figure 7-28, the received signals have been modeled for an AMCW Multifocal LIDAR Imaging System for a target at a distance of 11.25 m. The results show the generated signals for the FPA locations on 30.273 mm, 29.995 mm, 29.829 mm, and 29.719 mm. The highest signal level is gathered for the FPA position on 29.995 mm which refers to the second gating layer. Again it can be seen that phase shift is the same and it gives the displacement between the nearest N2π phase shift point which is 12 m for the second gating layer.
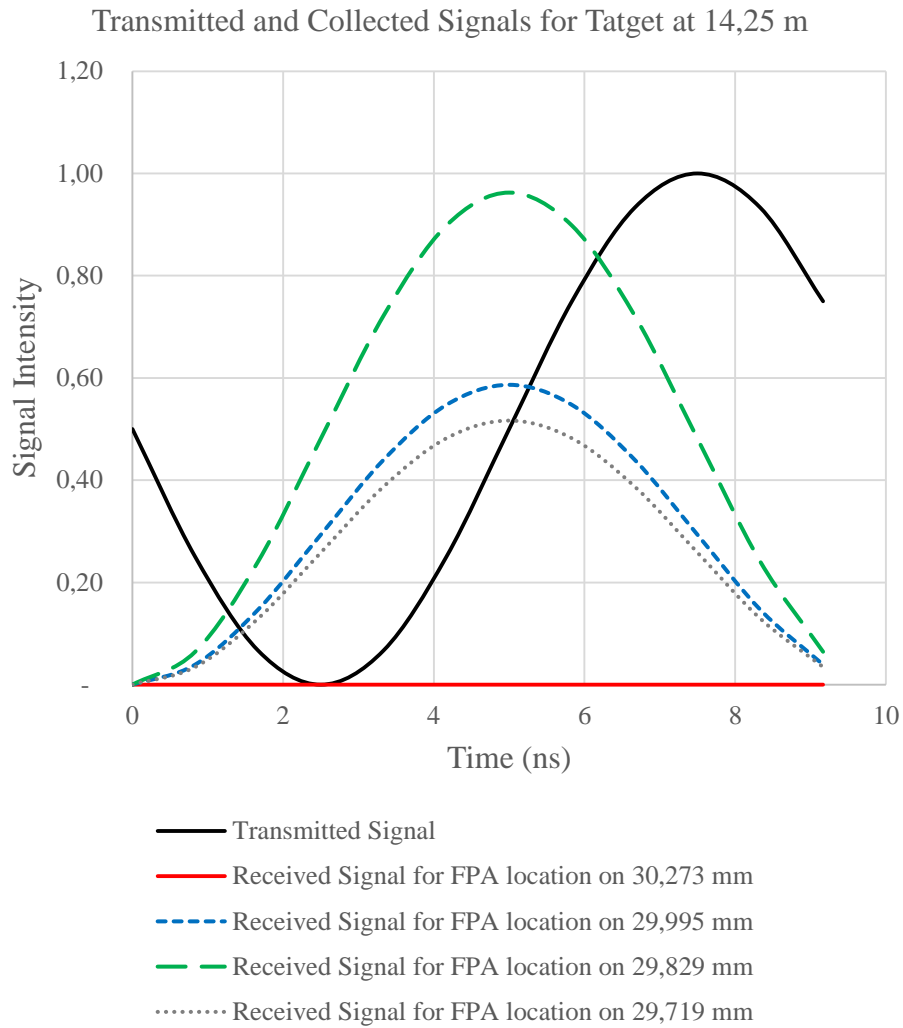
Figure 7-29: The Transmitted and Received signal Levels of AMCW Multifocal
LIDAR System for 14.25 m target distance

In Figure 7-29, the received signals have been modeled for an AMCW Multifocal
LIDAR Imaging System for a target at a distance of 14.25 m. The results show the
generated signals for the FPA locations on 30.273 mm, 29.995 mm, 29.829 mm, and
29.719 mm. The highest signal level is gathered for the FPA position on 29.829 mm
which refers to the third gating layer. It is seen that the signal levels between the FPA
position on 29.829 mm and other FPA positions are well distinguishable so it is easy
to say the target distance in the third gating layer. The phase shift is the same and it

gives the displacement between the nearest N2π phase shift point which is 15 m for the second gating layer.

Transmitted and Collected Signals for Tatget at 17,25 m
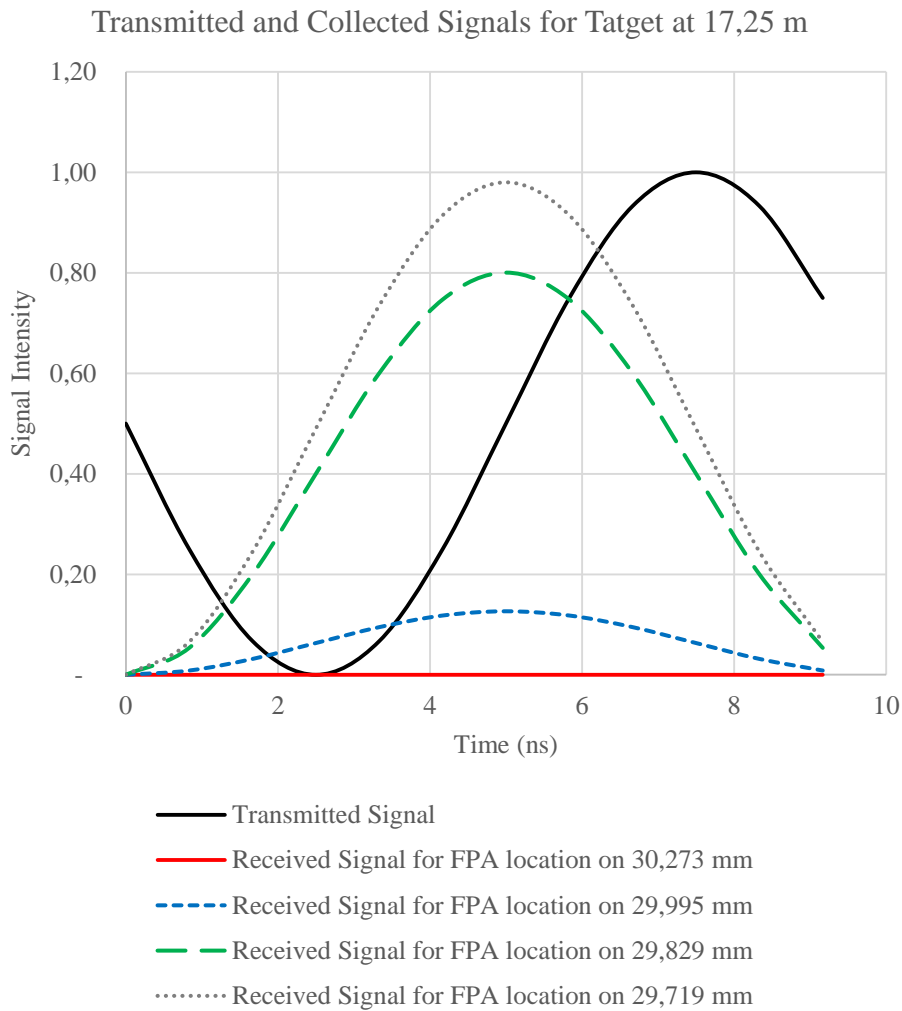
Figure 7-30: The Transmitted and Received signal Levels of AMCW Multifocal LIDAR System for 17.25 m target distance

In Figure 7-30, the received signals have been modeled for an AMCW Multifocal LIDAR Imaging System for a target at a distance of 17.25 m. The results show the generated signals for the FPA locations on 30.273 mm, 29.995 mm, 29.829 mm, and 29.719 mm. The highest signal level is gathered for the FPA position on 29.719 mm

which refers to the fourth gating layer. It is seen that the signal levels between the FPA position on 29.719 mm and other FPA positions are well distinguishable so the target distance in the fourth gating layer. Again, the phase shift is the same with previous examples and it gives the displacement between the nearest $N2\pi$ phase shift point which is 15 m for the second gating layer.

In the conclusion of the chapter, the results show that it is possible to use the depth of focus and multifocal imaging methods at creating gating layers for the AMCW LIDAR imaging system to enhance the measurement range to a few times of ambiguity range without any depth resolution losses. The results may enlarge the AMCW LIDAR application areas which are limited by the ambiguity problem.

CHAPTER 8

LIMITATIONS OF THE MULTIFOCAL LIDAR IMAGING

As described in chapter 1.2, multifocal imaging technique requires a narrow Field of Depth for distinguishing target layers from each other. The equation (1-33), can be re-written as;

$$d = \frac{2NCD^2}{f^2} = \frac{2CD^2}{f^2} \cdot \frac{f}{A} = \frac{2CD^2}{fA} \tag{8-1}$$

where N=f/A and A is the clear aperture of the optical system.

As shown in previous chapters, the width of the depth of field specifies the achievable depth resolution by the Multifocal LIDAR System. Regarding equation (8-1), we need a small circle of confusion diameter C, a small target distance D with high focal length f, and a high clear aperture to achieve higher depth resolutions.

On the other hand, the packaging is also a limiting factor for productibility. In Multifocal Lidar and Chromatic Multifocal LIDAR techniques, we need enough spacing to locate the pinhole detectors on the same optical axes. The distances between the detectors are limited with the depth of focus where The equation (1-35) can be re-written as,

$$s = \frac{2NCD}{f} = \frac{2CD}{f} \cdot \frac{f}{A} = \frac{2CD}{A} \tag{8-2}$$

So for achievable packaging or productibility of the system, we need a high circle of confusion diameter C, high target distance D, and a small clear aperture.

Another limiting factor of the system can be defined as the IFOV where small IFOV values will cause more scanning points to get the desired total field of regard area. The increasing focal length of the system for higher depth resolution will cause a loss from the total field of regard of the system.

Regarding described limitations, optimization on the desired depth resolution, field of regard, packaging, and cost-effectiveness (where high clear aperture values cause high optical system costs) shall be done depending on the application-specific requirements. The limiting results of the proof of concept works are defined below.

Table 8.1 The limitations of Multifocal, Chromatic Multifocal and Chromatic Multifocal with Dispersion Prism LIDAR Imaging Systems

Design	Depth Resolution	Maximum Measurement Range	Required Min. Distances Between Sensors
Multifocal LIDAR System	2 mm	0,974 m	0,65 mm
Chromatic Multifocal LIDAR System	2 mm	0,799 m	0,8 mm
Chromatic Multifocal LIDAR System with Dispersion Prism	2 mm	0,601 m	N/A
Multifocal LIDAR System	5 mm	1.541 m	1,03 mm
Chromatic Multifocal LIDAR System	5 mm	1.264 m	1,27 mm
Chromatic Multifocal LIDAR System with Dispersion Prism	5 mm	0,950 m	N/A

In Table 8.1, it is seen that the Multifocal LIDAR system can be used up to almost 1 m range with the current optimization. Also, this measurement range can be increased up to 1,5 m for 2 mm desired depth resolution, by increasing the clear aperture diameter to 10 cm and the focal length of the system up to 400 mm. It is also possible to extend the measurement range of the system up to 3,16 m with 2 cm desired depth resolution, 10 cm clear aperture, and 400 mm focal length. In any case, it is seen that basic Multifocal LIDAR Imaging is working in short distances and is good for applications that require high depth resolution in short ranges such as automation, robotic, etc.
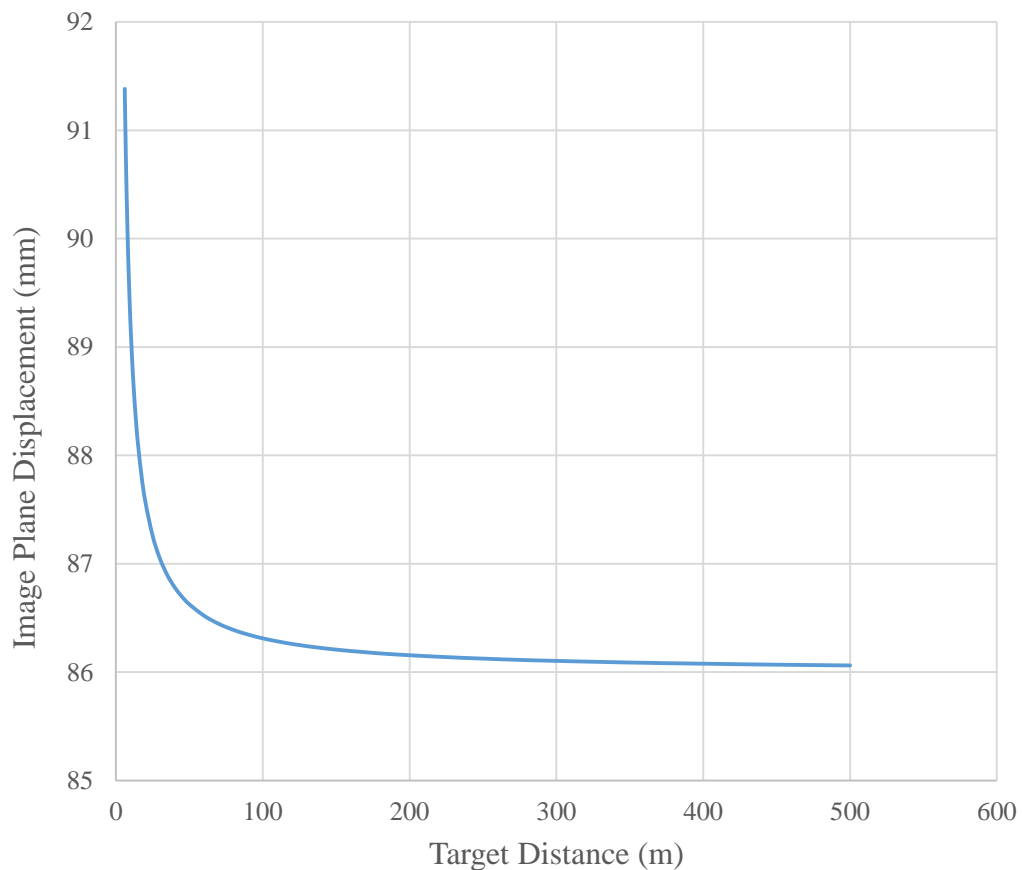
Figure 8-1: The Image Plane Position change regarding to Target Distances for Advanced Multifocal LIDAR Imaging System

For the Advanced Multifocal LIDAR Imaging system, although we are using the depth of field to distinguish the different target layers, we do not need to separate the target layers with the whole width of the field of depth. The image plane position change for different target distances for the Advanced Multifocal LIDAR Imaging system is given in Figure 8-1. In Figure 8-1 it is seen that the image plane position change exponentially decreases for high target distances. This shows that we will need nm step resolution at high distances, to observe the amplitude change that we get in chapter 6 with a 1.02 μm image plane position shift. So, the depth resolution that can be achieved at higher distances is limited by the step resolution of the high-resolution positioner system. Or in other words, for s specific required depth resolution, the maximum measurement range is limited by the step resolution of the high-resolution positioner system. The achievable maximum measurement ranges with the current optimized Advanced Multifocal LIDAR system are defined in Table 8.2. The results show that the Advance Multifocal Imaging system is good for mid-range applications such as autonomous driving applications in automotive, robotic, etc. Also, the Field of Regard, maximum measurement range, depth resolution, and clear aperture of the system can be optimized for different applications regarding application specific requirements.

Table 8.2 The Design Outputs of the AMCW Multifocal Imaging Optical System

Positioner Resolution	Maximum Measurement Range
1 μm	8 m
100 nm	25 m
10 nm	80 m
1 nm	250 m
0,5 nm	350 m

For the AMCW Multifocal Imaging system, depth of field is used as a tool to create gating layers for standard AMCW LIDAR systems for extending the measurement range above the ambiguity range. In chapter 7 it is shown that the maximum measurement range of a standard AMCW LIDAR system with 100 MHz modulation frequency, 5.9 mm depth resolution, and 3 m ambiguity range, is increased up to 6 times of ambiguity range without any loss at depth resolution. AMCW Multifocal LIDAR system can be used up to almost 18 m range with the current optimization. Also, this measurement range can be increased up to 80 m, by increasing the clear aperture diameter to 10 cm and the focal length of the system up to 400 mm. It is also possible to extend the measurement range of the system up to 250 m with a 5.9 cm desired depth resolution, 10 cm clear aperture, and 400 mm focal length. The results show that the AMCW Multifocal Imaging system is good for low-range and mid-range applications such as autonomous driving applications in automotive, robotic, etc. Another important advantage of the AMCW Multifocal LIDAR system is getting 500 different target layer information on a single measurement of each gating layer. So AMCW Multifocal LIDAR imaging is also suitable for applications that need near video rate imaging. Also, the Field of Regard, maximum measurement range, depth resolution, and clear aperture of the system can be optimized for different applications regarding application specific requirements.

CHAPTER 9

RESULTS AND GENERAL DISCUSSION

In this study, Multifocal LIDAR Imaging techniques have been introduced for high-resolution 3D imaging applications. The developed and introduced new hybrid methods, which use the narrow depth of field and so advantages of Multifocal Imaging, it is possible to achieve high depth resolutions beyond the Laser pulse rise time limitation of the LIDAR systems.

In the first step of this thesis, the basic design of a Multifocal LIDAR Imaging system is defined and designed with 3 separated pinhole detectors on the image plane for proving the concept theoretically. With this newly introduced method, it has been shown that multifocal imaging techniques can be combined with pulse-based direct ToF measurement techniques to enhance the depth resolution in units of mm, without complicated short pulsed light sources. The design and optical analysis results prove that; it is possible to use depth of focus as a tool in the LIDAR imaging system for getting depth information on the target surfaces with higher resolution than the standard LIDAR techniques. Our design paves the way for a simpler and cost-effective method for 3D imaging systems that use single-pixel detectors at a single photon sensitivity level.

During the design studies of the multifocal LIDAR system, it has been seen that the distances between the pinhole detectors are small for higher target distances which will create application and packaging problems for real-life applications. In the second step, a Chromatic Multifocal LIDAR method, which uses the increased chromatic aberrations as a tool for increasing the required distances between the pinhole detectors, has been developed and analyzed. The results of the developed

system show that increased chromatic aberrations can be used as a useful tool for increasing the required distances between the detectors.

Although the required detector separating distance issue has been solved and the packaging is improved by the Chromatic Multifocal LIDAR method, some complicated production techniques are still required such as alignment of the sensors on the optical axis precisely. So in step 3, the different wavelengths are separated by a dispersion prism to make all focal points on the same image plane with lateral distances to enable the usage of the linear detector arrays. The optical design and results of the third step also prove that using chromatic aberration as a tool and also dispersion mechanism for converting the distances on the optical axis to the lateral distance differences on a linear plane simplifies the system architecture and also makes it possible to measure the depth on the surface directly regarding used wavelength of light by high-resolution in units of mm.

With positive results and proof of the working concept of the Multifocal LIDAR Imaging System an advanced concept has been developed, as the fourth step of this study, for simpler packaging and easier productibility with higher numbers of depth layers and spatial resolution. The optical design and results of the fourth step also show that high numbers of the depth layers (in units of tens or even in units of hundreds depending on the full frame rate requirement of the application) can be measured with high depth resolution in units of mm at higher target distances. Also, high-resolution FPA's can be used with the developed Advance Multifocal LIDAR Imaging system which avoids the necessity of expensive scanning systems and also provides a compact design with easier productibility.

However, the depth resolution is limited by the de-magnification of the optical system for the longer ranges. The well-known AMCW LIDAR techniques can be combined with the depth of field technique to get higher depth resolution by avoiding the ambiguity problem of AM modulation by the depth of focus effect. As the final

step of this thesis, it has been shown that the new multifocal imaging concept can be combined with AMCW LIDAR systems for enlarging the measurement range without increasing the modulation period of AMCW and so decreasing the depth resolution. The main difference between the AMCW Multifocal Imaging System concept is using controlled depth of field and multifocal imaging technique indirectly for the range measurement. In this concept controlled depth of field is used for generating predefined gating (measurement) layers, which have equal width with the wavelength of the AMCW modulation, to distinguish the $\Delta\Phi$ phase shift between the transmitted and collected signals with the $N\Delta\Phi$ phase shifts for the distances bigger than ambiguity range. It is possible to use APD Arrays with high spatial resolution, so the system does not require expensive scanner systems.

The basic specifications of the new developed systems Multifocal LIDAR Imaging techniques are given below in Table 9.1.

Table 9.1 The Specifications of new Developed Multifocal LIDAR Imaging Techniques

Technique	Depth Resolution	Measurement Range	Frame Rate	# of Target Layers
Multifocal LIDAR	High (in mm)	Up to few meters	Video-Rate	3
Chromatic Multifocal LIDAR	High (in mm)	Up to few meters	Video-Rate	3
Chromatic Multifocal LIDAR with Dispersion Prism	High (in mm)	Up to few meters	Video-Rate	Up to hundreds
Advanced Multifocal LIDAR	High (in mm)	Up to hundreds of meters	Video-Rate / # of target layers	Up to hundreds
AMCW Multifocal LIDAR	High (in mm)	Up to hundreds of meters	Video-Rate /# of Gating Layers	~500 for per Gating Layer

In this study, Multifocal LIDAR Imaging techniques have been introduced for high-resolution 3D imaging applications. With the developed new hybrid methods, which use the narrow depth of field and so advantages of Multifocal Imaging, it is possible to achieve high depth resolutions beyond the Laser pulse rise time limitation of the LIDAR systems.

In a conclusion, new Multifocal LIDAR Imaging, Advanced Multifocal Imaging, and AMCW Multifocal LIDAR Imaging techniques and chromatic enhancement concepts have been designed and analyzed in this thesis. It has been shown that controlled depth of field effect and chromatic aberrations can be used as a tool for improving the depth resolution and frame rate of the LIDAR technique. Developed and theoretically proved Advanced Multifocal Imaging and AMCW Multifocal LIDAR Imaging techniques can be an important 3D imaging tool for many applications such as robotic

REFERENCES

[1]   Bochare Akshay, Saini Mukesh, Short Range Radar System using Arduino Uno, International Research Journal of Engineering and Technology, Volume: 04 Issue: 10, October, 2017

[2]   Grossman P., Depth From Focus, Volume 5, Issue 1, (1987)

[3]   TAKEMURA Kazumi, YOSHIDA Toshiyuki, Depth from Defocus Technique Based on Cross Reblurring, IEICE TRANS. INF. & SYST., VOL.E102–D, NO.11 (2019)

[4]   Whyte Refael, Streeter Lee, Cree Michael J., and Dorrington Adrian A., Application of LIDAR Techniques to Time-of-Flight Range Imaging, Applied Optics, October 14, 2015

[5]   Chen Zhaodong, Fan Rongwei, Ye Guangchao, Luo Tong, Guan Jiayu, Zhou Zhigang and Chen Deying;, Depth resolution improvement of streak tube imaging LIDAR system using three laser beams Chinese Optics Letters, COL 16(4), 041101 (2018)

[6]   Durand Frédo, Freeman Bill, MIT – EECS Lecture Notes

[7]   Lum Daniel J., Knarr Samuel H., and Howell John C., Frequency-modulated continuous-wave LIDAR compressive depth-mapping Optics Express, March 2018

[8]   Foix Sergi, Aleny`a Guillem and Torras Carme, Lock-in Time-of-Flight (ToF) Cameras: A Survey, IEEE Sensors Journal, Vol. 11, NO. 3, March 2011

[9]   Royo Santiago, and Ballesta-Garcia Maria, An Overview of LIDAR Imaging Systems for Autonomous Vehicles, Appl. Sci., 4093, 9, 2019,

[10]   Hwang Jeong-Yeon, Bu Jong-Uk, Ji Chang-Hyeon, Low Power Electromagnetic Scanning Micromirror for LIDAR System, IEEE Sensors Journal, VOL. 21, NO. 6, March 2021

[11]   Pentland Alex P., A New Sense for Depth of Field, Volume: PAMI-9, Issue: 4, (1987)

[12]   Wens Mike, Redoute Jean-Michel, Blanchaert Tim, Bleyaert Nicolas and Steyaert Michiel, An integrated 10A, 2.2ns rise-time laser-diode driver for LIDAR applications, 2009 Proceedings of ESSCIRC (2009)

[13]   Michael Moeller, Martin Benning, Carola Schönlieb, Daniel Cremers, Variational Depth from Focus Reconstruction, IEEE Transactions on Image Processing, Volume: 24, Issue: 12, Dec. 2015

[14]   Hazirbas Caner, Soyer Sebastian Georg, Staab Maximilian Christian, Leal-Taix´e Laura, and Cremers Daniel, Deep Depth From Focus, Computer Vision – ACCV 2018 pp 525–541, 2018

[15]   R.T.H.Collis, Advances in Geophysics, LIDAR, Volume 13, 1969,

[16]   McManamon Paul F., Banks Paul, Beck Jeffrey, Fried Dale G., Huntington Andrew S., and Watson Edward A., Comparison of flash LIDAR detector options, Optical Engineering 56(3), 031223 (March 2017)

[17]   Zhuo Shenglong, Zhao Lei, Xia Tao, Wang Lei, Shi Shi, Wu Yifan, Liu Chang, Wang Chill, Wang Yuwei, Li Yuan, Yu Hengwei, Xu Jiqing, Wang Aaron, Lin Zhihong, Chen Yun, Bai Rui, Chen Xuefeng, Chiang Patrick Yin, Solid-State dToF LIDAR System Using an Eight-Channel Addressable, 20W/Ch Transmitter, and a 128x128 SPAD Receiver with SNR-Based Pixel Binning and Resolution Upscaling, 2022 IEEE Custom Integrated Circuits Conference (CICC), 2022

[18]   Li Anhu, Liua Xingsheng, Sun Jianfeng, Lu Zhiyong, Risley-prism-based multi-beam scanning LIDAR for high-resolution three-dimensional imaging, Optics and Lasers in Engineering Volume 150, March 2022

[19]   Kato Yuichi, Sano Takuya, Moriyama Yusuke, Maeda Shunji, Yamazaki Takeshi, Nose Atsushi, Shina Kimiyasu, Yasu Yohtaro, Tempel Ward van der, Ercan Alper, Ebiko Yoshiki, 320x240 back-illuminated 10Pm CAPD pixels for high speed modulation Time-of-Flight CMOS image sensor, in Symp. VLSI Circuits Dig. Tech. Papers, Jun. 2017,

[20]   Lum Daniel J., Knarr Samuel H., and Howell John C., Frequency-modulated continuous-wave LIDAR compressive depth-mapping, Optics Express, Vol. 26, No. 12, 2018

[21]   Whyte Refael, Streeter Lee, Cree Michael J., and Dorrington Adrian A., Application of LIDAR Techniques to Time-of-Flight Range Imaging, Applied Optics, Vol.54, Issue 33, 2015

[22]   Godbaz John P., Cree Michael J. & Dorrington Adrian A., Extending AMCW LIDAR Depth-Of-Field Using a Coded Aperture, Computer Vision – ACCV, 2010

[23]   Lewis P., Modelling spatial video as part of a GIS video analysis framework, Proceedings of the 18th SIGSPATIAL International Conference on Advances in Geographic Information Systems, 2010

[24]   Badon Amaury, Bensussen Seth, Gritton Howard J., Awal Mehraj R., Gabel Christopher V.,Han Xue, Mertz Jerome, Video-rate large-scale imaging with Multi-Z confocal microscopy, Optica, Vol. 6, Issue 4, (2019)

CURRICULUM VITAE

Surname, Name: Ürkmen, Koray

EDUCATION:

Degree	Institution	Year of Graduation
MS	Bilkent University Physics	2005
BS	Izmir Institute of Technology Physics	2003
High School	Izmir Atatürk High School, Izmir	1998

FOREIGN LANGUAGES:

Advanced English,

CERTIFICATES:

- Introduction to Laser Radar
- MATLAB & Simulink Advanced Applications
- Engineering Approach to Imaging System Design
- Advanced Optical Design Using ZEMAX

PUBLICATIONS

1. Scanning Hall Probe Microscopy (SHPM) Using Quartz Crystal AFM Feedback; Dede M., Ürkmen K., Girişen Ö., Atabak M., Oral A., Farrer I., Ritchie D.; Journal of Nanoscience and Nanotechnology; Volume 8; Number 2; 2008 ; pp. 619-622(4)

2. Design of a High-Resolution Multifocal LIDAR: Enabling higher resolution beyond the laser pulse rise time; Ürkmen K., Yüce E., IEEE Transactions on Instrumentation and Measurement, in Review

3. High Resolution LIDAR Imaging System; Yüce E., Ürkmen K., TR Patent: 2021-GE-643595, (Pending)

4. High Resolution Dispersion Based LIDAR Imaging System; Yüce E., Ürkmen K., in Patent Office for Application

Hiking, Basketball, Gourmet, Movies,